DOI: 10.14753/SE.2013.1815

Prediction of intestinal absorption and brain penetration of drugs

Ph.D. Thesis

Éva Hellinger Pharm.D.

Semmelweis University
Doctoral School of Pharmaceutical Sciences

Supervisor:	Dr. Károly Tihanyi Ph.D.
Consultant:	Dr. Monika Vastag Ph.D.
Official reviewers:	Prof. Dr. Kornélia Tekes Ph.D. Dr. Katalin Jemnitz Ph.D.
Head of the Final Exam Committee:	Prof. Dr. Tamás Török D.Sc.
Members of the Final Exam Committee:	Prof. Dr. Imre Klebovich D.Sc. Dr. István Krizbai Ph.D.

Budapest
2012

DOI: 10.14753/SE.2013.1815

Table of content

DOI: 10.14753/SE.2013.1815

DOI: 10.14753/SE.2013.1815

DOI: 10.14753/SE.2013.1815

Abbreviations

ABC	ATP binding cassette
ADME	absorption, distribution, metabolism and excretion
AJ	adherens junctions
ATP	adenosine triphosphate
BBB	blood brain barrier
BBCEC	bovine brain capillary endothelial cells
BBMEC	bovine brain microvessel endothelial cells
BCRP	breast cancer resistance protein
BCSFB	blood-cerebrospinal fluid barrier
BCECF	2',7'-bis(2-carboxyethyl)-5(6)-carboxyfluorescein
BCECF-AM	2',7'-bis(2-carboxyethyl)-5(6)-carboxyfluorescein acetoxymethyl ester
Caco-2	colon adenocarcinoma cell line
calcein-AM	calcein–acetoxymethylester
CEC	cerebral endothelial cell
CNS	central nervous system
CSF	cerebrospinal fluid
CYP	cytochrome P450
EPA	triple co-culture of rat brain capillary endothelial cells with pericytes and astrocytes
fu	free (unbound) fraction
GI	gastrointestinal tract
GLUT	glucose transporter
HA	human absorption
HPT	human peptide transporter 1
IAM	immobilized artificial membrane assay
IRF	initial rate of fluorescence
ISF	interstitial fluid
KHB	Krebs-Henseleit buffer
K_M	Michaelis constant
Kp	total brain to total blood concentration ratio
Kp,uu	unbound brain to unbound blood concentration ratio at a steady state

LAT large neutral amino acid transporter
LDL low-density lipoprotein
MBUA mouse brain uptake assay
MCT monocarboxylic acid transporter
MDCK Madin-Darby canine kidney
MDCK-MDR1 MDCK cells transfected with the human MDR1 gene
MDR1 multidrug resistance protein
MOAT multispecific organic anion transporter
MRP multidrug resistance protein
mRNA messenger RNA
MW molecular weight
NaF fluorescein sodium
OAT organic anion transporter
OATP organic anion transporting polypeptide
OCTN organic cation transporter
PAMPA parallel artificial membrane permeation assay
PBCEC porcine brain capillary endothelial cells
PBMEC porcine brain microvessel endothelial cell
Papp apparent permeability
PBS phosphate buffered saline
PCR polymerase chain reaction
PD pharmacodynamics
Pe permeability coefficient
PEPT peptide transporter 1
P-gp P-glycoprotein, encoded by ABCB1, also termed MDR1
PK pharmacokinetics
PS permeability surface area product
SLC solute carrier
TEER trans epithelial/endothelial electric resistance
TJ tight junction
VB-Caco-2 vinblastine-treated Caco-2
ZO zonula occludens

DOI: 10.14753/SE.2013.1815

1. Introduction

A prerequisite of drug action is their presence in the molecular surroundings of the target in sufficient concentration and for sufficient length of time. Living organisms prevent drugs and other xenobiotics from entering a body by means of efflux transporters and eliminate them by means of highly adaptive metabolizing enzymes. The ADME properties of drugs (absorption, distribution, metabolism and excretion) will define their pharmacokinetic properties. Nowadays, all factors and traits that determine the pharmacokinetic profile of drugs are subject to modelling and serve as a ground of prediction. Pharmacokinetic properties of drug candidates are decisive data, either promote or block the development of NCEs.

The absorption, distribution, metabolism, excretion, and action of a drug all involve the crossing of cell membranes. In most cases, a drug must transverse the plasma membranes of many cells to reach its site of action. Bypassing cells by paracellular passage through intercellular gaps is a physiological mechanism e.g. in filtration across the glomerulus in the kidney. Generally, large lipophilic drugs do not penetrate paracellularly; they need to pass barriers through the cell membrane (transcellular diffusion). The capillaries of the central nervous system (CNS) and a variety of epithelial tissues have tight intercellular junctions, so paracellular passage through them is limited at best. Most drugs cross membranes by passive processes driven by the concentration gradient, but mechanisms involving the active participation of transporters or carriers also play an important role. Active transport is characterized by a direct requirement of energy, movement against a concentration gradient, saturability, selectivity and competitive inhibition by co-transported compounds (1).

Transporters are membrane proteins that control the influx of essential nutrients and ions and the efflux of cellular waste, environmental toxins, drugs, and other xenobiotics. Regarding drug transport, two groups of transporters are known; ABC (ATP binding cassette) and SLC (solute carrier) transporters. Most ABC proteins are primary active transporters, which need ATP hydrolysis to actively pump their substrates across membranes. These efflux transporters likely evolved as a defense mechanism against harmful substances, therefore, they have broad substrate specificity,

DOI: 10.14753/SE.2013.1815

consequently many drugs qualify as substrates for them. The SLC superfamily includes genes that encode facilitated transporters and ion-coupled secondary active transporters that generally mediate the cellular uptake of nutrients such as glucose and amino acid, and drugs that structurally resemble the endogenous ligands of the transporter.

Therefore, efflux and uptake transporters play substantial role in the pharmacokinetic and pharmacodynamic pathways of their substrate drugs, including pathways involved in both, therapeutic and adverse effects.

Transporters that are important in pharmacokinetics are generally located in the intestinal, renal, and hepatic epithelia, as well as in the capillary endothelia of blood-brain barrier (BBB). Transporters expressed in the liver and kidney work in concert with drug-metabolizing enzymes to eliminate drugs and their metabolites, thereby affecting exposure, and hence toxicity, in all organs (2). At the same time, efflux transporters control the tissue distribution and have a role in tissue penetration, therefore, may serve as protective barriers to particular organs and cell types. Access of solutes to several tissues such as the brain and testes is restricted and the efflux transporters in these barrier endothelia may limit penetration of drugs.

Among the best recognized transporters in the ABC superfamily are P-glycoprotein (P-gp, encoded by ABCB1, also termed MDR1) (**Fig. 1**) (3), which extrudes a large variety of xenobiotics (**Table 1**). The overexpression of P-gp (with other efflux transporters) is responsible for the multidrug resistance of tumours to some cancer chemotherapeutic agents. But P-gp is physiologically present on the apical surface of intestinal and kidney epithelial cells, on the luminal surface of brain capillary endothelial cells forming the BBB and on the canalicular membrane of hepatocytes. P-gp mediated efflux has been recognized as a serious limiting factor in brain entry of several substrate drugs (4,5,6), such as the HIV protease inhibitors and loperamide. Loperamide is a potent opioid that lacks the central effects characteristics of other opioids and therefore used for diarrhoea (1). P-gp also influences the intestinal absorption of low permeability or dissolution limited P-gp substrates. Consequently, these drugs have reduced or variable plasma levels and non-linear pharmacokinetics (7,8,9,10). The degree of absorption or the intestinal efflux of cyclosporine, talinolol and tacrolimus reportedly correlates with the intestinal MDR1 mRNA level in humans,

DOI: 10.14753/SE.2013.1815

and a decreased absorbed fraction has been reported in response to P-gp induction by carbamazepine or rifampicin or St. John's wort (11,12,13,14,15).

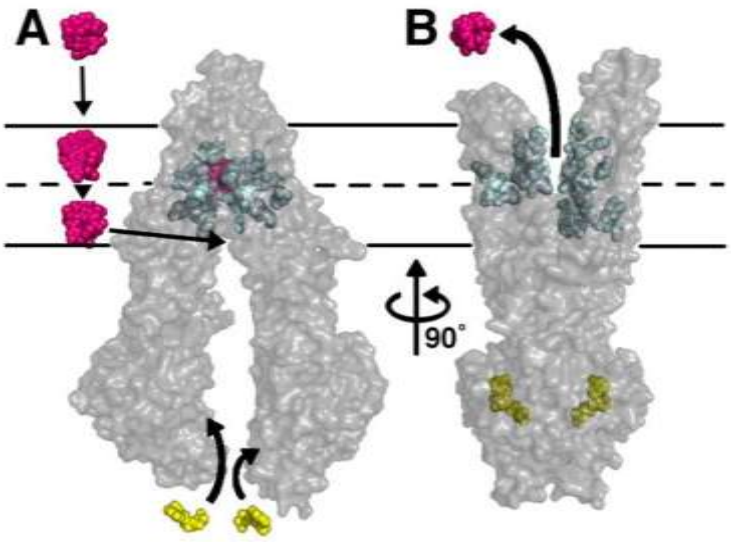

Fig. 1. Model of substrate transport by P-gp. **A:** Substrate (magenta) partitions into the bilayer from outside of the cell to the inner leaflet and enters the internal drug-binding pocket through an open portal. **B:** ATP (yellow) binds to the nucleotide-binding domains causing a large conformational change presenting the substrate and drug-binding site(s) to the outer leaflet/extracellular space (3).

Table 1. Reported substrates and inhibitors of P-gp (16).

Substrates: Acebutolol, Acetaminophen, Actinomycin D, β-Acetyldigoxin, Amitriptyline, Amprenavir, Apafant, Asimadoline, Atenolol, Atorvastatin, Azidopine, Azidoprocainamide methoiodide, Azithromycin, Benzo(a)pyrene, Betamethasone, Bisantrene, Bromocriptine, Bunitrolol, Calcein-AM, Camptothecin, Carbamazepine, Carvedilol, Celiprolol, Cepharanthin, Cerivastatin, Chloroquine, Chlorpromazine, Chlorothiazide, Clarithromycin, Colchicine, Corticosterone, Cortisol, Cyclosporin A, Daunorubicin (Daunomycin), Debrisoquine, Desoxycorticosterone, Dexamethasone, Digitoxin, Digoxin, Diltiazem, Dipyridamole, Docetaxel, Dolastatin 10, Domperidone, Doxorubicin (Adriamycin), Eletriptan, Emetine, Endosulfan, Erythromycin, β-Estradiol, Estradiol-17β-D-glucuronide, Etoposide (VP-16), Fexofenadine, GF120918, Grepafloxacin, Hoechst 33342, Hydroxyrubicin, Imatinib, Indinavir, Ivermectin, Levofloxacin, Loperamide, Losartan, Lovastatin, Methadone, Methotrexate, Methylprednisolone, Metoprolol, Mitoxantrone, Monensin, Morphine, 99mTc-sestamibi, *N*-desmethyltamoxifen, Nadolol, Nelfinavir, Nicardipine, Nifedipine, Nitrendipine, Norverapamil, Olanzapine, Omeprazole, PSC-833 (Valspodar), Perphenazine, Prazosin, Prednisone, Pristinamycin IA, Puromycin, Quetiapine, Quinidine, Quinine, Ranitidine, Reserpine, Rhodamine 123, Risperidone, Ritonavir, Roxithromycin, Saquinavir, Sirolimus, Sparfloxacin, Sumatriptan, Tacrolimus, Talinolol, Tamoxifen, Taxol (Paclitaxel), Telithromycin, Terfenadine, Timolol, Toremifene, Tributylmethylammonium, Trimethoprim, Valinomycin, Vecuronium, Verapamil, Vinblastine, Vincristine, Vindoline, Vinorelbine
Inhibitors: Amiodarone, Amitriptyline, Amlodipine, Astemizole, Atemoyacin-B, Atorvastatin, Aureobasidin A, Azelastine, Barnidipine, Benidipine, Bepridil, Bergamottin, Bergapten, Bergaptol, Biochanin A, Biricodar (VX-710), Bromocriptine, Buspirone, Caffeine, Carvedilol, Celiprolol, Cepharanthin, Chlorpyrifos, Cholesterol, Cimetidine, Clarithromycin, Clofazimine, Clomipramine, Clotrimazole, Colchicine, Cortisol, Cremophor EL, Cyclosporin, Cytochalasin E, Daunorubicin (Daunomycin), Desethylamiodarone, Desipramine, Desloratadine, Desmethylazelastine, Dexamethasone, Dexniguldipine, Digoxin, 6,7-Dihydroxybergamottin, Dihydrocytochalasin B, Diltiazem, Dipyridamole, Doxepin, Doxorubicin (Adriamycin), [D-Pen2, D-Pen5]-enkephalin, Efonidipine, Eletriptan, Emetine, Endosulfan, Epiabeodendroidin F, Ergometrine, Ergotamine, Erythromycin, Estramustine, Etoposide (VP-16), Fangchinoline, Felodipine, Fentanyl, Fluconazole, Fluoxetine, Fluphenazine, Fluvoxamine, Forskolin, Gallopamil, Genistein, GF120918, Haloperidol, Hydrocortisone, 1'-Hydroxymidazolam, Indinavir, Itraconazole, Ivermectin, Ketoconazole, Lansoprazole, Loperamide, Loratadine, Lovastatin, Manidipine, Methadone, Metoprolol, Mibefradil, Miconazole, Midazolam, Morin, Morphine, Naringenin, Nefazodone, Nelfinavir, Nicardipine, Nifedipine, Nilvadipine, Nisoldipine, Nitrendipine, Nobiletin, Norverapamil, Omeprazole, Pafenolol, Pantoprazole, Phenylhexyl isothiocyanate, Pimozide, Piperine, Pluronic block copolymer, Pristinamycin IA, Progesterone, Promethazine, PSC-833 (Valspodar), Quercetin, Quinacrine, Quinidine, Quinine, Ranitidine, Rapamycin, Reserpine, Ritonavir, Saquinavir, Silymarin, Simvastatin, Sirolimus, Mephenytoin, Spironolactone, Staurosporine, Sufentanil, Talinolol, Tamoxifen, Tangeretin, Taxol (Paclitaxel), Terfenadine, Tetrandine, Tetraphenylphosphonium, Trans-flupenthixol, Trifluoperazine, Triflupromazine, Trimethoxybenzoylyohimbine, Troleandomycin, Tween 80, Valinomycin, Verapamil, Vinblastine, Vincristine

DOI: 10.14753/SE.2013.1815

In the intestine the saturation of P-gp mediated efflux transport can occur due to high local concentration of dissoluted drugs and the simple diffusion may overcome P-gp activity (especially by high solubility - high diffusion drugs), still variable and non-linear pharmacokinetics along doses can occur and make drug development difficult. Saturation of P-gp function is less likely at BBB as usually low drug levels are present in the plasma; therefore, P-gp can limit severely brain penetration of P-gp substrate drugs (9).

Additionally, MRP2 (multidrug resistance protein, ABCC2), and BCRP (breast cancer resistance protein, ABCG2) are also expressed in the apical side of the intestinal epithelia, where they serve to pump out xenobiotics, including many orally administered drugs. At the BBB, beside P-gp, there is accumulating evidence for the roles of BCRP and MRP4 in limiting the brain penetration of drugs (17,2). **Fig. 2** shows the transporters in plasma membrane domains of intestinal epithelia, hepatocytes, kidney proximal tubules and brain capillary endothelial cells.

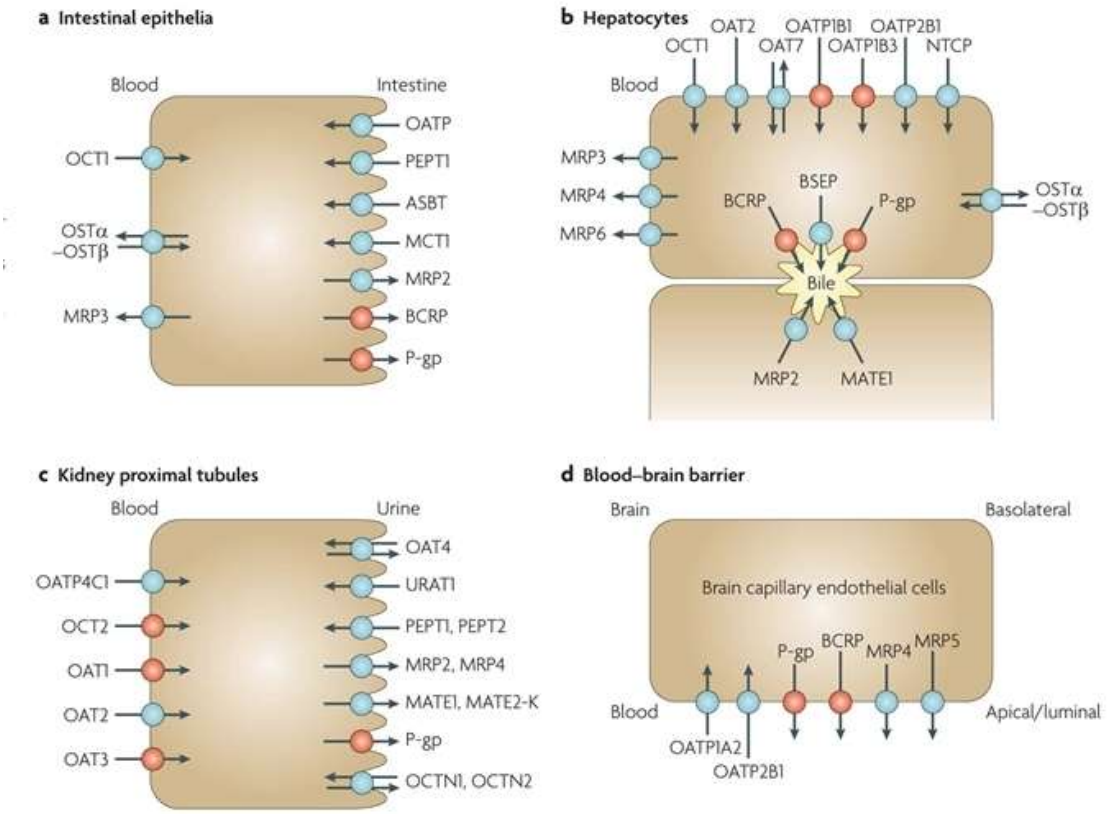

Fig. 2. Selected human transport proteins for drugs and endogenous substances. **a**: Intestinal epithelia contain in their apical (luminal) membrane several uptake transporters including one or more members of the organic anion transporting polypeptide (OATP) family; peptide transporter 1 (PEPT1;SLC15A1); ileal

apical sodium/bile acid co-transporter (ASBT; SLC10A2); and monocarboxylic acid transporter 1 (MCT1; SLC16A1). The apical ATP-dependent efflux pumps include multidrug resistance protein 2 (MRP2; ABCC2); breast cancer resistance protein (BCRP; ABCG2); and P-glycoprotein (P-gp; MDR1, ABCB1). The basolateral membrane of intestinal epithelia contains organic cation transporter 1 (OCT1; SLC22A1); heteromeric organic solute transporter (OSTα-OSTβ); and MRP3 (ABCC3). **b:** Human hepatocyte uptake transporters in the basolateral (sinusoidal) membrane include the sodium/taurocholate co-transporting peptide (NTCP;SLC10A1); three members of the OATP family (OATP1B1(SLCO1B1), OATP1B3 (SLCO1B3) and OATP2B1 (SLCO2B1)); organic anion transporter 2 (OAT2; SLC22A7)and OAT7 (SLC22A9); and OCT1. Efflux pumps in the hepatocyte basolateral membrane include MRP3, MRP4 (ABCC4) and MRP6 (ABCC6). Apical (canalicular) efflux pumps of the hepatocyte comprise P-gp; bile-salt export pump (BSEP or SPGP; ABCB11); BCRP (ABCG2); and MRP2. In addition, multidrug and toxin extrusion protein 1 (MATE1; SLC47A1) is located in the apical hepatocyte membrane. **c**: Kidney proximal tubules contain in the apical (luminal) membrane OAT4 (SLC22A11); urate transporter 1 (URAT1; SCL22A12); PEPT1 and PEPT2 (SLC15A2); MRP2 and MRP4; MATE1 and MATE2-K (SLC47A2); P-gp; organic cation/ergothioneine transporter (OCTN1; SLC22A4); and organic cation/carnitine transporter (OCTN2; SLC22A5). Basolateral uptake transporters in proximal tubule epithelia include OATP4C1 (SLCO4C1); OCT2; and OAT1, OAT2 and OAT3 (SLC22A8). **d:** Apical (luminal) transport proteins of brain capillary endothelial cells contributing to the function of the blood–brain barrier include the uptake transporters OATP1A2 and OATP2B1; and the efflux pumps P-gp, BCRP, MRP4 and MRP5 (ABCC5) (17).

1.1. Role of *in vitro* ADME predictions

In the early phase of drug discovery, PD- and PK-related aspects of molecules must be considered. Beyond the affinity and selectivity for the target pharmaceutical properties (stability, solubility, question of formulation), permeability across cell membranes and other ADME traits may require optimization (18). The cost and time taken to develop new medicines has continued to rise over recent times while the number of new drug approvals has declined. Therefore, the pharmaceutical industry is generally looking to improve success rates and reduce candidate attrition during the drug development process. One of the options for that is the early termination of drug development programmes that would ultimately fail, consequently resources can be focused on those compounds most likely to succeed (19).

Inappropriate pharmacokinetic behaviour, one of the causes of failure in drug development includes such factors as low bioavailability due to high extraction or poor

absorption characteristics, short elimination half-life leading to short duration of action and excessive variability due to genetic or environmental factors (19). In 1991, adverse pharmacokinetic and bioavailability results were the most significant cause of attrition in the clinic, and accounted for ~40% of all attritions (20). This observation has led to an increased emphasis on pharmacokinetic input to the drug discovery process throughout the pharmaceutical industry. Much progress has been made in developing tools for the prediction of drug absorption, drug clearance and drug–drug interactions, in addition to the scaling of pharmacokinetic parameters from animals to man. The use of pharmacokinetic predictions in the drug discovery phase has resulted in fewer compounds failing as a result of inappropriate clinical pharmacokinetics (19). By 2000, adverse pharmacokinetic and bioavailability had dramatically reduced as a cause of attrition in drug development, and contributed to it less than 10% (20). Moreover, consideration of the pharmacokinetic profile of a new chemical entity can also be beneficial in the assessment of safety and efficacy. Generally it is possible to make fairly robust predictions of the pharmacokinetic profile in man using *in vitro* systems and preclinical pharmacokinetic studies (19).

1.2. Intestinal absorption and its modelling

The oral route is a convenient way to administer drug products and it still remains the route of choice for a high patient compliance in most indications. Absorption across the intestinal barrier is a prerequisite for an orally administered drug to take effect. Absorption is the result of a complex process that begins when the dosage formulation is swallowed and proceeds through the liberation of the drug molecules from the formulation, crossing the biological membranes of enterocytes by passive diffusion and/or active transport, and metabolization by enzymes. Absolute bioavailability is the fraction of a dose that reaches systemic circulation following oral administration. The key determinants of the systemically available drug level are the fraction of the dose that enters the enterocytes and the fraction that escapes first pass metabolism. Current physiological properties of the gastrointestinal system, the physicochemical properties of the drug and its formulation will have impact on the systemic availability.

DOI: 10.14753/SE.2013.1815

1.2.1. Small intestine structure and function

The primary function of the gastrointestinal tract (GI) is the absorption of nutrients and water, but it also serves for drug absorption following oral administration. Furthermore, the protection of an organism from systemic exposure of various toxins, antigens, and microorganisms is also an important function. Therefore, the GI is also an interface between the outer world and an organism.

Drug absorption occurs in each anatomical segments of the GI, starting from the buccal mucosa, moving through the stomach, the small intestine (duodenum, jejunum and ileum) and ending in the colon. The pancreas and the biliary system of the liver secrete enzymes and detergents into the duodenum. Pancreatic secretions contain hydrolytic enzymes (proteases, lipases, amylases) that digest food, but also decompose drugs with sensitive groups. Biliary acids improve drug solubility and dissolution through micellization and wetting (21). Some metabolites and xenobiotics are subjects to entero-hepatic circulation, a process of intestinal reabsorption and repeated biliary excretion.

The functional layers of the small intestine are the mesothelium (serosa), muscularis propria, submucosa and the mucosa-containing absorptive epithelium. The intestine is richly supplied with blood vessels, nerve endings and lymphatics (**Fig. 3**).

The layer of columnar epithelial cells represents the most important barrier that nutrients and drugs must traverse to enter a body. The epithelium displays fingerlike projections, called villi, which provide increased surface area in order to achieve maximal absorption. The villi house the self-renewing population of epithelial cells with different functions, including secretory cells, endocrine cells and absorptive enterocytes. There are membrane invaginations at the feet of the villi, known as crypts, which consist of continuously dividing stem cells. Stem cells produce daughter cells, which are the source of both epithelial and crypt cells (22,23,24).

DOI: 10.14753/SE.2013.1815

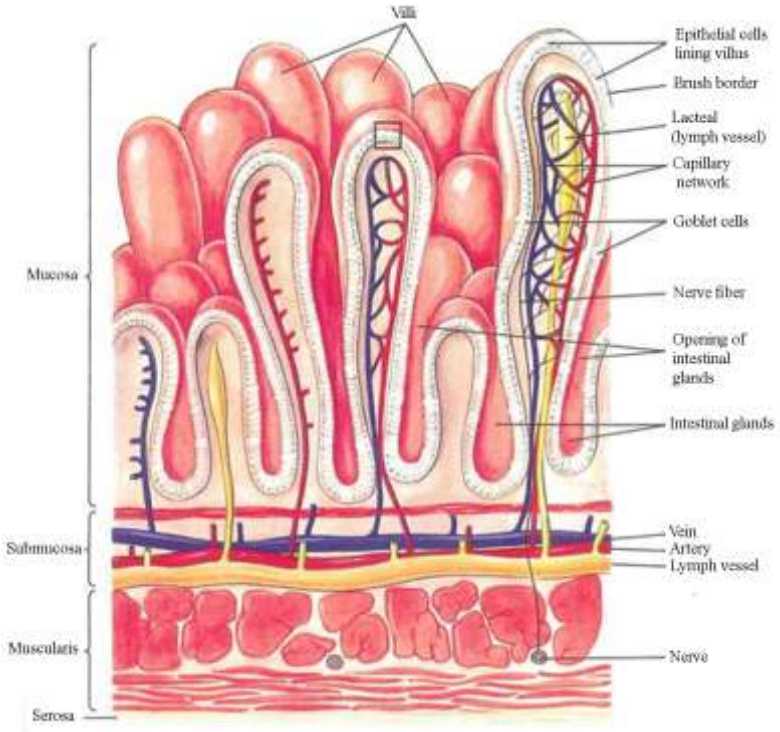

Fig. 3. Structure of the small intestine wall (25).

The microvilli-covered apical surface of the epithelium constitutes the brush border with enzymes such as sucrase, lactase and alkaline phosphatase. Brush border enzymes are involved in the digestion of carbohydrates. These enzymes hydrolyse sensitive drug substrates such as esters, amides etc. The brush border morphology is a special characteristic of the intestine that greatly increases the surface area of the absorptive cell and so provides increased contact with substances in order to achieve maximally efficient absorption (26,27). Special morphological features such as the brush border, villi and circular folds, together with the long transit time and variable pH, make the small intestine the primary site for drug absorption in the GI.

1.2.2. Factors influencing drug absorption

Drug absorption is influenced by the biological variables of gastrointestinal tract, like transit time, pH, presence of food, secreted detergents, gut motility and the expression level of transporters and enzymes. Moreover, the net pharmacokinetic

performance of the drug is also the consequence of the drug properties determining its solubility, penetrability and affinity to transporters and enzymes.

1.2.2.1. Biological variables of the small intestine that influence drug absorption

Residence time

Gastric residence and intestinal transit time influence drug absorption. This is especially true for dissolution-limited drugs. The mean gastric residence time is shorter than that of the intestine (28). Relatively high inter-individual variability also exists. Fed/fasted state, dosage form (tablet, capsule, solution, suspension etc.), drug particle size (an important physical parameter of the dissolution rate) and the volume of co-administered water all impact residence time.

pH

There is a pH gradient along the GI tract, which ranges from more acidic in the stomach to acidic/neutral in the small intestine. The solubility, dissolution and penetrability of ionizable drugs are sensitive to these pH variations. The pH range in the stomach and the jejunum varies greatly depending on the fasted/fed state (29).

Active transports

Drug absorption is particularly strongly influenced by both active influx and efflux transport processes for compounds with low passive penetrability. Based on gene expression levels, the most abundant active transporters in the human intestine are HPT1 (human peptide transporter 1), PEPT1 (peptide transporter 1), BCRP, MRP2, MDR1 and MCT1 (monocarboxylic acid transporter 1) (30). A compound with P-gp liability may overcome the intestinal barrier due to saturation at high intestinal dose and display a non-linear PK. The P-gp level increases distally along the segments of the small intestine, with relatively low interindividual variation (≤ 2-fold) compared to CYP3A4 (> 10-fold) (31,32).

Metabolism

Drug metabolism in the gut wall can severely reduce the drug level available for absorption. CYP3A4 is a major metabolic enzyme in the intestine (33). In the upper intestinal segments, it is assumed that there is interplay between P-gp and metabolic enzymes. P-gp and 3A4 have overlapping substrate specificity and so they act in concert: P-gp reduces intracellular drug levels, therefore CYP3A4 can act more effectively at lower substrate level.

Some drugs show varying solubility and stability in different regions of the intestine as a result of changes in environmental pH, degradation by enzymes present in the lumen of the intestine or interaction with endogenous solubilising agents such as bile. In other instances active efflux or uptake transport mechanisms will modify drug absorption to various extent in certain regions of the GI tract. Such drugs display region-specific absorption i.e. they can only be absorbed efficiently in specific segments of the GI tract that are named "absorption windows" (34).

1.2.2.2. Drug properties influencing absorption

Solubility and permeability are two major features of a drug that determine its oral absorption. The Biopharmaceutical Classification System has categorized drugs in terms of their solubility and intestinal permeability. Class I compounds are defined as those with high solubility and high permeability, and predicted to be well absorbed when given orally. All other compounds (classes II-IV) suffer either from low solubility, low permeability or both, and will present challenges to the development of products with acceptable oral bioavailability (34).

Penetration of xenobiotics is a virtually continuous process of traversing hydrophilic and lipophilic phases, so the lipophilic and hydrophilic features of drugs are important in this process. The Lipinski Rule defines the likelihood of poor absorption in humans, using the structural properties of over 2000 compounds that survived Phase I clinical trials (35). The ‘Rule-of-Five’ predicts that poor absorption or permeation is more likely when the number of hydrogen bond donors is more than 5, there are at least 10 hydrogen bond acceptors, the molecular weight is greater than 500 and the calculated

Log P is greater than 5. The 'Rule-of-Five' should be considered as a qualitative predictor of absorption and permeability. With large molecular size, solubility and passive penetrability decreases. If the number of hydrogen bonds and thus the drug's polar feature increases, aqueous solubility will increase, but passive penetration (partitioning in the lipid bilayer of the cell membrane) will decrease. Lipophilicity above a certain level limits molecular penetration, as drugs are simply trapped in the cell membranes. For optimal absorption, a good balance of permeability and aqueous solubility is deemed in the range of $0 < \log P < 3$ or $1 < \log D_{7.4} < 3$.

Veber et al. has defined additional critical properties that are required in order to achieve good oral bioavailability in rats (36). They reported the findings from a study of rat bioavailability data for 1100 drug candidates. They found that molecules possessing fewer than 10 rotatable bonds and having a polar surface area less than 140 $Å^2$ (or H-bond count less than 12) generally showed oral bioavailability in rats exceeding 20%.

Ionizability is also a critical drug property that influences drug absorption. Charged molecules display higher solubility than their neutral forms, yet they show lower rates of penetration. As there is a pH gradient along the gastrointestinal tract, the solubility and penetration of chargeable drugs may differ accordingly. Most drugs (75%) are weak bases, therefore less ionized and penetrate faster in the more basic segments of the GI, preferably in the small intestine.

High lipophilicity and therefore low aqueous solubility of new chemical entities is a common problem in recent drug research.

1.2.3. Models of intestinal absorption

In order to predict the absorption of new chemical entities, preclinical research generates data using *in silico*, *in vitro*, *ex vivo* and *in vivo* models previously correlated with human data. The availability of suitable human data is one of the most critical points of human prediction. High enough bioavailability (> 80%) may reflect good absorption and is a useful source of human data. The ratio of the cumulative urinary excretion of the drug and metabolites following oral and intravenous administration is another important form of data used for the human prediction endpoint. Low solubility, formulation-, salt- and dose-dependent absorption, and metabolism complicate the

evaluation of absorption (37). Some human single-pass perfusion data are also available, and present a good correlation with the extent of absorption determined by other pharmacokinetic studies (38).

1.2.3.1. In silico models

In silico methods use calculated physicochemical drug properties (*e.g.* lipophilicity, hydrogen bonding, molecular surface properties, solubility, solvatation energy, charge distribution) as descriptors for drug permeation, and frequently directly predict drug pharmacokinetic (PK) properties such as human absorption (39,40,41,42,37). The accuracy and the predictive value of *in silico* models are critically dependent on the reliability of the biological data on which the model is based (43). PSA, NPSA (non-polar surface area) and dynamic PSA_d appear to be important descriptors for the prediction of passive penetration (44,45). Prediction for active transports still needs to be proven (46,47). Otherwise, *in silico* models are high throughput, cost-effective techniques (requiring minimum usage of resources and manpower), as they are normally used for screening of virtual libraries, and a molecule will only be synthesized if it shows a satisfactory level of absorption.

1.2.3.2. Non-cell based in vitro systems

There are several methods that use artificial membranes or liposomes to predict drug absorption or drug-membrane interaction (48,49,50). The most widely used methods are IAM (immobilized artificial membrane assay) chromatography and PAMPA (parallel artificial membrane permeation assay). In IAM an artificial membrane is employed as the stationary phase of chromatography. A monolayer made up of phospholipid analogues is covalently bonded to the surface of silica particles. The technique can be performed coupled with a conventional HPLC instrument. Based on chromatographic retention time, it is possible to rank and classify a large number of drugs in a cost effective way (51). The method runs with small amounts of test articles and does not require either high purity samples or quantification. However, IAM models drug-membrane interaction rather than membrane permeation. Compounds that present

good lipid partition in this model do not necessarily cross the epithelial cell layer. The results simply represent passive transcellular uptake.

The PAMPA is a high throughput assay for permeability screening in early drug research. It is performed in two-part multi-well plates with an artificial lipid membrane impregnated with mixture of lecithin/phospholipids dissolved in an inert organic solvent (52,53). The drug concentration in the acceptor plate is followed by HPLC, or simply by a more efficient system coupled UV-plate reader. Due to its high throughput capacity, PAMPA can be used to pre-screen large sets of compounds for passive penetrability prior to cellular assays, and can provide information about ionization status, pH dependence of the absorption, and the influence of the unstirred water layer on drug permeability. PAMPA tolerates lower pH levels and a higher content of solubilizing agents than cell-based assays (54). The composition of the artificial membranes, type of filter material and the applied pH make PAMPA useful both for intestinal and BBB penetration measurement. Similarly to IAM, only passive transcellular transport can be predicted using PAMPA, as there is no consideration of paracellular pathway, carrier-mediated transport, drug metabolism, and active transporters, therefore, false positives and negatives may occur for active transporter substrates and for drugs capable of metabolism at the site of permeation.

1.2.3.3. Cell culture based in vitro models

For the majority of oral drugs, the intestinal epithelium forms the main barrier that must be permeated in order to enter the body. Epithelial cell-based systems are therefore expected to be the best *in vitro* models of oral drug absorption. *In vitro* models of drug penetration that display adequate passive permeability and efflux transporter functionality, especially those that offer both P-gp and good human predictability simultaneously, are much-needed tools for high throughput application in early drug research. Primary cultures of enterocytes have very poor viability (55,56,57), but immortalized cell lines such as Caco-2, HT-29, T-84, MDCK and 2/4/A/1 grow rapidly into confluent monolayers, and model absorption at some level. Reference compounds with known human absorption serve for validation of the models. Compared to the simpler IAM and PAMPA systems, the cell-based systems more closely resemble *in*

vivo conditions. Depending on the type and differentiation of the monolayers, these models display not only passive transcellular but also paracellular and active transport features. They have an advantage over *in vivo* animal models in that they require neither high amounts of test compounds nor animal test subjects.

Caco-2

Caco-2 is the preferred cell-based model for human drug absorption (58) (59). Caco-2 cells are derived from human colonic adenocarcinoma, but they have morphological and functional similarities to small intestinal enterocytes (60). The cells undergo spontaneous differentiation on permeable filters, depending on culture conditions. The advantage of the human origin of the cells is underlined by the results that many of the active transporter genes that are present in the human intestine, such as MDR1, MRP-2, -3, -5; BCRP, OCTN-1, -2, MOAT-C, PepT1 and OATP-B, are expressed at some level in Caco-2 cells (**Fig. 4**) (61,30,62,63). The functionality of several transporters were shown in native Caco-2 by measuring adequate substrates in bidirectional transport assay, for example: talinolol (64), cimetidine, vinblastine, colchicine, cyclosporine (65), digoxin, (66) for P-gp, dactinomycin, daunorubicin, dipirydamole, domperidone (65) for MRP2, adefovir, (67) for MRP4, daunorubicin, ciprofloxacin, furosemide, sulfasalazine (65,68) for BCRP, estrone-3-sulfate, (69), levofloxacin, (70), imatinib, (71) for OATP1A2 and estrone-3-sulfate (72,73,74) for OATP2B1.

A number of research labs have established a correlation between the permeability across Caco-2 monolayers and the human dose fraction absorbed for different sets of compounds (for reviews, see (75,76,77)).

The Caco-2 transport assay enables the measurement of permeability of both the absorptive (apical-to-basolateral) and secretive (basolateral-to-apical) directions. The apical compartment models the intestinal lumen, and the basal compartment models the blood stream. As an output, apparent permeability (Papp) is calculated and efflux ratio can be characterized by the ratio of $Papp_{\text{basolateral to apical}}$ vs. $Papp_{\text{apical to basolateral}}$. A ratio greater than 2.0 is generally accepted as an indicator of efflux (78). Preincubation of the cells with verapamil or quinidine is frequently used to confirm P-gp activity.

DOI: 10.14753/SE.2013.1815

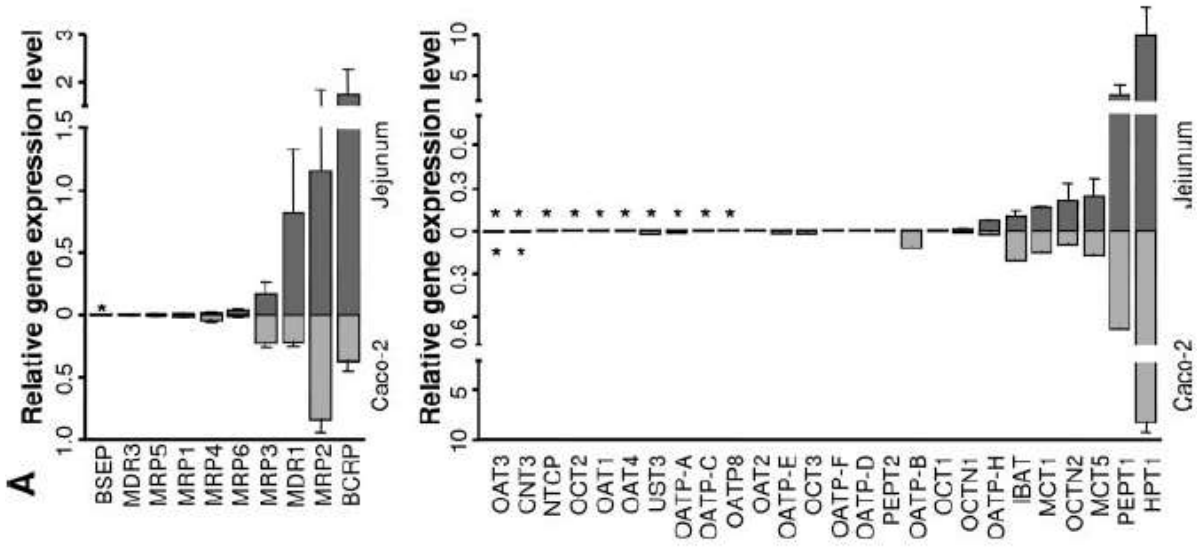

Fig. 4. Relative expression levels of ABC transporters (left panel) and SLC (right panel) transporters in human tissues isolated from jejunum mucosa. Each corresponding gene expression level in the Caco-2 cell line is shown in the opposing direction on the graph (light gray bars) for visualization of homologies and discrepancies in transporter expression profiles. The bars represent the mean relative expression levels; error bars indicate the standard deviation. *, absence of gene expression (30).

The Caco-2 cell model is widely accepted for permeability assessment, although it suffers from shortcomings such as long term cultivation of cells and the under-expression of active influx and efflux transporters and metabolic enzymes such as CYP3A4 (79,80,81,82,83). The permeability of hPEPT1 substrates such as cephalexin and amoxicillin are reported to be underestimated in Caco-2 (84). There is also a variable and low expression of P-gp in Caco-2 cultures, which seems to limit its use for screening P-gp substrates or studying P-gp related interactions (85,86). A number of laboratories have attempted to overcome some of the shortcomings of Caco-2. Improvement some functions of Caco-2 was our aim too, this is discussed later.

Other cell culture models of drug penetration

The HT-29 is a human intestinal colon cancer cell line that only differentiates after modifications of culture media, *e.g.* replacing of various components leads to clone selection and differentiation. The presence of galactose instead of glucose causes the formation of polarized cells. Clones differentiate into mucus-secreting goblet cells that can be used for studying the effect of mucin on intestinal absorption (87,88).

The T84 cell line, like Caco-2, differentiates spontaneously in culture after reaching confluency. However, the cells express fewer biochemical and morphological markers of differentiation (89). This cell line also expresses P-glycoprotein. It has been demonstrated that it is a good model for studying the induction of efflux transporters (90).

Madin-Darby canine kidney (MDCK) cells differentiate spontaneously into columnar epithelial cells and form tight junctions when cultured on semi-permeable membranes. A major advantage of MDCK cells over Caco-2 is the shorter cultivation period (3 days vs. 3 weeks) (91). Permeability data obtained for a large set of compounds (n=55) in MDCK model correlated well with human absorption and also with Caco-2 penetrability (92). MDCK cells derived from dog kidney cells may express transporters that are grossly different from those in the human intestine, which limits its usefulness for the prediction of human intestinal absorption. MDCK cells transfected with human MDR1 is a well accepted surrogate model of blood-brain barrier permeability (93).

2/4/A1 is a foetal rat intestinal epithelial cell line conditionally immortalized with a temperature-sensitive mutant of SV40 (94). 2/4/A1 is only useful for passively transported compounds (42). The transport rate of typical hydrophilic, poorly permeable paracellular compounds (*e.g.* mannitol and creatinine) in 2/4/A1 monolayers is comparable to that in the human jejunum, and much faster than in the Caco-2 cell model.

1.2.3.4. Excised tissues (ex vivo models)

The isolated tissues have the advantage of working with intact organs with physiological cell-cell contacts and normal intracellular matrices. In these models, the effect of variable tissue properties such as the distribution of transporters in the different segments of the GI may be examined (95).

In vivo, compounds passing the enterocyte are distributed to the systemic blood circulation by the blood and lymph vessels of the adjacent lamina propria. The underlying muscle layer does not represent a barrier to the absorptive process. The musculature can therefore be stripped off the tissues, consequently the tissue can be

oxygenated more efficiently. If the tissues are sufficiently supported with oxygen, they can be used for several hours. However, as the tissue is separated from its *in vivo* blood circulation, its viability is hampered and may lead to incorrect and non-reproducible permeability data (96), which is the main disadvantage of these *ex vivo* models.

Isolated-perfused intestinal segments

The entire small intestine, or alternatively, just a segment of it, is cannulated at both ends. After removal, the intestine or intestinal segment is placed in a perfusion apparatus and circulated luminally with an oxygenated buffer containing the test compound (97). In a more elaborate version of this method, the intestine is perfused both luminally and vascularly, so the superior mesenteric artery and the portal vein are cannulated and perfused (98,99). Wei *et al.* recently adapted this technique for human intestinal segments (100). The drug disappearance is calculated and an equal level of drug absorption is assumed, which is only valid when apical uptake is a rate-limiting step in drug absorption. If drug metabolism or accumulation occurs in the mucosa, then this approach leads to an overestimation of drug absorption (101). Using luminally and vascularly perfused method, both drug appearance in the vascular perfusate and its disappearance from the lumen can be followed.

The technique is valuable in the elucidation of transport mechanisms and may also be useful in evaluating the absorption of poor solubility drugs that require formulation (101).

Everted gut sacs

The small intestine of rodents (mostly rats) is removed, flushed and placed into an oxygenated special tissue culture medium. The intestine is everted, divided into sacs, and then laced up at both ends. In one end of the sac, a blunt needle syringe is inserted to inject the required volume into the sac lumen. The sac is placed in a tank of oxygenated buffer with the test compound (102). The drug content is analyzed in the solution of the serosal side and in the digested tissue/sacs. The transport of drugs, nutrients, liposomes, proteins and macromolecules can be studied with this method (103), and kinetic parameters can be determined with high reliability and

reproducibility. Examination of the paracellular transport of hydrophilic molecules makes possible to study the effect and toxicity of potent enhancers (104).

Drug absorption can be measured at different parts of the intestine, and the region, where drug absorption is maximal, may be identified. (105). It has been demonstrated that this method is suitable to study the effect of P-gp on xenobiotic transport by co-administered P-gp inhibitors (106,107), the role of influx transporters like PepT1, LAT2 (105,108), intestinal drug metabolism (109), hydrolysis of prodrugs (110,111), food effect (112) and the effects of excipients and different formulations on absorption (113,78).

Even using well-oxygenated buffers, the destruction of the intestinal mucosa is rapid. Apart from this issue, it is an inexpensive, relatively simple technique that is useful in examining site specific intestinal absorption. Paracellularly-transported compounds had similar permeability values to those obtained with human perfusion studies.

Ussing chambers

Ussing and Zerahn (114) first introduced Ussing chambers to study the active transport of sodium in isolated frog skin. Since then, the method has been used to study ion transport, drug absorption and permeability across the intestinal sheets of rats, rabbits, hamsters and mice (115,116). Using human biopsies of gastric, jejunal and colon mucosa barriers, the functions of the human GI tract can also be studied (117,118,119). Ussing chambers have also been used to study the intestinal metabolism of xenobiotics (120,121).

The technique is applied to opened, isolated intestinal sections mounted between two halves of a diffusion chamber. The intestinal section, as a flat sheet, separates the buffers from the drug containing buffers so that the transport of molecules across the tissue and between the chambers can be measured.

Both mucosal-to-serosal (m-s) and serosal-to-mucosal (s-m) directional fluxes can be studied, enabling the differentiation of passively and actively absorbed drugs (122). Different segments of the GI can be used, enabling the evaluation of site-specific absorption. Even the electro-physiological properties of the intestinal membrane during drug absorption can be monitored (123). Determination of species differences with

respect to intestinal characteristics may support the selection of suitable animal models for drug bioavailability studies (124,125). The short viability of the tissues in simple media due to the lack of blood flow and the sensitivity of the mounted sheets in the diffusion cells to mechanical damage may limit the generation of reliable data.

1.2.3.5. In situ models

In situ experiments involve perfusion of the drug solution through isolated cannulated intestinal segments. The perfused organ stays connected with the systemic blood circulation of the animal (126). Drug permeability, absorption kinetics, intestinal transport and metabolism, regional absorption and drug secretion into the intestinal lumen after *i.v.* administration are frequently studied in *in situ* models (127,128,129).

Using *in situ* models, drug absorption is generally estimated on the basis of drug disappearance from the intestinal lumen, but the rate of decrease in the drug concentration in the perfusate is not always equal to the rate of absorption into the portal vein. Sampling from mesenteric vessels or the portal vein can give a better estimation of drug absorption (130). Perfused flow rate and anaesthesia can influence the rate of drug absorption (89,131,132). Non- or low-absorbable volume markers such as PEG 4000, mannitol or Lucifer Yellow should be used to take into consideration the change in the luminal drug solution due to absorption or secretion of water. This method requires a large number of animals to obtain statistically significant absorption data and relatively high amounts of test compounds (> 10 mg).

A particular advantage of this method is that by bypassing the stomach acidic compounds are not likely to be precipitated, and the process is not complicated with biliary excretion and entero-hepatic circulation as is the case in *in vivo* methods. The presence of an intact blood supply and intact innervation mimics *in vivo* conditions well, and the model provides useful kinetic data.

1.2.3.6. In vivo animal models

Animal models are commonly used to predict the extent of the absorption of drug candidates. In practical terms, oral bioavailability is determined through this

method. However, drug bioavailability is influenced by far more factors than intestinal absorption alone. Sampling from the portal vein may rule out the metabolism in the liver, and intra duodenal administration of dissolved compounds makes possible to eliminate the role of dissolution, gastric acidity and emptying (124).

In vivo models integrate all of the biological factors that may affect drug absorption, such as the mucus layer, the dynamic components of the mesenteric blood circulation and all of the other factors that can influence drug dissolution. However, there are numerous species differences that influence absorbed drug levels. The gastric volume available for drug dissolution and gastric pH differ between species. Rodents have a less acidic pH than humans (133). There are also significant species differences in the activity, type and distribution of metabolic enzymes and also in the expression of transporters in the different species. GI volume, motility and transit time also show species specificity. Dogs are known to overpredict the human bioavailability of hydrophilic drugs. Rats seem to be better predictors of the bioavailability of compounds with paracellular and carrier-mediated processes (133,134,135,125). Generally, for low solubility, dissolution-limited, metabolism-subjected drugs, the bioavailability may not reflect absorption alone, and may contain numerous species-related factors.

1.2.3.7. Conclusions to models of absorption

Predictive, cost-effective, high-throughput absorption models are necessary tools for drug research (**Table 2**). The choice of method depends largely on the questions to be answered and the stage of intended application. At more advanced levels of drug research, the questions are more complex. In the design phase, *in silico* approaches using relatively simple rules can orient chemistry thinking; later, when drug substances are available, fast screens such as PAMPA followed by the relevant cell-based assay can reveal drug candidates with highly limiting passive and/or active penetrability and metabolic liabilities.

Table 2. Summary of absorption models.

Model	Origin	Throughput	Advantages	Disadvantages
In silico models	Virtual	High	No synthesized drug is needed	Only predictive for passive transcellular transport
IAM chromatography	Artificial	High	Very low amount of drug needed Simple, easy technique	Models the drug-membrane interaction and not permeability Only predictive for passive transcellular transport
PAMPA	Artificial	High	Relatively low amount of drug needed Excellent reproducibility, ease of automation Enables the study of pH effect and role of unstirred water layer	Only predictive for passive transcellular transport High membrane retention
Cell based model (Caco-2)	Human	Moderate	Relatively low amount of drug needed Widespread use, amount of data and practice Enables the study of active transport mechanisms with bidirectional assay and with inhibitors and drug-drug interactions	Interlaboratory variability (also in expression of P-gp) Low expression of CYP3A Long term cultivation Underestimation of paracellularly diffusible compounds and uptake substrates
Ussing chambers	Animal/ human	Low	Relatively low amount of drug needed Monitoring of electro-physiological properties during the experiment Enables the study of species differences, site-specific absorption, intestinal metabolism, active transport mechanisms with bidirectional measurement and with inhibitors, effect of excipients and drug-drug interactions	Short viability Sensitivity of the mounted sheets in the diffusion cells to mechanical damage
Everted gut sacs	Animal	Low/ moderate	Relatively simple, reproducible method Enables the study of site-specific absorption, intestinal metabolism, active transport mechanisms with inhibitors, effect of excipients, drug-drug interactions and food effect	Species specific properties Relatively high amount of drug needed Short viability
Isolated-perfused intestinal segments	Animal/ human	Low	Enables the study of species differences, intestinal metabolism, active transport mechanisms with inhibitors, effect of excipients, drug-drug interactions and food effect	Relatively high amount of drug needed Analytical difficulties if blood sample is taken Possibility of incorrect data if rate of drug disappearance is measured Short viability
In situ model	Animal	Low	Intact blood and nerve supply Enables the study of site-specific absorption, intestinal metabolism, active transport mechanisms with the secretion of drug or with inhibitors, effect of excipients, drug-drug interactions and food effect	Species specific properties Relatively high amount of drug needed Analytical difficulties if blood sample is taken Possibility of incorrect data if rate of drug disappearance is measured Effect of anaesthesia
In vivo model	Animal	Low	Integrate all biological factors affecting absorption Enables the study of active transport mechanisms with inhibitors, effect of excipients, complex formulations, drug-drug interactions and food effect	Species specific properties Bioavailability measurement, not absorption Analytical difficulties Relatively high amount of drug needed

DOI: 10.14753/SE.2013.1815

DOI: 10.14753/SE.2013.1815

Drugs that survive the first sets of *in vitro* ADME test batteries may enter the advanced phase of *in vivo* pharmacological testing. Prior to this, animal PK studies that answer specific questions about dosage size, formulation and food effects may support successful pharmacodynamic testing. Species specific properties may limit the use of *ex vivo*, *in situ* and *in vivo* animal models.

Among the models, cell-based assays provide information not only for passive transcellular permeation of the drug but also for paracellular and transporter mediated processes with medium throughput. For prediction of human absorption Caco-2 culture based models are especially good in the early phase of drug discovery. Experiments on this culture form the base of this work.

No single model can provide sufficient data as a stand-alone method. However, cumulated information from the various *in vitro* and *in vivo* approaches can direct scientists in predicting human drug presence and in planning appropriate clinical studies in order to reach sufficient effective drug levels. Multilevel strategies drawing on the differing strengths of models with different levels of complexity appear to be the best approach to generating reliable human predictions.

1.2.4. Improving the properties of Caco-2 cultures

As mentioned before, several labs have established a correlation between permeability measured across Caco-2 monolayers and human dose fraction absorbed for different sets of passively penetrating compounds (for review, see (75,76)); although the permeability data do display significant interlaboratory differences (136,137,91).

A number of laboratories have attempted to overcome some of the shortcomings of Caco-2. Reducing the three-week differentiation period to three days mostly resulted in less differentiated cultures (138) and lower P-gp levels (139). Application of butyrate for differentiation in short-term cultures (140,141) induced not only differentiation but apoptosis as well (142). The traditional 3-week culture is still preferable (75,58).

The Caco-2 model was found to be the most predictive (r^2=0.9), even for passive brain penetration, in a comparative study using different cell types (e.g. MDCK-MDR1, BCE etc.) (143). However, Caco-2 was unable to identify P-gp substrates as correctly as the frequently used surrogate BBB model MDCK-MDR1. In our hands Caco-2

frequently failed to recognise P-gp substrates which has been described by others as well (144,145,77). Generally, the variable and low expression level of P-gp in Caco-2 cultures seems to be the limiting factor for its use in screening P-gp substrates or studying P-gp related interactions (79,85,86).

Improved P-gp expression and functionality of Caco-2 cells was set as an objective by several laboratories for different purposes. Horie and co-workers isolated subclones of Caco-2 cells expressing high levels of MDR1 and recommended their use for profiling drugs for P-gp activity and structure-transport relationships (146). The transfection of Caco-2 with hPXR, mCAR nuclear receptor genes regulating the expression of both metabolic enzymes and efflux transporters (MDR1 and MRP2) (147,80), or transfection with the hMDR1 gene, resulted in elevated expression of P-gp and improved efflux functionality. Others have also attempted to stimulate P-gp expression with agents such as vinblastine or vincristine. P-gp expression and functionality for a limited number of test compounds were studied in vinblastine-treated Caco-2 cells, and recommended for the identification of P-gp substrates using short or long term growth protocols (148,145,149,150). For the time being transfected or vinblastine treated Caco-2 cells have not been validated for use in drug penetration screening. At the same time vinblastine- or vincristine-treated cultures are routinely applied, albeit only at early passages in Calcein AM (151,152) and in radioligand-binding assay (153,154). Therefore, we set out to characterize the vinblastine-treated Caco-2 culture for using as a drug penetration model and for the prediction of human absorption and brain penetration (see later).

1.3. Brain penetration and models of blood-brain barrier permeability

1.3.1. Barriers of the CNS

Three barrier layers limit and regulate molecular exchange at the interfaces between the blood and the neural tissue or its fluid spaces. The first is the blood-brain barrier (BBB) formed by the cerebrovascular endothelial cells between blood and brain interstitial fluid (ISF). The second interface is formed by the epithelial cells of the choroid plexus facing the ventricular cerebrospinal fluid (CSF), which constitute the

DOI: 10.14753/SE.2013.1815

blood-cerebrospinal fluid barrier (BCSFB). The third barrier is provided by the avascular arachnoid epithelium between blood and subarachnoid CSF (155), and completely enclose the CNS (156,157). Individual neurons are rarely located more than 8–20 μm from a brain capillary (158); however, they may be millimetres or centimetres far from a CSF compartment. Furthermore, the surface area of the BBB microvessels constitutes the largest interface for blood–brain exchange. This surface area, depending on the anatomical region, is between 150 and 200 cm^2 /g tissue giving a total area for exchange in the brain of between 12 and 18 m^2 for the average human adult. Because of the large surface area of the BBB and the short diffusion distance between neurons and capillaries, the BBB exerts the greatest control over the immediate microenvironment of brain cells from the various CNS barriers, so the endothelium has the predominant role in regulating the brain microenvironment (157).

1.3.2. The neurovascular unit

The anatomical substrate of the BBB is the cerebral microvascular endothelium together with astrocytes, pericytes and neurons, which are organized into well-structured neurovascular units (**Fig. 5**) (156).

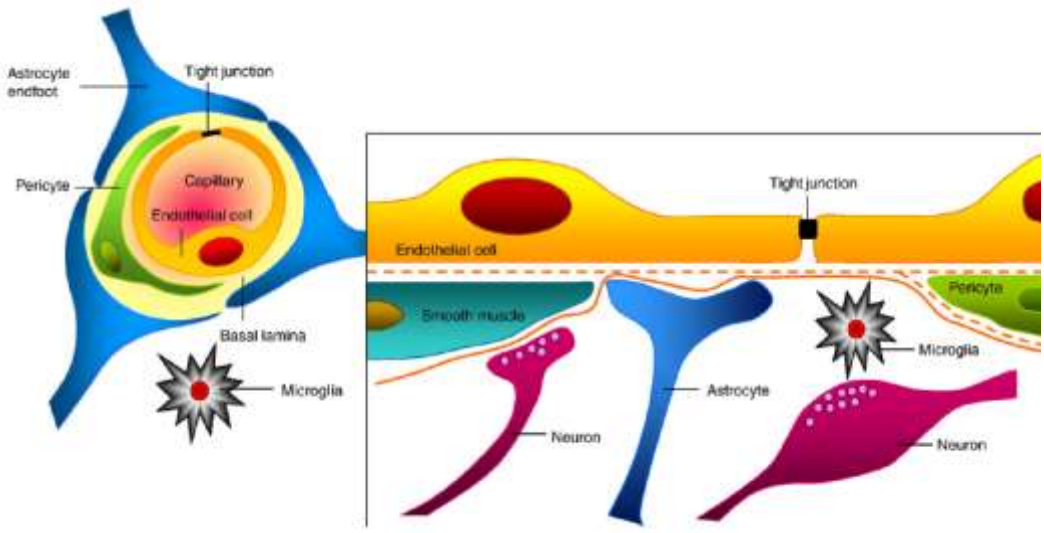

Fig. 5. Cellular constituents of the blood-brain barrier. The barrier is formed by capillary endothelial cells, surrounded by basal lamina and astrocytic perivascular endfeet (157).

The cerebral endothelial cells (CECs) form a continuous sheet covering the inner surface of the capillaries. Brain endothelial cells have both endothelial-like features

(i.e., expression of von Willebrand factor, uptake of acetylated LDL, high activity of alkaline phosphatase and gamma-glutamyl transpeptidase) and epithelial-like features (i.e., continuous line of tight junctions, low level of pinocytosis, high TEER) (159). The nearest neighbours of endothelial cells are brain pericytes which are sharing a common basal membrane consisting of collagen IV, fibronectin, laminin and proteoglycans. Pericytes have a fundamental role in stabilizing the brain capillary structure *in vivo* (160,161), and they participate in the development, maintenance and regulation of the BBB (162). Endfeet of astrocytes cover a significant part of the endothelial surface (163). Astrocytes are also capable to induce BBB properties in endothelial cells (156). Cerebral capillaries are innervated by different neurons (164), which can regulate important aspects of BBB function and induce the expression of BBB-related enzymes in cultured cerebral endothelial cells (165). Microglial cells are also found in the perivascular space, playing an immunological role; however, their contribution to the BBB properties is not well characterized (159).

1.3.3. The barrier function

The barrier function of BBB results from a range of passive and active features of the brain endothelium. Owning to the anatomy of the BBB, it acts as a *'physical barrier'*, because the complex tight junctions between adjacent endothelial cells reduce most molecular motion paracellularly through the junctions, in contrast to most endothelia (164,166). An additional line of defence is the highly negatively charged glycocalyx at the luminal surface of brain endothelial cells. Absence of fenestrations and low number of pinocytotic vesicles further decrease molecular movement through the cells (167).

The presence of specific transport systems (solute carriers, efflux pumps, adsorptive and receptor-mediated transendothelial transport) (167) on the luminal and abluminal membranes of endothelial cells regulates the transcellular traffic of molecules, which provides a selective *'transport barrier'* (168). These transporters and carriers provide the CNS with nutrients, vitamins, minerals and metabolic precursors. The efflux transporters participate in the protection of the brain from potentially toxic

molecules and xenobiotics, and in the regulation of the level of neurotransmitters and metabolites in the brain (167).

Finally, a combination of intracellular and extracellular enzymes provides a *'metabolic barrier'*, which modify endogenous and exogenous molecules that could bypass the barrier and affect neuronal functions (169,162). Phase I enzymes (aldehyde and alcohol dehydrogenases, alkaline phosphatase, aminotransferases, aromatic L-amino decarboxylases, butyrylcholinesterase, catechol-O-methyl transferase, epoxy hydrolases, γ-glutamyl transpeptidase, ketone and alcohol oxidoreductases, monoamine oxidases A and B and transaminases), as well as phase II enzymes (glutathione S-transferase-π (GSTπ), GSTα, Sult1a1, Sult1a2, and UDP-glucuronosyl-transferase Ugt1a1) are expressed at the BBB (170,167,171). The metabolic enzymes, together with the efflux pumps, provide an important line of defence for the CNS from neurotoxic substances circulating in the blood, like endogenous metabolites or proteins, or xenobiotics ingested in the diet or otherwise acquired from the environment (167).

The barrier function is not fixed, but can be modulated and regulated, both in physiology and in pathology. With these features the BBB provide a stable fluid microenvironment that is critical for complex neural function, and protect the CNS from chemical insult and damage (156). The BBB restricts ionic and fluid movements between the blood and the brain, and protects the brain from fluctuations in ionic composition, which would disturb synaptic and axonal signalling (172). The barrier helps to keep separate the pools of neurotransmitters and neuroactive agents that act centrally and peripherally (157,173). The BBB prevents many macromolecules from entering the brain. The protein content of CSF is much lower than that of plasma, and plasma proteins such as albumin, pro-thrombin and plasminogen are damaging to nervous tissue (174,175).

1.3.4. Elements of the barrier

1.3.4.1. Transport pathways

As shown on **Fig. 6**, six transport pathways can be distinguished at the level of the BBB (167).

1. Passive transcellular pathway for lipophilic molecules

Small gaseous molecules such as O_2 and CO_2 can diffuse freely through the lipid membranes, and this is also a route of entry for small lipophilic molecules (MW less than 400-500), including drugs such as barbiturates, caffeine, nicotine and ethanol (156,176,177).

2. Passive paracellular pathway for hydrophilic molecules

In contrast to peripheral microvessels, the restricted paracellular pathway by the tight interendothelial junctions of cerebral microvessels prevents hydrophilic molecules from entering the CNS freely. Therefore, most proteins, peptides and polysaccharides cross the BBB poorly (177).

3. Carrier-mediated transport

The BBB express saturable, bi-directional transport systems for nutrients, vitamins and minerals at the BBB (157,177). About 40 members of the solute carrier (SLC) transporter family were identified in brain microvessels by serial analysis of gene expression (178). Drugs which resemble nutrients or vitamins may be substrates of these transporters therefore can reach high concentrations in the CNS. The most important BBB uptake transport proteins involved in drug transport are the organic anion transporting polypeptide, OATP1A2 (methotrexate, statins), OATP2B1 (fexofenadin) and the large neutral amino acid transporter (LAT) (L-DOPA, gabapentin) (179,17).

4. Active efflux transport

The ABC transporters in the BBB function as active efflux pumps consuming ATP and transporting a diverse range of potentially neurotoxic endogenous or xenobiotic molecules out of the brain capillary endothelium and the CNS (180). The most important ABC transporters identified in brain capillaries are P-glycoprotein (ABCB1, substrates: digoxin, loperamide), multidrug resistance proteins MRP-1, -4, -5 and -6 (ABCC1-6, substrates: topotecan, furosemide), and breast cancer resistance

protein (BCRP/ABCG2, substrate: methotrexate) (157,178,181,17,182,183). Many drugs that are substrates of these ABC efflux transporters have significantly reduced brain penetration (5), resulted in inefficient treatment of CNS diseases (brain tumours, HIV and epilepsy), or avoidance of side effects in the brain (184).

5. Receptor-mediated transcytosis

Receptor-mediated transport which can be bidirectional is responsible for the brain penetration and clearance of peptides and proteins (185) like transferrin, melanotransferrin, insulin, leptin, low density lipoprotein and many other important regulatory proteins (177,162).

6. Adsorptive-mediated transcytosis

Adsorptive-mediated transcytosis is highly downregulated at the BBB. It transfers albumin through peripheral endothelial cells, but unregulated leakage of serum proteins into the CNS would be toxic to neurons (176,186).

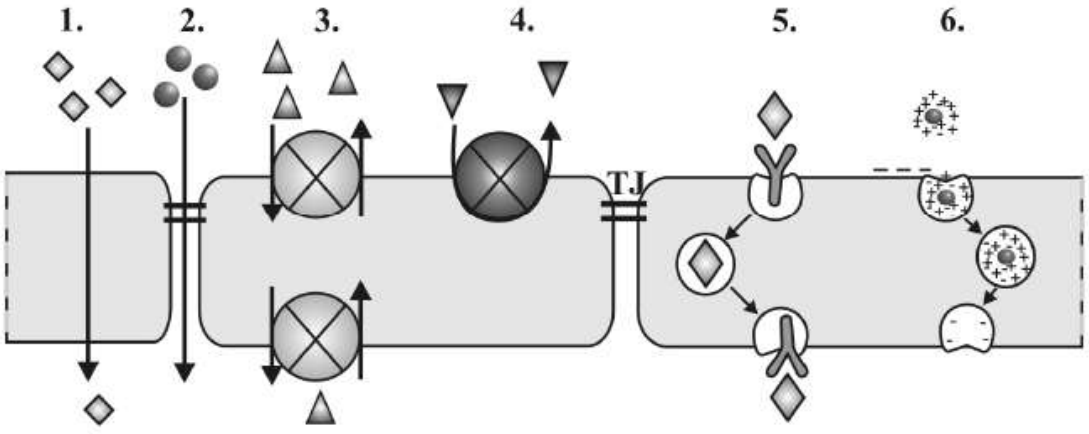

Fig. 6. Transport pathways at the BBB. 1, passive transcellular diffusion; 2, paracellular diffusion; 3, carriers; 4, active efflux transport; 5, receptor-mediated transport; 6, adsorptive-mediated transcytosis (167).

1.3.4.2. Intercellular junctions

The junctional complexes between endothelial cells, that include adherens junctions (AJs) and tight junctions (TJs, zonulae occludentes), play a crucial role in determining paracellular permeability (159).

Tight junctions

Presence of a continuous line of TJs at the cell-cell borders of endothelial cells is one of the most important elements of the BBB phenotype. The TJs are not only responsible for the restriction of the paracellular pathway (‘gate function’), but also for segregating the apical and basal domains of the cell membrane (‘fence function’) which enables the polarized (apical–basal) properties of the endothelial cells similar to epithelial cells (187). The molecular components of the TJs can be separated into transmembrane and cytoplasmic plaque proteins. Transmembrane proteins of endothelial TJs include occludin (188), junctional adhesion molecules (189) and members of the claudin family (190). Plaque proteins link transmembrane proteins to the actin cytoskeleton. Occludin and claudins are linked to a number of cytoplasmic scaffolding and regulatory proteins ZO-1, ZO-2, ZO-3 and cingulin (157).

Adherens junctions

Cell–cell interaction in the junctional zone is stabilized by AJs (156). AJs mediate adhesion of endothelial cells to each other and – in part – regulation of paracellular permeability. The transmembrane proteins of the adherens junctions are the cadherins, in the case of vascular endothelial cells mainly VE-cadherin (191), which is linked through the catenins (alpha, beta and gamma) to the cytoskeleton. In brain endothelial cells, tight and adherens junctions are intermingled (192), and it has been shown that ZO-1 and ZO-2 can interact with alpha-catenin (193).

1.3.5. *In vitro* BBB models

The insufficient presence of drugs at their brain targets due to the barrier function of brain capillary endothelial cells is a common cause of failure of drugs that

target the CNS; therefore, prediction of BBB permeability is important in drug development. In drug discovery for the prediction of brain penetration several types of models are used. Such models are *in silico* prediction, PAMPA, cell culture-based approaches and also animal models (BUI, *in situ* perfusion, etc). Due to the higher complexity of information derived on both passive penetration and active transport processes, cell cultures are favoured tools for BBB drug penetration modelling (194,195). Basically, there are two types of models. Firstly, the "real BBB models" that are based on cultures of brain capillary endothelial cells supplemented and/or co-cultured with astrocytes/pericytes. Secondly, the well accepted surrogate BBB models that use epithelial-like cells like Madin-Darby Canine Kidney (MDCK) cells transfected with human MDR1 gene and the possibly the recently challenged colon carcinoma cell line (Caco-2) (196,197,194).

In vitro models always involve compromises. The loss of complexity is made up for by the higher throughput, lower costs and the simplicity that makes it easier to analyze individual phenomena. Understandably, efforts are made to ensure that *in vitro* models be as similar as possible to *in vivo* conditions, since the closer a model mirrors the *in vivo* situation, the more accurate the predictions it can yield. However, sacrificing some complexity while retaining the critical *in vivo* features may be worthwhile when weighed against the advantages in terms of simplicity, higher capacity and reproducibility (198).

1.3.5.1. Critical features of in vitro cell-based BBB penetration models

For the predictive modelling of CNS permeation, it is critical that drug transport in the cellular assay is free of leakiness and that the model presents BBB features of passive and active transport (198).

In vivo the gap between endothelial cells is tight enough to prevent compounds passing in a paracellular manner through the tight junctions between the overlapping membranes of interconnected cells. Therefore, the *in vitro* BBB model must display restrictive paracellular pathways. The functional tightness of the junctions can be measured in terms of the TEER and by junctional permeability tracers. High TEER and low penetrability of hydrophilic markers may guarantee controlled paracellular

pathways in the models. Although *in vivo* the TEER of brain endothelium is greater than 1000 Ωcm^2 (199), a consensus has been reached that reasonable data can be obtained in *in vitro* BBB models if the system shows a sufficiently high TEER, at least 150 to 200 Ωcm^2 (200). In industrial drug permeability screening, use of permeability markers of a size similar to small drug molecules (100 to 400 Da) to estimate junctional permeability is favoured over TEER measurement. Such markers include fluorescein, Lucifer Yellow or sucrose and mannitol (194). *In vivo* the permeability of the disaccharide sucrose (MW = 342, molecular radius = 4.4 Å) is very low – between 0.025 and 0.1 x 10^{-6} cm/s (197,201). Ideally, tracer permeability *in vitro* should not exceed the *in vivo* value of BBB permeability estimated. Until now those extremely low values could not be reproduced in cell cultures. As a reasonable *in vitro* cut-off value of Pe approximately 1 x 10^{-6} cm/s might be acceptable.

Selective transcellular permeability is also a critical characteristic of BBB models, as the passive transcellular pathway is a major route for drugs crossing membrane barriers. Less well understood are the effects of lipid membranes and cellular architecture of cerebral versus peripheral cells on permeability rankings of various BBB models (202).

In the emerging new concept, P-gp efflux functionality is a critical feature of CNS permeation modelling. Based on our current knowledge, P-gp is the main efflux pump, which drastically affects both the penetration rate and the extent of brain distribution unless counteracting mechanisms, such as high passive penetrability and/or adequate plasma-protein binding and brain-tissue binding, compensate for its action. The accurate prediction of these *in vivo* characteristics is best performed with *in vitro* BBB models that comprise efflux functionality as well as the passive permeability. In *in vitro* models, the P-gp functionality (verified by specific inhibitors) is described as the fold difference of basolateral-to-apical and apical-to-basolateral drug transport. It is understandable that an interlaboratory comparison of efflux substrates is often contradictory, since the P-gp expression level and pump functionality of the applied BBB models varies greatly (198). It is suggested, that as for P-gp substrate properties and their impact on permeability, species differences are more critical than the tissue origin of the cell model to be used (203).

1.3.5.2. Primary brain endothelial cell-based BBB models

Understandably, brain capillary endothelial cell-based models are believed to be the best *in vitro* BBB models as they show the highest resemblance to *in vivo* BBB based on various parameters including lipid composition of cell membranes, complexity of tight junctions and expression of BBB enzymes. Brain capillary endothelial cells are genetically programmed to possess most BBB features. When cultured correctly, cerebral endothelial cells show the basic features of BBB endothelium including complete tight junctions and expression of BBB-specific transporters and enzymes.

Under *in vivo* conditions, the development, maintenance and function of the capillary endothelial cells are under the complex influence of the surrounding astrocytes, pericytes and even neuronal contacts. Many functions such as paracellular tightness (inulin permeability, TEER), γ-glutamyl transpeptidase activity (204), P-gp and MRP functionality (205) are downregulated *in vitro* in cultured capillary endothelial cells. Co-culturing of endothelial cells with astrocytes/pericytes, adding astrocyte conditioned media or media supplements, such as cyclic adenosine monophospate and glucocorticoid hormone can greatly improve a number of diminished properties like paracellular tightness (inulin sucrose, and sodium fluorescein permeability, TEER) (204,206), γ-glutamyl transpeptidase activity (204), P-gp, GLUT1 (207,208), LDL-receptor and transferrin receptor (156,204). However, the culture conditions used still do not let perfect reconstruction of *in vivo* endothelial features in culture.

Unfortunately, these models are not convenient for routine industrial use because they are labour intensive, monolayer integrity is sensitive for experimental conditions, and the models are very expensive. The characterization of these models is still uneven; while monolayer tightness is in high focus, the transporter functionality is not fully characterized even in the best models of BBB penetration in use. Data on the on the efflux functionality in brain capillary endothelial models are also scarce.

Cerebral endothelial cells were isolated from many species (200), but only a few BBB models are well-characterized for permeability and have sufficient tightness as measured in terms of TEER and/or paracellular tracer permeation. The preferred models of brain capillary endothelial cells display a sufficiently high TEER, of 300–500 Ω cm^2 and interestingly, a fairly broad range of Pe for paracellular tracers, from as low as 3.9 ×

10^{-6} to as high as 80×10^{-6} cm/s. Such models include the porcine brain microvessel endothelial-cell model reported by Zhang et al. (209), the 4D/24w bovine brain capillary endothelial-cell model of Culot et al. (210) and the rat brain capillary model established by triple co-culture with pericytes and astrocytes by Nakagawa et al. (211).

A great advantage of the rodent models is that they can be easily compared to *in vivo* results and measurements, and it is simple to prepare syngeneic cultures. Furthermore, in the case of mouse models, the use of transgenic animals is possible. However, due to their small size, relatively low amounts of endothelial cells can be obtained from them (195,159). Many syngenic model were prepared with co-culture of astrocytes, and puromycin treatment were also used (212,195). Puromycin, a P-gp ligand drug, is applied in a method of purification in which the P-gp expressing capillary endothelial cells can be selected from contaminating cells in the culture (brain pericytes, fibroblasts, smooth muscle or leptomeningeal cells). With the addition of brain pericytes, triple co-culture models were developed by Nakagawa et al. (206). The model, which closely mimickes the anatomical position of the cells at the BBB *in vivo*, displayed better barrier properties, than models without pericytes. Drug permeability assays were also performed with this model, using a set of 19 compounds with known *in vivo* BBB permeability. Advantageously, it can be frozen, transported and stored for 6 months. The ready-to-use nature of the Nakagawa system may lead to its widespread use for rapid BBB screens.

Pig or bovine endothelial models have the advantage that large quantity of cells is easy to obtain. The bovine model is widely used in both basic and applied research. Cecchelli et al. developed a bovine BBB model from co-culture of cloned and passaged bovine capillary endothelial cells and rat glia, and used for several permeability studies (213,214). A new, 24-well format version of the model that uses a special inducing medium was introduced by Culot et al. (210). Some similarities between porcine and human vascular physiology make the porcine model suitable for drug screening (195). Zhang et al. developed a porcine brain microvessel endothelial cell (PBMEC) based model and recommended it to predict the *in vivo* BBB permeability of drugs (209).

There are only a few human models that are characterized for permeability properties and transporters. The use of human primary cells is restricted, the access to

human brain tissue is difficult. The first syngeneic BBB model using human cerebral endothelial cells and astroglia in co-culture showed a tight paracellular barrier (215).

Efflux functionality, especially for P-gp, seems to be an essential feature of the best *in vitro* BBB models. Hardly any data is available from capillary endothelial cells concerning P-gp functionality characterized by efflux ratio from bidirectional assay of P-gp substrate drugs. There is some data available with regard to the efflux ratio of the P-gp and MRP substrate dyes, or inhibition of its transport. In rat brain capillary endothelial cells, P-gp, BCRP and MRP functionality has been shown by the inhibition of daunorubicin uptake with specific inhibitors (216). Efflux ratio of 2.5 was shown for the P-gp substrate rhodamine 123, and protein of P-gp and MRP was detected by Western blot in the triple co-culture of rat brain capillary endothelial cells (211). P-gp functionality was shown by the transport kinetics of 2',7'-bis(2-carboxyethyl)-5(6)-carboxyfluorescein acetoxymethyl ester (BCECF-AM) and MRP functionality by BCECF in BBMEC (205). Uptake of rhodamine 123 was inhibited by verapamil and S9788 in BBCEC, and P-gp, MRP1, MRP4, MRP5 mRNA were shown (210). Efflux ratio of 1.73 was shown for rhodamine 123, and mRNA of P-gp, BCRP, MRP1,MRP4 was detected in the culture of PBMEC (209). Despite the numerous experimental approaches, there is still a great need for models of BBB that could provide P-gp functionality with good predictivity to the *in vivo* situation.

1.3.5.3. Brain endothelial cell line-based BBB models

Since primary cultures are expensive, time consuming and technically difficult, the use of immortalized brain endothelial cell lines is widespread. Unfortunately, immortalized cell lines do not express all the critical features necessary for modelling BBB permeability, as they do not form sufficient barrier, despite the significant research invested in improving BBB differentiation using extracellular matrices, factors that induce cell differentiation and conditioned media. After all, brain endothelial cell lines are still useful in studying the physiology and pathology of the BBB.

Immortalized brain capillary endothelial cells like t-BBEC (bovine brain capillary endothelial), hCMEC/D3 and SV-HCEC (human), bEnd5 (mouse) or RBE4

(rat) are easier to maintain and handle than primary cultures (214,197,194). One of the best characterized cell lines, RBE4, was generated by transfection of rat brain endothelial cells with a plasmid containing the E1A adenovirus gene (217). Although RBE4 demonstrates several BBB-like properties, including expression of P-gp, these cells, unfortunately, show incomplete tight junctions and therefore form leaky monolayers. The first stable, well-characterized human brain endothelial cell line, hCMEC/D3, shows several endothelial and BBB characteristics, including chemokine receptors, TJ proteins and drug efflux mechanisms. D3 cell layers in mono-culture give a low value of TEER (40 Ωcm^2), and high permeability coefficients for sucrose, inulin, and FITC-dextran (218). When D3 cells were maintained in a dynamic system, the paracellular barrier properties were significantly improved and TEER exceeded 1000 Ωcm^2 (219,218).

1.3.5.4. Epithelial cell based surrogate BBB models

The tight paracellular barrier and efflux pumps are two major features of BBB, therefore, surrogate cell culture models possessing these two characteristics have been established and tested for their predictive value on brain penetrability of drug candidates (195).

The Madin-Darby canine kidney (MDCK) epithelial cell line is widely used in tight junction (TJ) research. This cell line and its subclone transfected with the human MDR1 gene, MDCK-MDR1, has been used in several permeability studies and it is now a well-accepted surrogate BBB model (220,143,221,93).

Native Caco-2 which is the preferred choice of the industry for the prediction of intestinal absorption (75,58,59) is also increasingly scrutinized in comparative studies for BBB permeability prediction (143,222,223). However, a serious disadvantage of Caco-2 is that the activity of P-gp in native culture is low and highly variable (79,85,86), as mentioned before.

In spite of the fact that these cells originate from the periphery with appropriate organ-specific sets of membrane proteins (224,30,225), and they have a cell membrane lipid composition that differs from that of brain capillary endothelial cells (202), high *in*

vitro – in vivo BBB permeability correlations were demonstrated with epithelial cell based Caco-2 and MDCK-MDR1 models (143,222).

In summary, among the wide variety of models, only a few of the primary brain capillary endothelial-based models and surrogate models have sufficient tightness as measured in terms of TEER and/or paracellular tracer permeation. In comparison with endothelial BBB models, epithelial cell-based surrogate BBB models are more cost-effective and easier to handle. A drawback is that the cells originate from peripheral organs with specialized physiological functions; therefore they cover fewer *in vivo* BBB properties.

1.3.6. Modelling CNS permeation

In several studies permeability data derived from the *in vitro* model is correlated with *in vivo* brain penetration data. Brain distribution or *in vivo* permeability data often guides researchers in their choice of reference compounds to characterize BBB models. The limited availability of *in vivo* permeability data makes the otherwise essential validation process challenging.

1.3.6.1. Factors influencing brain penetration in vivo

In the understanding of CNS penetration, a new concept has emerged for rationalizing brain penetration. The central component of the new concept is the clear differentiation between 1.) the rate of BBB permeation, 2.) the extent of brain penetration (=distribution between brain and plasma) and 3.) the intra brain drug distribution (=distribution within the CNS) which all affect the success of drug therapy (226,227,228). Moreover, the *in vivo* pharmacokinetic parameters that correlate with efficacy (e.g., unbound concentration in the brain and distribution within the brain) were identified, as well as factors that affect those pharmacokinetic parameters (**Table 3**).

DOI: 10.14753/SE.2013.1815

Table 3. Factors that affect the rate and the extent of brain penetrability.

Rate of permeability across BBB is a function of:	**Extent of brain penetration is a function of:**
passive permeation	plasma protein binding
active transport processes	brain tissue binding
plasma protein binding	efflux pumps at BBB
cerebral blood flow	ISF bulk flow

Based on (228).

Active efflux transporters such as P-gp, may drastically modify both processes of the rate and the extent of drug penetration, which all affect the success of drug therapy (226,227). Therefore, models of brain penetration possessing predictive P-gp functionality are of great importance (198).

1.3.6.2. In vivo models of brain penetration

Cell-based BBB models can potentially predict at least two clearly decisive parameters of drug delivery to the brain: 1) The permeability surface area product (PS) which represents the rate at which drugs penetrate. 2) The extent of brain exposure to the drug relative to the concentration of total or unbound drug in blood.

PS, typically derived from the unidirectional uptake coefficient (K_{in}) using an *in situ* saline-based perfusion method, is a measure of the permeability of a compound across the brain capillary endothelium (194).

The most common method to study brain penetration *in vivo* is the determination of the total brain to plasma ratio (Kp) in rodents; however, these data do not provide reliable information on the concentration at the target site (228).

To circumvent this key limitation of measurement of total levels in brain, sampling of CSF (229) and/or brain microdialysis of ISF can be carried out (230). However, both methods have their drawbacks, in particular practicability (microdialysis) and reliability (CSF sampling) which weaken their applicability in routine drug discovery (196,203).

Alternatively, measurement of the total brain to total plasma ratio can be complemented by some additional methods. The free fraction (unbound fraction, fu) in the brain and plasma can be determined by equilibrium dialysis (231).

Using fu brain and fu plasma data, Kp can be transformed into the unbound Kp,uu (232). Kp,uu is a measure of the extent of the distribution equilibrium of a compound between the unbound fractions in brain and in plasma. If the value is close to unity, passive diffusion across the BBB can be assumed (228).

In vivo permeability coefficient measured by the tissue distribution model in mice (mouse brain uptake assay/MBUA) is also used in a few *in vitro – in vivo* correlations (143). In that approach the distribution of compounds to brain tissue is measured only five minutes after the injection of the compounds in mice. From the ratio of the concentration in the brain to plasma (Kp), in this case, the rate of brain penetration (apparent permeability coefficient) can be calculated, because of the short experimental time, and presuming that metabolism and back-flux are negligible at that time point.

1.3.6.3. In vitro - in vivo correlations using BBB models

In the *in vitro - in vivo* correlations permeability data generated on primary brain capillary endothelial cell-based models are more frequent than that of surrogate epithelial BBB models (210,211,209). Highly comparable *in vitro – in vivo* BBB permeability correlations were also achievable with epithelial cell-based Caco-2 and MDCK-MDR1 models (**Table 4**) (143,222).

There are only a few comparative studies between brain capillary endothelial cell based models and epithelial based surrogate models (**Table 4**) (143,222,223). One of these studies showed, that for passive brain penetration the Caco-2 model was the most predictive, followed by the primary BBEC, the MDCKwt and the MDCK–MDR1 models (143). Among the models, the MDCK-MDR1 model provided the best separation of passively and effluxed compounds. However the BBEC was not evaluated for P-gp functionality.

The BBB transporters may severely modify drug penetration to the brain (226,227). The under-representation of transporters in the models is reflected in the few

available studies where high *in vitro – in vivo* permeability correlations appear more frequently if transporter substrates, especially uptake substrates, are excluded (143,222,209). Correcting *in vivo* data with brain and plasma protein binding has been reported to improve the strength of correlations (228,221,233).

Table 4. *In vitro - in vivo* and *in vitro - in vitro* correlations using primary brain endothelial and surrogate epithelial BBB models.

Correlation between		All compounds (n)	Excluded from the correlation	R^2 value	Ref.
In vitro BBCEC model	*In vivo* PS	10		0.81	(210)
In vitro PBMEC model	*In vivo* PS	15	3	0.89	(209)
In vitro EPA model	*in vivo* Papp (mouse brain distribution model)	19		0.89	(211)
In vitro BBEC	*In vivo* Papp (MBUA)	22	12	0.74	(143)
In vitro Caco-2	*In vivo* Papp (MBUA)	22	12	0.86	(143)
In vitro MDCK-MDR1	*In vivo* Papp (MBUA)	22	12	0.64	(143)
In vitro BBMEC	*In vivo* unbound brain/blood (microdialysis)	9	2	0.98	(222)
In vitro Caco-2	*In vivo* unbound brain/blood (microdialysis)	9	2	0.83	(222)
In vitro MDCK-MDR1	*In vivo* unbound brain/blood (microdialysis)	9	2	0.72	(222)
In vitro Caco-2	*In vitro* BBMEC	11		0.86	(222)
In vitro MDCK-MDR1	*In vitro* BBMEC	11		0.83	(222)
In vitro Caco-2	*In vitro* MDCK-MDR1	11		0.96	(222)

BBCEC: bovine brain capillary endothelial cells, **PBMEC**: porcine brain microvessel endothelial cells, **BBEC**: bovine brain endothelial cells, **BBMEC**: bovine brain microvessel endothelial cells, **MBUA**: mouse brain uptake assay, **PS**: permeability surface area product.

For the time being no standard model has yet emerged for the prediction of BBB penetration; therefore, cost, time, labour and quality of the models are all contributing factors in deciding which model to use.

DOI: 10.14753/SE.2013.1815

2. Aims

The Caco-2 model, which is very often used for prediction of human absorption in drug discovery, suffers from several drawbacks like low and variable P-gp functionality. This makes the identification of P-gp substrates difficult. There are a few studies where the Caco-2 model was used for prediction of brain penetration, but correlation only occurred if transporter substrates were excluded.

Currently, industry-standard BBB drug penetration model is not available. Comparative studies of different BBB models are scarce, especially those that examine the transporter functionality.

Therefore, our aims were:

-To establish a culture with higher and steady P-gp functionality by the modification of Caco-2 cells.

-To examine the effect of sustained vinblastine treatment of Caco-2 cells on the expression and functionality of P-gp (VB-Caco-2).

-To characterize and validate VB-Caco-2 model for long term use for drug penetration screening, P-gp substrate and inhibitor identification in bidirectional transport assay, and in Calcein-AM assay.

-To elucidate the mechanism of vinblastine effect on P-gp level.

-To compare the primary brain capillary endothelial BBB model (EPA) and the epithelial cell-based (Caco-2, VB-Caco-2, MDCK-MDR1) models as possible surrogate BBB models, with special respect to the critical BBB features (presence of discriminative paracellular pathway, BBB-like selective transcellular penetration and expression and function of P-gp)

-To test these models for prediction of *in vivo* BBB penetration.

-To compare a large set of *in vitro* permeability data obtained in parallel with the well accepted surrogate BBB model MDCK-MDR1 and the high P-gp expressing VB-Caco-2 models of drug penetration.

DOI: 10.14753/SE.2013.1815

3. Materials and methods

3.1. Chemicals

Acetaminophen, fluorescein sodium and quinidine were from Fluka (Buchs, Switzerland). Caffeine was originated from Merck (Darmstadt, Germany) and cimetidine from ICN Biomedicals Inc. (Aurora, OH, USA). Doxorubicin HCl was obtained from LGC Standards GmbH (Teddington, Middlesex, UK). The 7-ethoxyresorufin, 4-OH-tolbutamide, and bufuralol HCl were purchased from Ultrafine (Manchester, UK) and 6α-hydroxypaclitaxel from BD Biosciences (Woburn, MA, USA). Tolbutamide and paclitaxel were from RBI (Natick, MA, USA) and USP (Rockville, MD, USA), respectively. Talinolol was purchased from TRC (Toronto Research Chemicals Inc., North York, ON, Canada). All other chemicals were from Sigma–Aldrich (St. Louis, MO, USA).

3.2. Cell cultures

3.2.1. Caco-2 cells

Caco-2 cells (HTB-37) at passage 17 were obtained from the ATCC (American Type Culture Collection, Rockville, MD, USA). The cells were routinely cultured and differentiated in standard tissue culture medium consisting of Minimal Essential Medium supplemented with 20% foetal bovine serum, penicillin (100 unit/ml), streptomycin (0.1 mg/ml) and sodium pyruvate (1mM).

3.2.2. VB- Caco-2 cells

VB-Caco-2 cultures were created from Caco-2 cultures by growing cells in 10 nM vinblastine supplemented standard tissue culture medium during subcultivation in flasks and differentiation in Transwell inserts. In vinblastine withdrawal experiments a batch of VB-Caco-2 cultures were separated into two parts; one line continued to be

kept in 10 nM vinblastine, while the other was grown in the absence of vinblastine for a further 33 passages.

Both Caco-2 and VB-Caco-2 cultures were grown at 37 °C in an atmosphere of 5% CO_2 and 95% relative humidity. Cells were passaged at subconfluence (every 3-4 days) at a split ratio of 1:3-1:4 using Trypsin-EDTA solution (0.25%).

For transport assay, Western blot, RT-PCR, CYP activity measurements and electron microscopy the cells were seeded at 5 x 10^5 cells per 1.12 cm^2 density on EC Matrix (ATCC, USA) covered Costar Transwell inserts (polycarbonate, 12 mm diameter, 0.4 μm pore size; Corning Incorporated, Corning, NY, USA) and used for the assays on days 19-21. VB-Caco-2 cultures were studied between passages 48 to 201 and Caco-2 between 35 to 93. All chemicals used for tissue culture were purchased from Gibco BRL (Grand Island, USA).

3.2.3. MDCK cells

Parent and MDR1 transfected Madin-Darby canine kidney epithelial cells (234) were obtained from the Netherlands Cancer Institute (Amsterdam, The Netherlands). The cells were cultured in a tissue culture medium consisting of 4.5 g/l glucose containing Dulbecco's Modified Eagle's Medium supplemented with 10 % foetal bovine serum, penicillin (50 units) and streptomycin (0.05 mg/ml) all from Gibco. Cultures were grown at 37 °C in an atmosphere of 5% CO_2 and 95% relative humidity. Cells were passaged at subconfluence (every 3-4 days) at a split ratio of 1:3-1:6 using Trypsin-EDTA solution (0.25%). The cells were used for up to 20-30 passages as long as their original properties were preserved. For transport assay and Western blot, the cells were seeded at 5 x 10^5 cells per 1.12 cm^2 density on Costar Transwell inserts (polycarbonate, 12 mm diameter, 0.4 μm pore size) and used for the assays on days 3-4. All chemicals used for tissue culture were purchased from Gibco BRL (Grand Island, USA).

DOI: 10.14753/SE.2013.1815

3.2.4. Rat BBB model

Rat brain capillary endothelial cells were used in a triple co-culture model (**Fig. 7**). Primary cultures of brain endothelial cells, astrocytes and pericytes, and construction of the *in vitro* BBB model were prepared by Nakagawa et al. (Nagasaki University, Japan) and Deli et al. (Biological Research Centre of the Hungarian Academy of Sciences, Szeged, Hungary) as described in (211) with the difference that cells were seeded on collagen and fibronectin coated Costar Transwell polycarbonate membranes (12 mm diameter, 3 μm pore size; Corning Incorporated, Corning, NY, USA) for the permeability measurements.

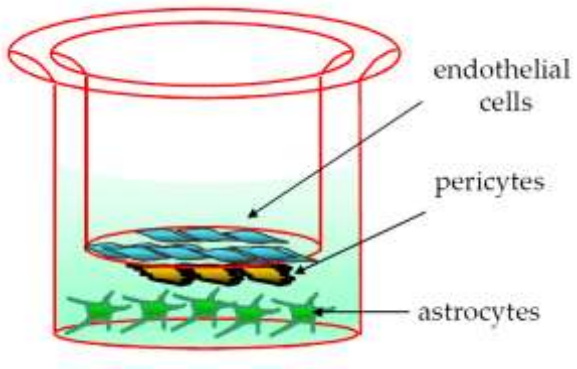

Fig. 7. Schematic drawing of the *in vitro* BBB model.

3.3. Cell morphology

The morphology of native cells in flasks and toluidine blue stained cells on Transwell inserts was monitored using inverse phase contrast microscopy. Micrographs were taken from cells cultured in T75 flasks. The selected micrographs from both Caco-2 and VB-Caco-2 cultures are representations of the culture characteristics.

3.4. Electron microscopy

Cells grown on the membrane of the culture inserts were fixed with 3 % paraformaldehyde containing 0.5% glutaraldehyde in phosphate buffer (pH 7.4) for 30

min at 4 ºC. After washing with the buffer several times, the cells on the membrane were postfixed in 1 % OsO_4 for 30 min. Following a rinse with distilled water, the cells were dehydrated in graded ethanol, block-stained with 1 % uranyl acetate in 50 % ethanol for 1 h. After the last step of dehydration, inserts were placed in the 1:1 mixture of abs. alcohol and Taab 812 (Taab; Aldermaston, Berks, UK) for 30 min at 30 ºC. Finally, the membranes of the culture inserts with the cells were removed from their support and embedded in Taab 812. Polymerization was performed overnight at 60 ºC. Ultrathin sections were cut perpendicularly for the membrane using a Leica UCT ultramicrotome (Leica Microsystems, Milton Keynes, UK) and examined using a Hitachi 7100 transmission electron microscope (Hitachi Ltd., Tokyo, Japan).

3.5. Immunostaining

Cells cultured on polyester membrane Transwell-Clear inserts (12 mm diameter, 0.4 μm pore size; Corning Incorporated, Corning, NY, USA) were stained for the junctional proteins β-catenin (Sigma–Aldrich, St. Louis, MO, USA), ZO-1 and claudin-1 (Invitrogen, Carlsbad, CA, USA), claudin-4 and -5, (Zymed Laboratories, San Francisco, CA, USA), and monolayers grown on glass coverslips were stained for P-glycoprotein (Calbiochem, La Jolla, CA, USA). The cultures were washed in PBS and fixed with ethanol (95 vol.%)–acetic acid (vol.5 %) for 10 min at -20 °C (ZO-1, β-catenin), with ethanol for 30 min at 4 °C (claudins) and with 4 % paraformaldehyde for 30 min at 4 °C (P-glycoprotein). Cells were blocked with 3% BSA and incubated with primary antibodies (anti-β-catenin, ZO-1, claudin-1, -4, -5 in 1:200 and P-glycoprotein in 1:10 for 1 h 30 min). Incubation with secondary antibody Cy3-labeled anti-rabbit IgG (Sigma–Aldrich) or anti-mouse-IgG-Alexa 488 (Invitrogen), dilution 1: 500, lasted for 1 h. To counterstain the cell nuclei, bis-benzimide (Sigma–Aldrich) was used in a dilution of 1:400. Between incubations cells were washed three times with PBS. Coverslips were mounted in Gel Mount (Biomeda, USA) and the staining was examined by a NikonEclipse TE2000 fluorescent microscope (Nikon, Japan) and photographed using a Spot RT digital camera (Diagnostic Instruments, USA).

3.6. Real-time PCR

RNA was extracted from cells cultured in flasks and Transwell inserts using RNeasy Mini Kit (Qiagen, Hilden, Germany), following the manufacturer's protocol. The reverse transcription of RNA (1 μg) was performed in a final volume of 40 μl containing 4 μl 10-fold-concentrated buffer, 8 μl $MgCl_2$ (25 mM), 4 μl dNTP, 2 μl RNasin, 1 μl random primers (Promega, Madison, WI, USA) and 1 μl MuLV reverse transcriptase (PE Applied Biosystems, Branchburg, New Jersey). The reverse transcription was carried out in a Gene ATAQ Controller thermal cycler (Pharmacia LKB, Uppsala, Sweden), under the following conditions: all samples were incubated at 42 ºC for 45 min and 99 ºC for 5 min. PE Applied Biosystems designed real-time PCR primers for MDR1 and the housekeeping 18S ribosomal RNA and TaqMan universal PCR master mix reagent were used to perform the PCR in 96-well optical reaction plates in an ABI Prism 7000 Sequence Detection System (PE Applied Biosystems). The analysis was carried out with ABI Prism 7000 SDS software (PE Applied Biosystems). Samples were run in triplicate.

3.7. Western blot

Cells were washed in ice-cold PBS (phosphate buffered saline) and scraped into 8 M urea/PBS containing 0.1% Triton-X, 1 μg/ml leupeptin, 10 ng/ml aprotinin, 100 μM phenylmethylsulphonyl fluoride (PMSF), 100 μM dithiothreitol, 200 μM sodium orthovanadate and 1 mM sodium fluoride. Cells were lysed with three cycles of snap-freezing and thawing. The extracts were centrifuged at 12000 g for 20 min and protein concentration in the supernatant was determined using the method described by Lowry et al. (235). For Western blotting, 25 μg protein samples were loaded on 7.5% Tris-HCl Ready Gels (BioRad Laboratories, Hercules, CA, USA) and blotted onto polyvinylidene difluoride membrane (BioRad Laboratories). Blots were probed overnight at 4 ºC with primary mouse anti-P-glycoprotein monoclonal antibody (Clone C219, Calbiochem, La Jolla, CA, USA in a dilution of 1:100 in the blots of **Fig. 12** and **15** or 1:20 in **Fig. 21**), or for loading control with primary rabbit anti-actin polyclonal antibody (1:200, Sigma-Aldrich) for 1 hour at room temperature. Then, secondary antibodies (goat anti-mouse

HRP-conjugated IgG; 1:10 000; Calbiochem, for anti-P-gp; or goat anti-rabbit HRP-conjugated IgG antibody 1:3000, Bio-Rad, for anti-actin) were added for 1 hour at room temperature. Chemoluminescence method (SuperSignal West Pico Chemiluminescent Substrate, Thermo scientific Rockford, IL, USA) was applied for detection of P-gp. For loading control, 3,3'-diaminobenzidine (Sigma-Aldrich) was used.

3.8. Bidirectional transport assay

The permeability of the test compounds was measured using bidirectional transport assay, in the apical-to-basolateral (A-B) and basolateral-to-apical (B-A) directions (**Fig. 8**) at 37 °C with moderate shaking (120 rpm). For highly permeable compounds, the "sink condition" was maintained by transferring the wells with cells to fresh buffer, HBSS-Hepes (Hank's Buffered Salt Solution containing 25 mM Hepes) at given time points (after 15 or 30 or 60 min). For the B-A direction, samples were taken after incubating the inserts for 30 or 60 or 120 min. The final incubation time for each reference compound was set on the basis of pilot experiments. At least three independent experiments were performed with triplicate inserts in both directions for reference compounds. Permeability screening was routinely performed under iso pH condition (pH 7.4 $_{A}$-7.4 $_{B}$), but reference compounds were measured under both gradient (pH 6.5 $_{A}$-7.4 $_{B}$) and iso pH conditions. Better prediction of human absorption is expected for ionisable drugs using gradient pH in the penetration assay. Therefore, the gradient pH permeabilities of reference compounds with acidic (ibuprofen, warfarin) or basic properties (alprenolol, doxorubicin, labetalol, loperamide, verapamil) were used in the plots with human absorption. As for weak bases, a "false efflux" effect occurs due to the dominance of ionized, less permeable molecular forms over the more penetrable neutral forms in the acidic apical pH; the P-gp classification for drugs is based on iso pH Papp values.

Before initiation of the transport studies, TEER (trans epithelial electric resistance) was measured (EVOM-2, WPI Inc, Sarasota, FL). Upon completion of the experiments, epithelial integrity was examined by toluidine blue (1%) staining. Lucifer Yellow (100 μM) and sodium fluorescein (100 μM), markers for the paracellular pathway, were used to verify tight junction integrity.

DOI: 10.14753/SE.2013.1815

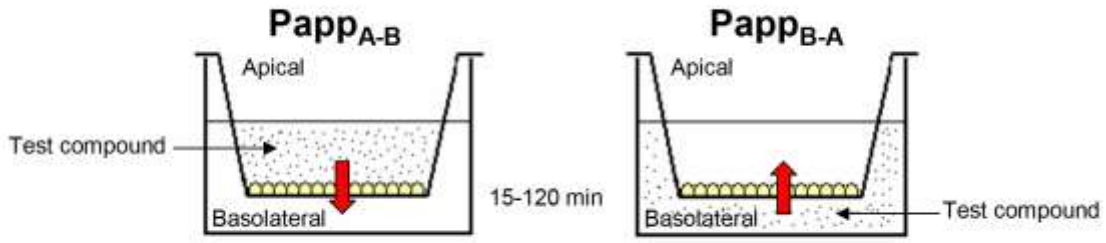

Fig. 8. Set-up of bidirectional transport assay with Transwell inserts

The concentration of test compounds in the samples was determined by HPLC with UV-VIS or a fluorescence detector (Merck-Hitachi LaChrom). Digoxin was measured on a Thermo LTQ XL linear ion trap mass spectrometer coupled with a Thermo Surveyor HPLC (San Jose, CA USA). Lucifer Yellow (at 485/530 nm excitation/emission) and sodium fluorescein (at 490/514 nm excitation/emission) were quantified using a fluorescence plate reader (Safire (2), Tecan Deutschland GmbH, Crailsheim, Germany).

Apparent permeability (Papp) was calculated with the following equation:

$$\text{Papp} = \frac{(dQ/dt)}{A x C_0}$$

where dQ/dt is the rate of permeability, C_0 is the initial concentration in the donor compartment, and A is the surface area of the filter (1.12 cm^2). The efflux ratio was calculated, as the ratio of $Papp_{B-A}$ to $Papp_{A-B}$. A ratio greater than 2.0 was accepted as an indicator of the efflux mechanism involvement (78). Verapamil HCl or quinidine (100 μM, 30 min preincubation) were used as efflux inhibitors to confirm P-gp activity.

Recovery (mass balance) was calculated according to the equation:

$$\%\text{Recovery} = \frac{C_f^D V^D + C_f^A V^A}{C_0^D V^D} x100\%$$

where C_0^D and C_f^D are the initial and final concentrations of the compound in the donor compartment, respectively; C_f^A is the final concentration in the acceptor compartment; V^D and V^A are the volumes of the solutions in the donor and acceptor compartments. With the exception of loperamide (50-60%), the recovery was over 70% for all the tested compounds. No mass balance correction was performed.

For MDCK-MDR1 cells, the corrected efflux ratio was also calculated (efflux ratio measured in MDCK-MDR1 cells divided by the efflux ratio measured in the parent cells). By this FDA recommended correction, the fold recombinant MDR1 activity is obtained over the effect of the constitutive canine transporter (78).

3.9. Calcein-AM extrusion assay

VB-Caco-2 cells were seeded onto 96-well plates (TPP, Trasadingen, Switzerland), at a concentration of 50 000 cells per well (200 µl/well) in vinblastine free cell culture medium, and cultured at 37°C and 5% CO_2 for 3 days.

The Calcein-AM assay was performed as described by Eneroth et al. (151), with slight differences. Briefly, after 3 days in culture the medium was removed, and the wells were washed three times with HBSS-Hepes. Then 50 µl of the test solution was added to the wells by a multichannel pipette and preincubated for 15 min at 37 °C. Thereafter 2.64 µM of Calcein-AM was added in an additional 150 µl of test solution, to produce a final concentration of 2.0 µM of Calcein-AM. After adding Calcein-AM the plates were immediately placed in a TECAN fluorescence plate reader (SAFIRE II, TECAN) and calcein fluorescence was monitored at 37 °C for 30 min at 485/529 nm excitation/emission with linear shaking. Compounds were tested at 10-100 µM final concentrations in HBSS-Hepes, 6 parallels were run at each concentration. Verapamil (250 µM) was used as a positive control. See **Fig. 9** for the explanation of working Calcein AM assay.

In accordance with (236) the initial rate of fluorescence generation (IRF) was determined from the time-dependent increase of cellular fluorescence and the final results, P-gp inhibition % was calculated using the following equation:

DOI: 10.14753/SE.2013.1815

$$\%\,\text{inhibition} = \frac{IRF_{\text{test compound}} - IRF_{\text{background}}}{IRF_{\text{verapamil}} - IRF_{\text{background}}} \times 100$$

where $IRF_{\text{test compound}}$ represents the initial rate of fluorescence generation in wells with test compound and calcein AM; $IRF_{\text{background}}$ the initial rate in wells with calcein AM alone and $IRF_{\text{verapamil}}$ the initial rate with verapamil and Calcein-AM. Compounds were indicated as P-gp inhibitor when they caused at least 25% of the inhibition of P-gp evoked by the positive control verapamil.

The P-gp functionality of each culture was characterized by the ratio of $IRF_{\text{verapamil}}$ and $IRF_{\text{background}}$. $IRF_{\text{verapamil}}/IRF_{\text{background}} > 3$ made only a culture eligible for using in Calcein-AM assay.

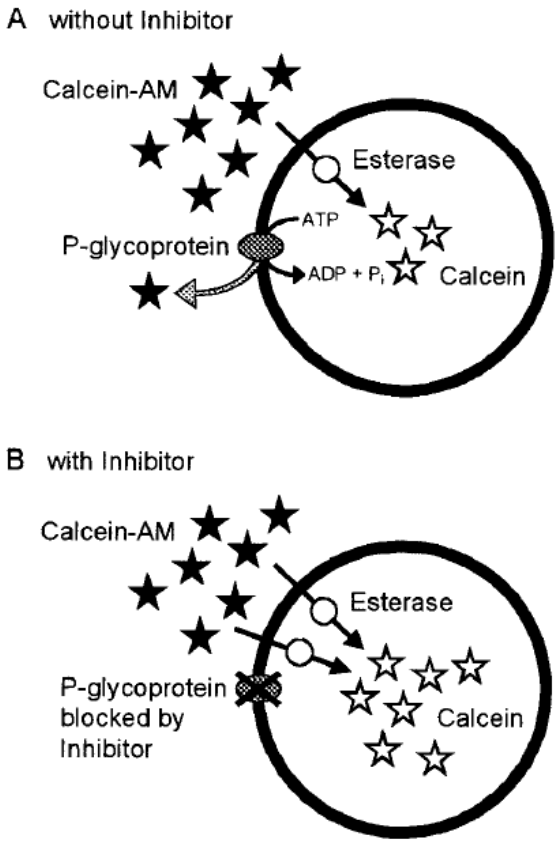

Fig. 9. Mechanism of Calcein-AM assay. Calcein-AM is a nonfluorescent P-gp substrate, capable of entering the cell by passive diffusion. In the cell, Calcein-AM is hydrolysed to fluorescent calcein by cytosolic esterases. Calcein accumulation is an indicator of P-gp inhibition as well as P-gp functionality in different cells (237,151).

DOI: 10.14753/SE.2013.1815

3.10. CYP activity

Cells grown on Transwell inserts for 20-21 days were washed with (37 °C) Krebs-Henseleit buffer (KHB) (Sigma-Aldrich) supplemented with amikacin-sulfate (42 g/l), gentamicin (83.5 mg/l), Hepes (20 mM), Heptanoic acid (4.2 μM), and salicylamide (3 mM). The CYP substrates were added to the apical and basolateral compartments in supplemented KHB buffer in a concentration that was at least twice as high as their K_M values (1A1: phenacetin, 1600 μM; 2C8: paclitaxel, 25 μM; 2C9: diclofenac, 100 μM and tolbutamide, 3500 μM; 2D6: bufuralol, 80 μM and dextromethorphan, 100 μM; 2E1: chlorzoxazone, 400 μM; 3A4: testosterone, 200 μM) determined in-house in other sets of experiments (details not added) using human liver microsomes. After two hours of incubation (37 °C), samples were collected from both sides of the inserts and enzyme specific metabolites were tracked using HPLC/UV or HPLC/Fluorometric techniques (Merck-Hitachi LaChrom). Finally, the cells were collected from the inserts by trypsinisation and counted. Results are added as pmol metabolites formed/min/10^6 cells.

3.11. Equilibrium dialysis measurements

This method was performed as described in (221), with slight differences. In brief, a 96-well equilibrium dialysis apparatus was used to determine the free fraction of the drugs in the plasma and brain (HTDialysis LLC, USA). Membranes (3.5-kDa cut-off) were conditioned in PBS for 60 min, then in 80:20 PBS/ethanol for 20 min, and then rinsed before use. Balb/C mouse (25-30 g, obtained from Harlan Laboratories, Eystrup, Germany) blood and brain were obtained fresh on the day of the experiment. Animal care followed the recommendations of European Convention for the Protection of Vertebrate Animals Used for Experimental and other Scientific Purposes (Council Directive 86/609/EEC). Procedures on animals were approved by the local ethics committees. The brain tissue was homogenized with PBS to a final composition of 1:2 brain/PBS using an Ultra-Turrax T10 (IKA Werke GmbH & Co., Staufen, Germany). Fresh plasma was separated from fresh whole blood by centrifugation at 2000*g* for 20 min. Diluted brain homogenate and plasma were spiked with the test compound to give

a nominal final concentration of 10 μM of test substance and a final DMSO concentration of 0.1%. 150 μl aliquots were loaded into the 96-well equilibrium dialysis plate. Dialysis against PBS (150 μl) was carried out for 5.5 h at 37 °C with moderate shaking. At the end of the incubation period, aliquots of plasma, brain homogenate or buffer sample were transferred to polycarbonate tubes (Tomtec Ltd., Budapest, Hungary), plasma and brain homogenate samples were diluted 10x in PBS, then acetonitrile was added 1:1 both to samples from the buffer and from the diluted plasma or brain side. Samples were mixed and kept at -20ºC until analysis. Before analysis, the samples were centrifuged at 3000*g* for 20 min.

The unbound (free) fraction (fu) for plasma and the apparent fu for brain was determined as the ratio of concentration in buffer to that in plasma or brain. Fu for the brain was calculated with correction for the dilution factor (D):

$$fu = \frac{1/D}{1/fu_{apparent} - 1 + 1/D}$$

3.12. *In vivo* studies of drug permeability in mice

The distribution of compounds to brain tissue *in vivo* was measured using a tissue distribution model in mice. The experiment was done by Nakagawa et al. in Japan as described in (211) and the Kp values were shared with us. Five min after the injection of a single dose of the compounds in anesthetized mice (Balb/C) via the tail vein (n = 3), blood samples were collected from vena cava and the whole brain was removed. The concentration of the compounds in brain and plasma samples was measured by liquid chromatography-tandem mass spectrometry (LC-MS/MS). The ratio of the concentration in brain and plasma (Kp) was determined for each drug. The ratio was then used to calculate the apparent permeability coefficient (Papp), presuming that metabolism and back-flux are negligible at that time point.

DOI: 10.14753/SE.2013.1815

4. Results

4.1. Drug penetration model of vinblastine-treated Caco-2 (VB-Caco-2) cultures

4.1.1. VB-Caco-2 culture

VB-Caco-2 cultures were established by cultivation of Caco-2 cells in a tissue culture medium containing vinblastine. The morphological characteristics of VB-Caco-2 cultures showing compact, homogenous monolayers of mostly small diameter cells (**Fig. 10B**) appeared after approx. 6 passages of initiation of 10 nM vinblastine exposure, and were maintained throughout the whole observation period up to 200 passages with continued vinblastine treatment.

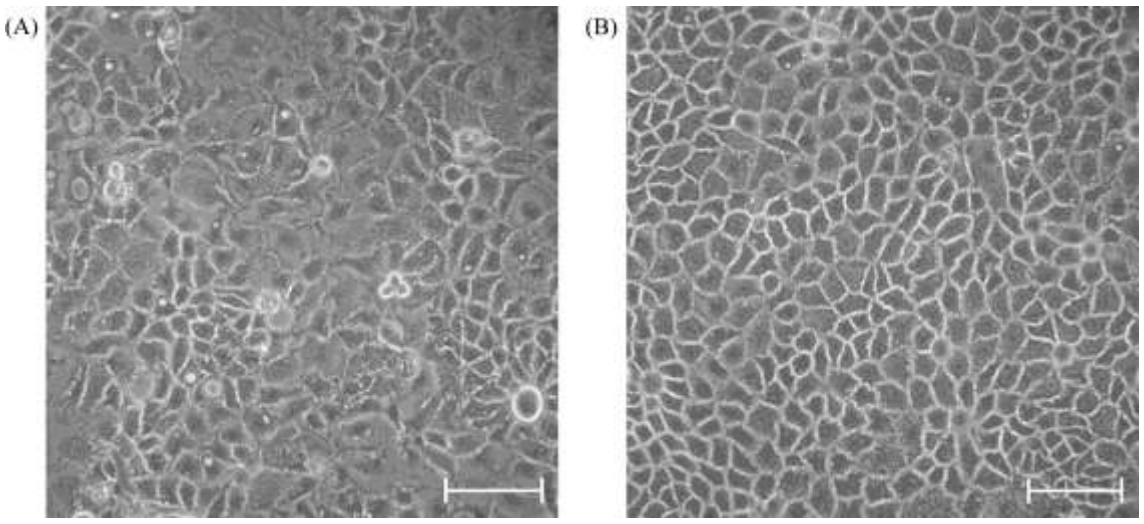

Fig. 10. Morphology of Caco-2 (A) and VB-Caco-2 (B) monolayers. Cells seeded at a density of 1x 10^6 cells/T-75 flask and cultured for 4 days. Phase contrast images, scale bars: 100 μm.

Contrary to VB-Caco-2, Caco-2 cultures grown in normal tissue culture medium (no vinblastine is added) showed heterogeneous appearance of monolayers consisting of a mixture of patches of small cells among areas covered with relatively large diameter cells (**Fig. 10A**). The morphology of Caco-2 cultures changes with the increase in passage number, containing a growing number of large cells.

DOI: 10.14753/SE.2013.1815

4.1.2. P-glycoprotein mRNA and protein levels in VB-Caco-2 and in Caco-2 cultures

The P-gp mRNA and protein levels were determined in VB-Caco-2 and Caco-2 cultures using RT-PCR and Western blot techniques, respectively. In VB-Caco-2 cultures the level of MDR1 mRNA was 2.2 and 4.3 times higher than in differentiated and undifferentiated Caco-2 cultures, respectively (**Fig. 11**).

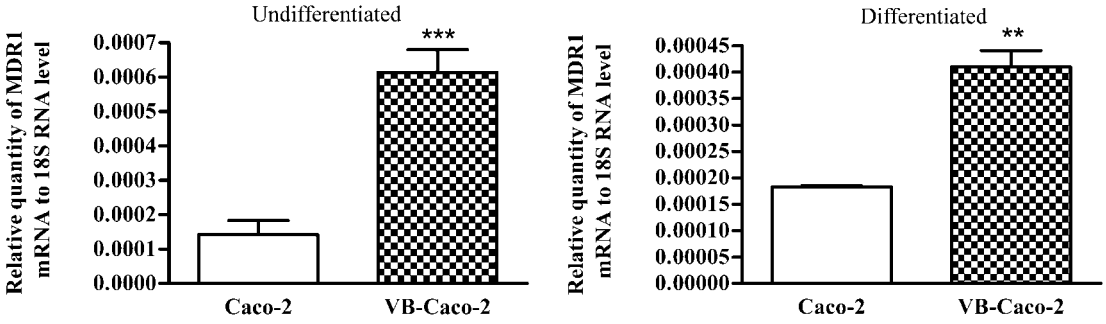

Fig. 11. Relative quantity of MDR1 mRNA level determined by RT-PCR in Caco-2 and VB-Caco-2 cultures. Mean and S.D. were calculated from cultures with different passage numbers. Significantly higher MDR1 mRNA level was seen in VB-Caco-2 cultures (**$p < 0.01$; ***$p < 0.001$).

Immunoblots (**Fig. 12**) show most intense expression of P-gp in VB-Caco-2 cultures. Cells allowed to differentiate spontaneously by growing for 19-21 days on Transwell inserts display an even higher level of P-gp protein than their undifferentiated equivalents cultured for only a few days (2-3 days) in tissue culture flasks. In native Caco-2 cultures hardly any detectable level of P-gp protein was observed.

DOI: 10.14753/SE.2013.1815

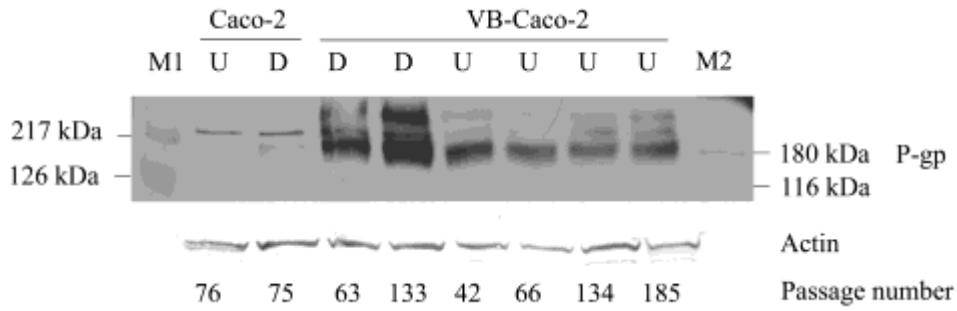

Fig. 12. Western blot of differentiated (D) and undifferentiated (U) Caco-2 and VB-Caco-2 cell lysates probed for P-gp. Molecular weight markers: **M1**: Kaleidoscope Prestained Standards (Bio-Rad) and **M2**: Prestained Molecular Weight Marker (Sigma-Aldrich).

4.1.3. Functionality of VB-Caco-2 in comparison to Caco-2: passive penetration

The apparent permeability ($Papp_{A-B}$) values obtained for the passively penetrating reference compounds correlated strongly (r^2 = 0.9830), indicating no substantial difference in the passive drug penetration between the two models. Penetrability of the paracellularly transported Lucifer Yellow and fluorescein sodium was also at the same degree in the two models (**Table 5**). Furthermore, both the VB-Caco-2 and the Caco-2 displayed TEER (transepithelial electric resistance, 2011 ± 332 and 1024 ± 187 Ω x cm^2, respectively) that was comparable to literature data (238).

4.1.4. Prediction of human absorption by VB-Caco-2

The apparent permeabilities ($Papp_{A-B}$) of all reference drugs (passively penetrating and efflux mediated) measured in VB-Caco-2 and Caco-2 models were plotted against literature values for HA (human absorption) (85,238,37). Theoretically, a sigmoidal curve can be obtained if high enough number of drugs with broad enough range of permeability/HA values are plotted.

DOI: 10.14753/SE.2013.1815

Table 5. Apparent permeability ($Papp_{A-B}$, pH 7.4_A-7.4_B), efflux ratio and classification of drugs (Y: efflux ratio > 2; N: efflux ratio < 2) in Caco-2 and VB-Caco-2 bidirectional transport assays.

				Caco-2					VB-Caco-2				
			Working conc.(µM)	$Papp_{A-B}$ ($x10^{-6}$ cm/s)		efflux ratio		effluxed	$Papp_{A-B}$ ($x10^{-6}$ cm/s)		efflux ratio		effluxed
Compound	Transport	HA (%)		Mean	± S.D.	Mean	± S.D.		Mean	± S.D.	Mean	± S.D.	
Caffeine	passive	100 [c]	10	84.0	± 4.2	0.9	± 0.1	N	83.6	± 5.6	0.8	± 0.0	N
Antipyrine	passive	100 [d]	10	80.7	± 5.8	0.8	± 0.0	N	80.9	± 6.9	0.9	± 0.1	N
Ibuprofen	passive	95 [c]	10	69.8	± 5.9	0.9	± 0.0	N	76.2	± 3.7	0.7	± 0.0	N
Lamotrigine	passive	98 [c]	10	58.5	± 2.9	0.8	± 0.1	N	51.0	± 1.3	0.8	± 0.1	N
Corticosterone	passive	100 [c]	10	57.8	± 5.5	0.8	± 0.0	N	62.7	± 10.7	0.9	± 0.2	N
Alprenolol	passive	93-96 [c]	10	55.7	± 2.3	0.7	± 0.0	N	51.7	± 5.7	0.9	± 0.1	N
Warfarin	passive	98 [c]	10	50.6	± 8.4	0.9	± 0.1	N	53.6	± 3.4	0.9	± 0.1	N
Verapamil	P-gp	100 [c]	10	36.6	± 6.0	0.8	± 0.0	N	36.3	± 1.8	0.9	± 0.1	N
			1	26.5		**1.5**		N	17.0		**4.4**		Y [b]
Acetaminophen	passive	80-100[c]	10	36.0	± 1.8	0.8	± 0.1	N	34.4	± 2.0	0.9	± 0.0	N
Quinidine [a]	P-gp	80-90 [c]	10	29.1	± 6.9	**1.2**	± 0.1	N	13.1	± 2.1	**3.6**	± 0.5	Y [b]
			1	25.5		**1.7**		N	3.2	± 0.6	**23.5**	± 4.7	Y [b]
Ketoconazole	passive		10	26.5	± 3.1	1.2	± 0.1	N	27.1	± 4.6	1.2	± 0.1	N
Dexamethasone [a]	P-gp	80-100[c]	10	20.3	± 2.0	**1.1**	± 0.1	N	13.5	± 2.1	**2.9**	± 0.4	Y [b]
			3	22.7		**1.1**		N	12.0		**2.9**		Y [b]
Loperamide [a]	P-gp		10	17.0	± 3.5	**0.8**	± 0.4	N	8.8	± 1.9	**3.0**	± 0.5	Y [b]
			3	13.6		**1.1**		N	2.3		**20.0**		Y [b]
Labetalol [a]	P-gp	90-95 [c]	50	15.8	± 2.1	**1.2**	± 0.1	N	10.4	± 2.5	**2.9**	± 0.6	Y [b]
			3	29.2		**0.8**		N	7.9		**5.2**		Y [b]
Vinblastine	P-gp, MRP2		10	4.1	± 0.6	8.5	± 1.8	Y	0.3	± 0.1	248.0	± 78.0	Y
Cimetidine	P-gp, BCRP	64 [c, e]	50	1.9	± 0.3	2.1	± 0.2	Y	0.6	± 0.1	4.8	± 0.6	Y
Ranitidine [a]	P-gp	64 [d, e]	50	1.8	± 0.6	**1.3**	± 0.3	N	0.5	± 0.0	**3.9**	± 1.0	Y [b]
			10	2.2		**1.1**		N	0.5		**3.5**		Y [b]
Chlorothiazide	P-gp, BCRP, MRP4	25 [d, e]	50	1.4	± 0.4	3.7	± 1.3	Y	0.1	± 0.0	21.9	± 7.5	Y
Atenolol [a]	paracell., P-gp	50-54 [c]	50	0.7	± 0.3	**1.2**	± 0.1	N	0.2	± 0.1	**2.6**	± 0.8	Y [b]
			10	0.8	± 0.1	**1.3**	± 0.4	N	0.2	± 0.0	**2.1**	± 0.4	Y [b]
Furosemide	BCRP, MRP4	61 [c]	50	0.6	± 0.2	29.6	± 6.5	Y	0.3	± 0.2	72.6	± 41.5	Y
Sulfasalazine	BCRP	12 [d, e]	50	0.4	± 0.3	64.8	± 36.5	Y	0.2	± 0.0	65.8	± 21.5	Y
Doxorubicin	P-gp	0.7-23 [c]	50	0.4	± 0.1	6.3	± 2.2	Y	0.1	± 0.0	60.3	± 17.1	Y
Na-fluorescein	paracell.		100	1.4	± 0.3				0.5	± 0.2			
Lucifer Yellow	paracell.		100	0.5	± 0.3				0.1	± 0.1			

Results are mean and interassay S.D. values obtained with 3-6 different passages of cultures (VB-Caco-2 between 48-195; Caco-2 between 35-93) at iso pH conditions.

[a] Drugs measured in two concentrations. At lower concentration only a single experiment was performed.

[b] P-gp substrates identified only by VB-Caco-2.

HA (%): human absorption from [c] (37); [d] (238);

[e] http://www.who.int/medicines/services/expertcommittees/pharmprep/QAS04_109Rev1_Waive_invivo_bioequiv.pdf.

BCRP: breast cancer resistance protein; MRP: multidrug resistance-associated protein

The efflux ratio is the ratio of $Papp_{B-A}$ to $Papp_{A-B}$

DOI: 10.14753/SE.2013.1815

In our case two groups of compounds were clearly distinguishable. High permeability compounds with HA of higher than 85% with an apparent permeability of at least 8.5 x 10^{-6} cm/s or 15.4 x 10^{-6} cm/s in the VB-Caco-2 or Caco-2 model, respectively; and low permeability compounds with lower than 0.6 x 10^{-6} cm/s $Papp_{A-B}$ values in the VB-Caco-2 model and with lower than 1.9 x 10^{-6} cm/s $Papp_{A-B}$ in the Caco-2 model. The higher threshold Papp values with Caco-2 for the two groups were most probably attributable to the lower P-gp sensitivity of those cells (**Fig. 13**).

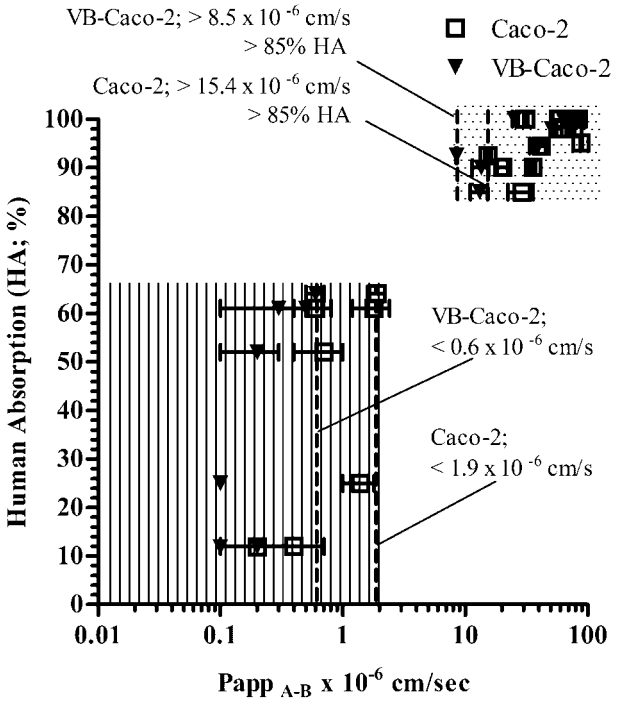

Fig. 13. The fraction absorbed (HA%, literature data) plotted against apparent permeabilities ($Papp_{A-B}$) of reference drugs (as listed in **Table 5.**) in VB-Caco-2 and Caco-2 bidirectional transport assay. The models differentiate two groups of drugs with slightly differing penetrability thresholds (dotted area: high permeability compounds; lined area: low permeability compounds). Weak acids (ibuprofen, warfarin) and weak bases (alprenolol, doxorubicin, labetalol, verapamil) are demonstrated with their $Papp_{A-B}$ values obtained at gradient pH; other drugs are shown with their $Papp_{A-B}$ at iso pH. Bars represent S.D.

DOI: 10.14753/SE.2013.1815

4.1.5. P-gp functionality of VB-Caco-2 compared to Caco-2 in bidirectional transport assay

The VB-Caco-2 assay sensitively detected the P-gp substrates (efflux ratio > 2). It correctly classified all low permeability P-gp substrates such as vinblastine, cimetidine, ranitidine, chlorothiazide, atenolol and doxorubicin, and it identified all high permeability P-gp substrates like verapamil, quinidine, dexamethasone, loperamide and labetalol (**Table 5**). In contrast to this, the Caco-2 was unable to identify the high permeability reference P-gp substrates, and it also failed to recognize two of the low penetrability references: ranitidine and atenolol (**Table 5**). Although other low permeability P-gp substrates such as vinblastine, cimetidine, chlorothiazide and doxorubicin were recognized by Caco-2, the notably higher efflux ratio by the VB-Caco-2 also points to the superior sensitivity of the latter. The P-gp inhibitor verapamil reduced the efflux ratio of the test compounds by at least 50% (**Table 6**), which accords with the regulatory classification for P-gp substrates (78).

Table 6. Apparent permeability (Papp $_{A-B}$) of selected reference drugs in the presence or absence of the P-gp inhibitor verapamil.

		VB-Caco-2		VB-Caco-2 + 100μM verapamil	
		Papp $_{A-B}$ ($x10^{-6}$ cm/s)	efflux ratio	Papp $_{A-B}$ ($x10^{-6}$ cm/s)	efflux ratio
Compound	Working conc. (μM)	Mean ± S.D.	Mean ± S.D.	Mean ± S.D.	Mean ± S.D.
Vinblastine	10	0.4 ± 0.1	**203.3** ± 13.7	8.6 ± 0.0	**4.4** ± 0.2
Dexamethasone	10	12.8 ± 0.3	**3.2** ± 0.1	22.3 ± 1.0	**0.9** ± 0.1
Quinidine	10	13.0 ± 0.0	**5.8** ± 0.2	60.9 ± 2.5	**0.6** ± 0.0
Loperamide	10	7.7 ± 0.4	**2.9** ± 0.4	19.5 ± 1.8	**1.0** ± 0.1
Labetalol	10	8.1 ± 0.1	**6.0** ± 0.2	19.8 ± 3.1	**0.9** ± 0.2
Cimetidine	10	0.9 ± 0.0	**3.8** ± 0.5	1.5 ± 0.1	**1.2** ± 0.1
Atenolol	50	0.2 ± 0.0	**3.6** ± 0.5	0.2 ± 0.0	**1.8** ± 0.6
Ranitidine	10	0.9 ± 0.2	**3.0** ± 0.7	0.8 ± 0.5	**0.8** ± 0.4
Doxorubicin	50	0.1 ± 0.0	**58.7** ± 31.3	0.1 ± 0.0	**1.9** ± 0.6

The P-gp functionality of VB-Caco-2 was monitored through a broad passage range between 35 and 195. During this interval, each P-gp substrate showed an efflux ratio of higher than 2 at each reading (**Fig. 14**).

DOI: 10.14753/SE.2013.1815

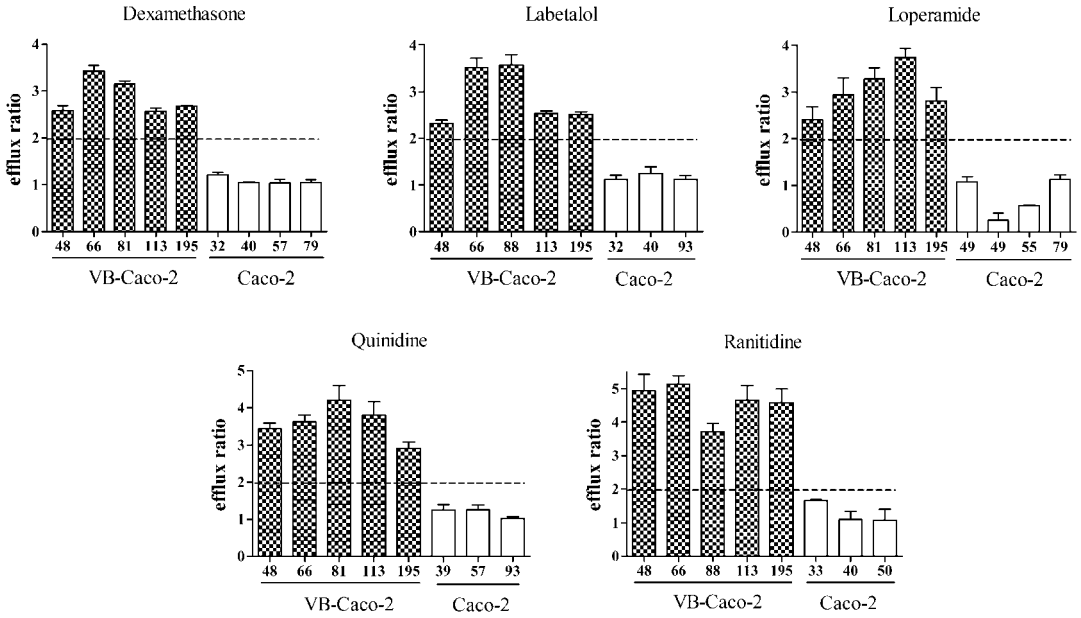

Fig. 14. Distribution of efflux ratios (mean and S.D. n = 3) of selected P-gp substrates in VB-Caco-2 (filled column) and in Caco-2 cultures (empty column) through a broad passage range. VB-Caco-2 model recognizes with efflux ratio > 2 the known P-gp substrates along the whole observation period. Passage numbers are indicated under the columns.

4.1.6. The effect of vinblastine withdrawal on P-gp level and functionality in VB-Caco-2 cultures

Vinblastine withdrawal following its sustained presence in VB-Caco-2 cultures (through 70 passages) did not decrease the P-gp protein level or functionality (**Fig. 15**). The protein level of differentiated cultures and bidirectional transport of selected efflux substrates were investigated at 10 and 33 passages after the drug withdrawal.

DOI: 10.14753/SE.2013.1815

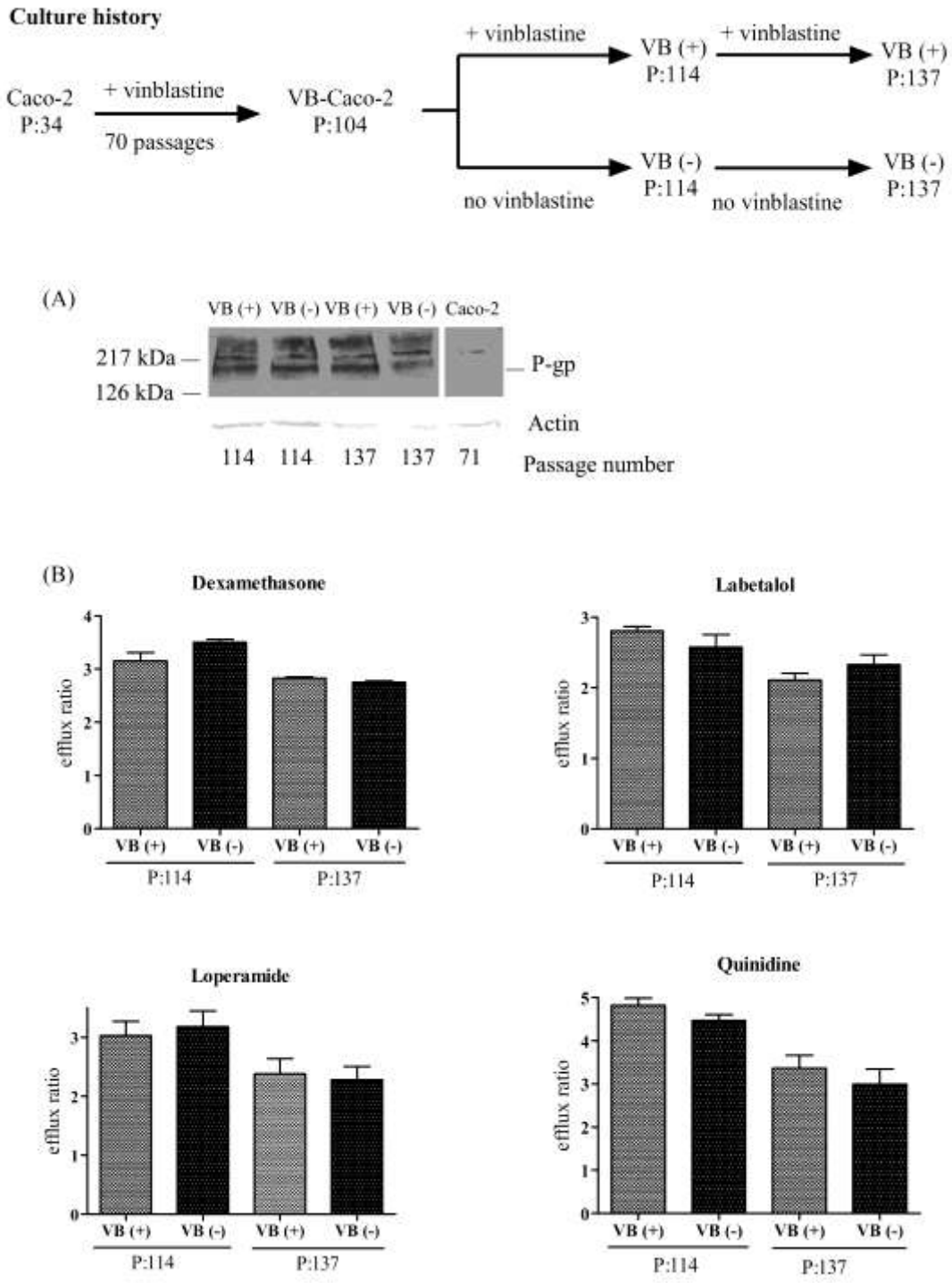

Fig. 15. Western blot of cell lysates probed for P-gp (A) and comparison of efflux ratios (B) in VB-Caco-2 and in vinblastine withdrawn VB-Caco-2 cultures. No decrease in P-gp protein level or significant differences of P-gp activities characterized by efflux ratios were detected between the VB (+) and VB (-) cultures. VB (+): VB-Caco-2 cultures kept continuously in vinblastine containing medium between passages 34 and 137; VB (-): vinblastine was withdrawn from the medium of VB-Caco-2 from passage 104 and kept without vinblastine up to passage 137. Bars represent S.D.

DOI: 10.14753/SE.2013.1815

4.1.7. Screening of NCEs using VB-Caco-2 and Caco-2 bidirectional transport assay

A structurally diverse set of 91 compounds (16 structure families) synthesized in Richter's preclinical research program in four different indication areas underwent permeability screening at a 3 or 10 μM concentration (depending on their aqueous solubility) using both VB-Caco-2 and Caco-2 assays. The results revealed that 34 out of 91 tested NCEs in VB-Caco-2 assay were P-gp substrates displaying an efflux ratio of > 2, while Caco-2 identified only 8 of them (**Fig. 16**). The Caco-2 failed to identify ~ 76% of compounds, the efflux of which was inhibited by at least 50% by verapamil, which confirms that those compounds were indeed P-gp substrates (data not shown).

For passively transported compounds (efflux ratio < 2), similar apparent permeability values (r^2 = 0.8706) were obtained in both models in agreement with the observations made on reference drugs as described in Section 4.1.3.

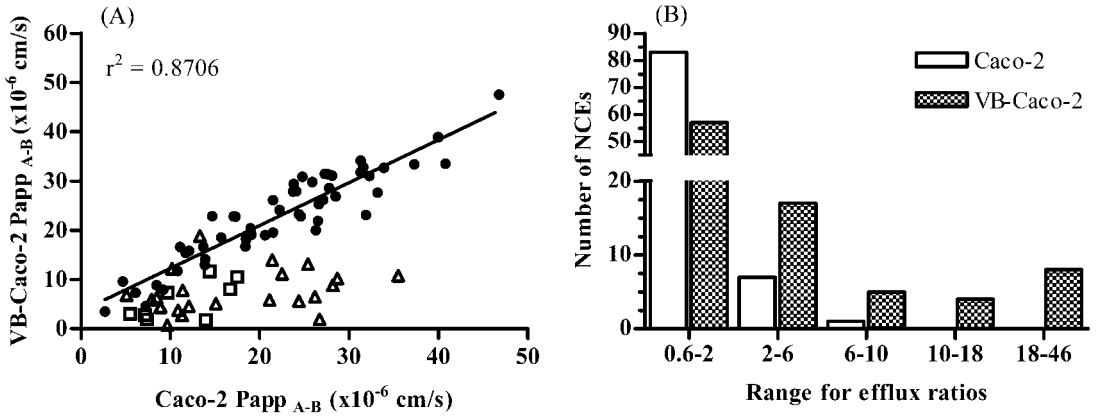

Fig. 16. Apparent permeabilities (Papp $_{A-B}$) (A) and distribution of efflux ratio values (B) of new chemical entities (NCEs) (n = 91) determined both in VB-Caco-2 and Caco-2 bidirectional permeability assays at iso pH conditions; filled circles: efflux ratio < 2 both in VB-Caco-2 and Caco-2 models (n = 57); open triangles: efflux ratio > 2 only in VB-Caco-2 model (n = 26); open square: efflux ratio > 2 both in VB-Caco-2 and Caco-2 models (n = 8). A correlation (r^2 = 0.8706) was detectable for the groups of NCEs with passive penetration (filled circles). Some 37% of NCEs are assumed to be P-gp substrates (open triangles plus squares) in the VB-Caco-2 model and only 9% in the Caco-2 (open squares); therefore, Caco-2 failed to identify ~ 76% of NCEs potentially interacting with P-gp. More assumed P-gp substrates and higher accompanied efflux ratios appeared with the VB-Caco-2 model. The range for efflux of 0.6-2 covers compounds identified as subjects to passive penetration.

DOI: 10.14753/SE.2013.1815

4.1.8. P-glycoprotein functionality of VB-Caco-2 in Calcein AM assay

The VB-Caco-2 culture was examined in four different passage ranges (67-73, 94-97, 128-131, 199-201) using reference compounds (n = 17) to test its suitability for long term use in calcein AM assay. The data in **Table 7** show that the reference P-gp inhibitors were correctly identified by VB-Caco-2, in keeping with the literature values, throughout the observation period.

Table 7. Percentage of P-gp inhibition by reference compounds tested in Calcein AM assay using VB-Caco-2 cells. Results are presented in mean ± S.D. of cells with four different passages between 67 and 201.

Compound	Working conc. (μM)	% inhibition of P-gp Mean	± SD	Test result	Literature result
Cyclosporin A	10	169.7	± 4.4	+	+
Ketoconazole	100	114.8	± 9.0	+	+
Verapamil	250	100.0		+	+
Loperamide	100	85.8	± 12.9	+	+
Vinblastine	100	84.0	± 11.4	+	+
Quinidine	100	79.1	± 13.7	+	+
Testosterone	100	53.3	± 7.2	+	+
Terfenadine	10	45.6	± 6.6	+	
Labetalol	100	43.8	± 8.2	+	+
Alprenolol	100	37.9	± 8.2	+	
Dexamethasone	100	3.8	± 2.4	-	-
Ranitidine	100	2.1	± 0.9	-	-
Furosemide	100	2.1	± 2.8	-	
Chlorothiazide	100	1.8	± 1.8	-	
Cimetidine	100	1.8	± 2.4	-	-
Antipyrine	100	0.6	± 0.5	-	-
Caffeine	100	0.4	± 1.8	-	
Sulfasalazine	100	0.3	± 1.9	-	-

Literature results using MDCK-MDR1, vinblastine selected Caco-2 and other cell lines based calcein AM assay from: (152,239,236).
Test results: % inhibition of P-gp > 25%: positive (+); < 25%: negative (-)

Calcein retention in the presence of verapamil relative to calcein retention without verapamil ($IRF_{verapamil}$ /$IRF_{background}$) was constantly higher than 3 in the VB-Caco-2 cultures, up to at least 201 passages, displaying high enough functionality for P-gp in the assay. This ratio was only 1.3-1.7 in the Caco-2 cultures at any passages.

DOI: 10.14753/SE.2013.1815

4.1.9. CYP enzyme activity

The CYP3A4 and CYP1A1-mediated reactions in differentiated VB-Caco-2 and Caco-2 cultures (**Table 8**) were similar as they were measured by testosterone 6-ß-hydroxylation and phenacetin O-deethylation, respectively. Detectable activities of CYP2C8, CYP2C9, CYP2D6 and CYP2E1 (paclitaxel 6α-hydroxylation, diclofenac 4'-hydroxylation or tolbutamide 4-hydroxylation, bufuralol 1'-hydroxylation or dextromethorphan O-demethylation and chlorzoxazone 6-hydroxylation, respectively) were not found either in differentiated or undifferentiated cells.

Table 8. CYP enzyme activities in differentiated VB-Caco-2 and Caco-2 cultures.

CYP enzyme	Substrate	Working conc. (μM)	Metabolite	Activity (pmol/min/10^6 cells) Caco-2	VB-Caco-2
1A1	Phenacetin	1600	Acetaminophen	2.62 ± 0.5	2.14 ± 0.4
2C8	Paclitaxel	5	6-α-OH-paclitaxel	< 2.05	< 2.87
2C9	Diclofenac	100	4-OH-diclofenac	< 0.26	< 0.36
	Tolbutamide	3500	OH-tolbutamide	< 1.03	< 1.43
2D6	Bufuralol	80	OH-bufuralol	< 1.03	< 1.43
	Dextromethorphan	100	Dextrorphan	< 0.21	< 0.29
2E1	Chlorzoxazone	400	OH-chlorzoxazone	< 0.51	< 0.72
3A4	Testosterone	200	6-β-OH-testosterone	0.94 ± 0.1	0.86 ± 0.1

Activities are expressed as mean ± S.D. (n = 3)

DOI: 10.14753/SE.2013.1815

4.2. Challenging brain penetration modelling with VB-Caco-2:

Comparison of brain capillary endothelial cell-based and epithelial cell-based surrogate BBB penetration models

4.2.1. Morphology: electron microscopy and immunohistochemistry

4.2.1.1. Rat brain capillary endothelial cells co-cultured with pericytes and astrocytes (rat BBB)

Brain capillary endothelial cells co-cultured with pericytes and astrocytes were grown on Transwells in regular monolayers. The height of cells at the perinuclear region was only at about 1.5-2 μm or even less (0.2-0.4 μm) in the plasmalemmal processes where adjacent endothelial cells typically overlap and contact each other (**Fig. 17**). Between the overlapping plasma membranes, the tight junctions, long rows of "kissing points", can be seen. The surface of the endothelial cells is typically smooth but often interrupted by caveolae and caveolae-like invaginations (**Fig. 18**). In the brain capillary endothelial cells, the adherens junctions and desmosomes are in structural unity with the tight junctions (**Fig. 19**).

Brain endothelial cells stained positively for the endothelial specific claudin-5 but not for the epithelial type claudins (e.g., claudin-1 and -4) and they also yielded positive immunostaining for ZO-1 and β-catenin as well (**Table 9**). The brain capillary endothelial cells are thin and elongated (**Fig. 20**), and show a swirling pattern in the monolayers.

DOI: 10.14753/SE.2013.1815

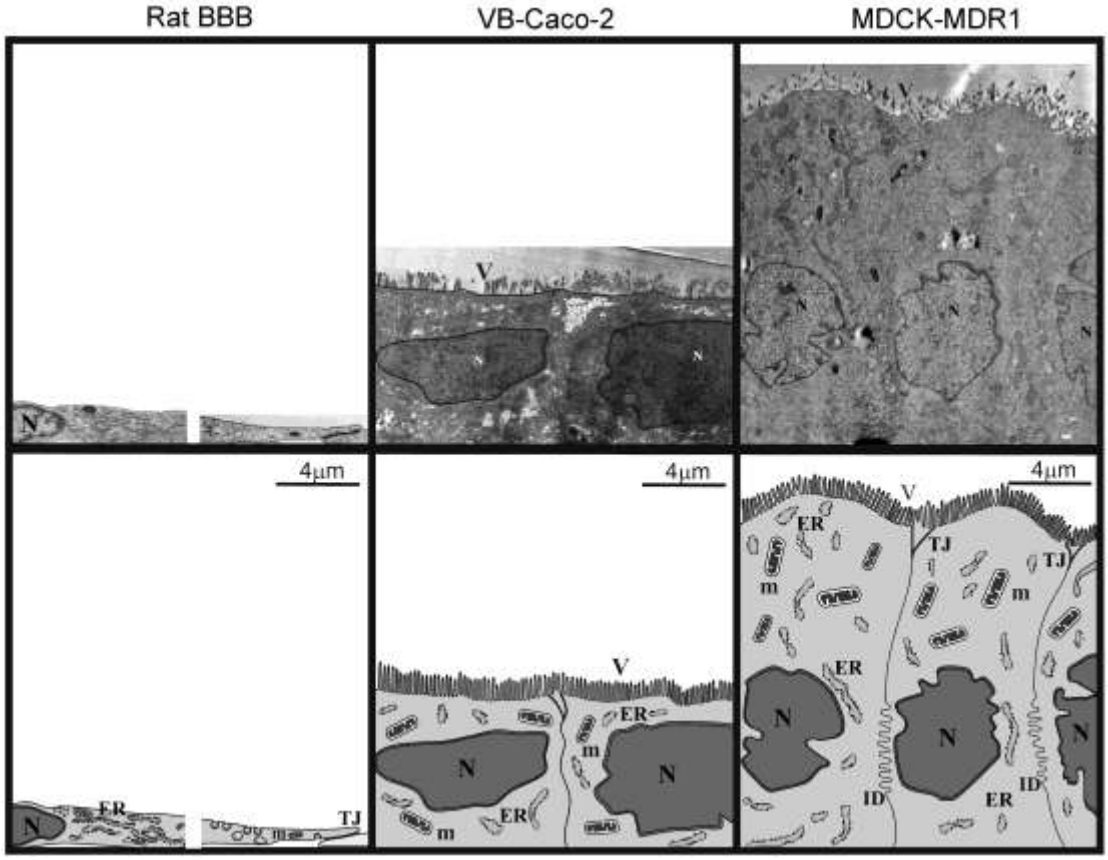

Fig. 17. Electron micrographs of rat BBB, VB-Caco-2 and MDCK-MDR1 cell cytoarchitecture. ER, endoplasmatic reticulum; ID, interdigitations; m, mitochondrion; N, nucleus; TJ, intercellular tight junctions; V, microvilli.

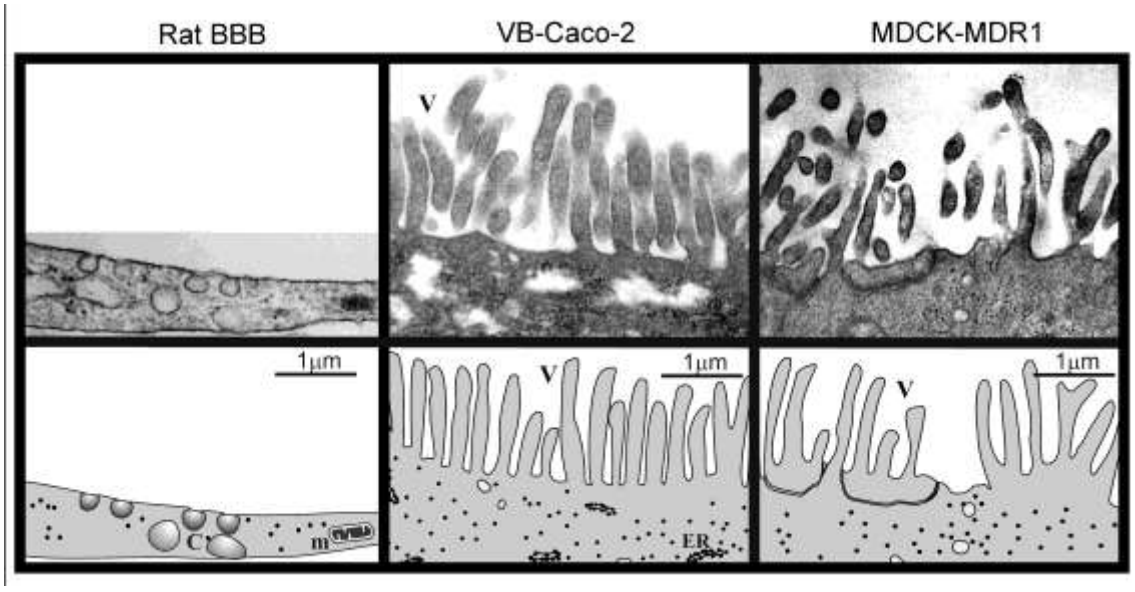

Fig. 18. Electron micrographs of rat BBB, VB-Caco-2 and MDCK-MDR1 cell surface morphology. C, caveolae; ER, endoplasmatic reticulum; m, mitochondrion; V, microvilli.

DOI: 10.14753/SE.2013.1815

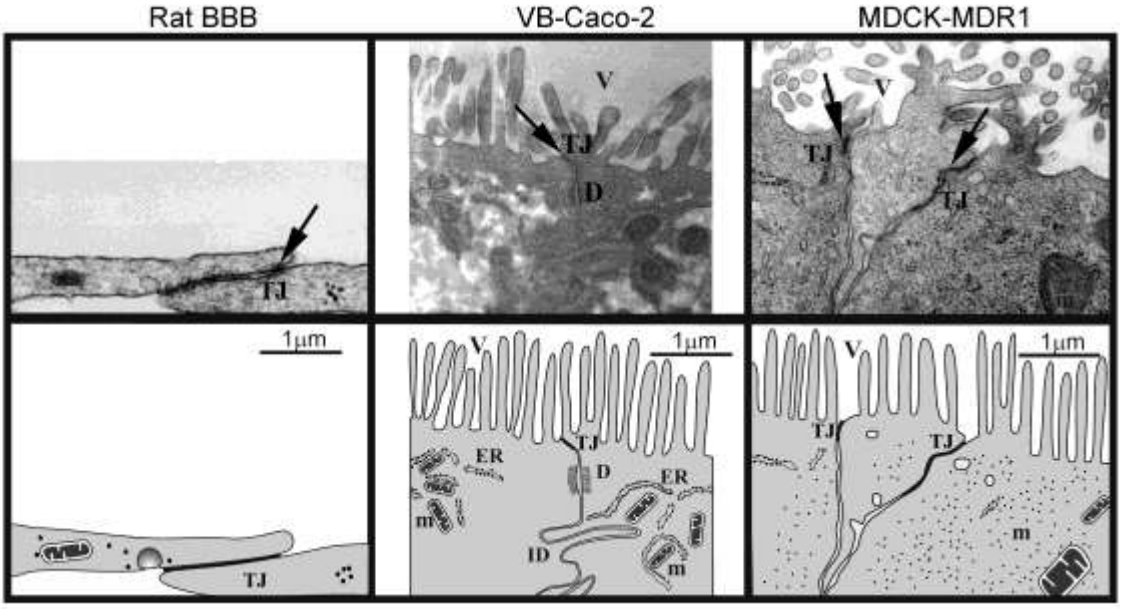

Fig. 19. Electron micrographs of rat BBB, VB-Caco-2 and MDCK-MDR1 intercellular junctions. D, desmosome; ER, endoplasmatic reticulum; ID, interdigitations; m, mitochondrion; N, nucleus; TJ, intercellular tight junctions; V, microvilli. Arrows point to tight intercellular junctions.

Table 9. Summary of the expression of tight junction (TJ) and adherens junction related proteins in rat brain capillary endothelial blood-brain barrier (BBB) and in epithelial models (Caco-2, VB-Caco-2, MDCK-MDR1) using immunostaining. For staining see **Fig. 20**.

Model	β-catenin	ZO-1	Claudin-1	Claudin-4	Claudin-5
Rat BBB	+	+	+/–	–	+
Caco-2	+	+	+	+	–
VB-Caco-2	+	+	+	+	–
MDCK-MDR1	+	+	+	+	–

+: positive staining, –: negative staining

DOI: 10.14753/SE.2013.1815

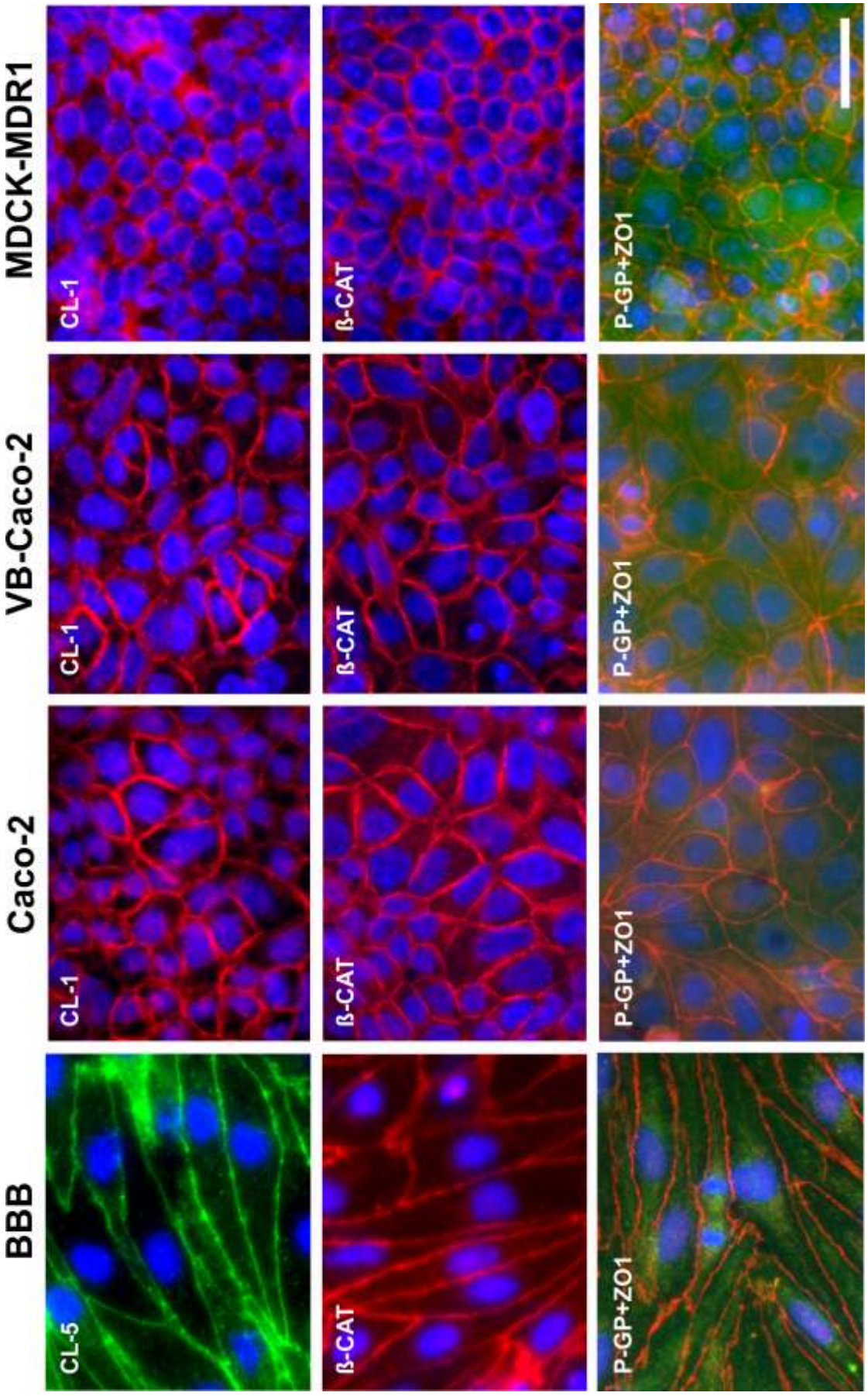

Fig. 20. Primary rat brain microvessel endothelial cells and epithelial cell lines stained for tight junction (TJ) and adherens junction related proteins and for P-glycoprotein. Cell nuclei (blue) are counterstained with bis-benzimide. In the double immunohistochemistry P-glycoprotein is seen as green staining spreading over cell bodies, while ZO-1 TJ associated protein demarks cell to cell borders (red). BBB, blood-brain barrier model; β-CAT, β-catenin (red); CL-1, claudin-1 (red); CL-5, claudin-5 (green); P-GP, P-glycoprotein (green); VB, vinblastine-treated; ZO-1, zonula occludens protein-1 (red). Scale bar: 20 μm

4.2.1.2. Native human Caco-2 and VB-Caco-2; dog kidney epithelial cell lines: MDCK and MDCK-MDR1

Native Caco-2, VB-Caco-2 and dog kidney epithelial cultures (MDCK, MDCK-MDR1) grow on Transwells in non-overlapping monolayers and have a cuboidal shape (**Fig. 17**). An obvious morphological difference is that the kidney epithelial cells are usually higher than the colon carcinoma cells (MDCK-MDR1: 10-20 μm versus VB-Caco-2: 8-15 μm). The apical surface of both cell types is similarly covered with microvilli (**Fig. 18**). Between the adjacent cells, the tight junctions are relatively short (0.3-1 μm), and are positioned apically and well separated from other junctional structures like desmosomes and adherens junctions, so they could be identified as independent structures (**Fig. 19**). At the basolateral region, fingerlike projections (interdigitations) were observed between neighbouring cells.

Positive staining for the integral membrane TJ proteins claudin-1 and claudin-4, for the cytoplasmic TJ associated ZO-1 protein and for the adherens junction protein β-catenin was demonstrated in both human colon carcinoma and dog kidney epithelial cells (**Table 9**). Pericellular staining appeared for all the listed TJ proteins. Epithelial type cells were not stained positively for the endothelial-specific claudin-5 TJ protein (**Table 9**). There was a typical cobblestone pattern in both epithelial cultures, but the VB-Caco-2 cultures grow in a lower density than MDCK-MDR1 (**Fig. 20**). Generally, there were no ultrastructural morphological or TJ immunostaining-related differences between native Caco-2 versus VB-Caco-2 or parental MDCK versus MDCK-MDR1 cultures.

DOI: 10.14753/SE.2013.1815

4.2.2. P-glycoprotein expression in rat BBB EPA and in epithelial cell lines (native Caco-2, VB-Caco-2, MDCK and MDCK-MDR1)

The expression of P-gp protein was assayed by using the Western blot technique in cell lysates and by the immunostaining of P-gp on cell monolayers. Western immunoblots revealed comparably intense staining of P-gp in VB-Caco-2 and MDCK-MDR1 cultures (**Fig. 21**). The P-gp staining in rat brain capillary endothelial cells was less intense and the bands appeared at a lower molecular weight than in the other cells with human P-gp. In MDCK and in native Caco-2 cell lysates, the protein level of P-gp was under the detection limit.

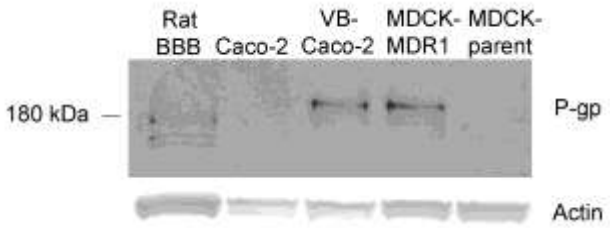

Fig. 21. Western blot analysis of lysates of rat brain capillary endothelial cells, native Caco-2, VB-Caco-2, MDCK-MDR1 and MDCK-parent cell lines probed for P-glycoprotein (P-gp).

P-gp immunostaining revealed comparably weaker staining of P-gp for Caco-2, while staining differences were not obvious for the other types of cultures (**Fig. 20**).

4.2.3. Comparison of paracellular tightness of the models

The Trans Epithelial Electric Resistance (TEER) in rat BBB (548 ± 125 Ωcm^2), native Caco-2 (1024 ± 184 Ωcm^2) and VB-Caco-2 (2012 ± 347 Ωcm^2) models was well above the critical value (150-200 Ωcm^2), signifying acceptable integrity (**Table 10**). The MDCK(II) and MDCK(II)-MDR1 cultures presented a TEER that was typically below 100 Ωcm^2.

The VB-Caco-2 and the MDCK-MDR1 models were the least permeable for fluorescein sodium (NaF), a low molecular weight marker of paracellular integrity, with values of 0.47 ± 0.17 x 10^{-6} cm/s and 0.59 ± 0.06 x 10^{-6} cm/s, respectively. The rat BBB

and native Caco-2 models were looser, as demonstrated by the significantly higher Papp for NaF; (rat BBB: 2.72 ± 0.03 x 10^{-6} cm/s; Caco-2: 1.34 ± 0.29 x 10^{-6} cm/s; **Table 10**).

4.2.4. Comparison of efflux of P-gp substrate drugs and permeability of mixed mechanism drugs

In bidirectional assays with rat BBB, native Caco-2, VB-Caco-2, MDCK or MDCK-MDR1 monolayers, the Papp of different mechanism reference drugs (both passively permeated and effluxed) was determined in two directions and the ratio of Papp values (efflux ratio) was calculated (**Table 10**). Among the various models, MDCK-MDR1 and VB-Caco-2 identified the highest number of efflux transporter substrates, characterized with an efflux ratio higher than 2, which indicates more sensitive P-gp recognition of these models compared to the others. Accordingly, the MDCK-MDR1 (using a corrected efflux ratio) and the VB-Caco-2 models identified five out of the seven known P-gp substrates tested (**Table 10**, bolded figures). The rat BBB model could only identify digoxin as a P-gp substrate.

Permeability of most compounds from **Table 10** was also measured in the previous experiments (**Table 5**) using Caco-2 and VB-Caco-2 drug penetration models. Permeability and efflux ratio were in the same classification range; however, for atenolol at 10 μM the mean efflux ratio was 2.1, but in the following experiments, it was 1.95, which is above or below the limit of the classification for efflux substrates, respectively.

Table 10. Permeability (Papp) and efflux ratio values of drugs and Trans Epithelial Electric Resistance (TEER, Ωcm2) measured in the rat blood-brain barrier (BBB), native Caco-2, VB-Caco-2, MDCK and MDCK-MDR1 models.

Compound	Primary transport mech.	Major efflux transporters	Rat BBB			Caco-2			VB-Caco-2			MDCK			MDCK-MDR1			
			$Papp_{A-B}$ x10^{-6} cm/s		efflux ratio	$Papp_{A-B}$ x10^{-6} cm/s		efflux ratio	$Papp_{A-B}$ x10^{-6} cm/s		efflux ratio	$Papp_{A-B}$ x10^{-6} cm/sec		efflux ratio	$Papp_{A-B}$ x10^{-6} cm/s		efflux ratio	efflux ratio corrected
			mean	S.D.		mean	S.D.		mean	S.D.		mean	SD		mean	S.D.		
Antipyrine	PT		51.8	1.5	0.88	82.3	3.5	0.80	78.1	2.5	0.97	72.6	2.3	0.98	74.6	3.1	0.96	0.98
Caffeine	PT		64.9	1.9	0.92	84.7	1.0	0.94	85.7	3.0	0.84	79.3	3.2	0.98	78.5	5.6	0.98	1.00
Verapamil	PT/E	P-gp	23.4	2.2	1.36	44.6	8.9	1.33	40.0	7.9	1.60	25.6	10.6	1.59	15.2	0.3	**2.78**	1.75
Indomethacin	PT		33.6	1.3	1.31	50.9	1.4	1.08	50.3	0.5	1.10	47.1	4.4	1.11	45.5	4.3	1.16	1.05
Quinidine	PT/E	P-gp	6.28	0.04	1.93	40.2	3.7	1.06	16.3	3.6	**4.90**	31.8	3.4	1.22	5.19	1.51	**16.4**	**13.5**
Loperamide	PT/E	P-gp	15.6	2.30	1.40	18.1	1.2	1.46	11.5	0.7	**3.13**	9.48	1.03	1.81	4.70	2.67	**17.8**	**9.79**
Atenolol	PP/E	P-gp	1.36	0.20	1.66	0.83	0.19	1.21	0.25	0.09	1.95	0.58	0.20	1.42	0.43	0.14	**2.33**	1.64
Vinblastine	E	P-gp, MRP2	2.42	0.97	0.57	6.97	0.95	**10.5**	0.28	0.07	**270.2**	2.09	0.92	**7.32**	0.21	0.12	**368.5**	**50.5**
Cimetidine	E	P-gp, BCRP	3.86	0.73	0.72	1.97	0.24	**2.23**	0.96	0.56	**3.90**	1.04	0.18	1.32	0.78	0.10	**4.54**	**3.45**
Digoxin	E	P-gp	1.25	0.27	**2.46**	6.50	0.42	**4.72**	0.55	0.17	**65.5**	2.37	0.12	**7.0**	0.57	0.09	**53.1**	**7.56**
Fluorescein-Na	PP		2.72	0.03		1.34	0.29		0.47	0.17		0.65	0.16		0.59	0.06		
			TEER (Ωcm^2), mean ±S.D.															
			548	125		1024	184		2012	347		74	4		84	8		

Compounds were measured at 10 µM, except for sodium fluorescein (100 µM). Bold numbers indicate efflux mechanism (efflux ratio higher than 2). Results for Caco-2, VB-Caco-2, MDCK and MDCK-MDR1 are added as their mean and inter assay S.D. values obtained in at least 3 independent experiments with 3 parallels of identical treatments within assays. For rat BBB model a single experiment (with triplicate inserts) was performed. PT: passive transcellular; PP: passive paracellular; E: Efflux

DOI: 10.14753/SE.2013.1815

DOI: 10.14753/SE.2013.1815

4.2.5. Correlation of in vitro and in vivo drug permeability in rat BBB and in native Caco-2, VB-Caco-2, MDCK and MDCK-MDR1 models

4.2.5.1. Brain tissue and plasma protein binding of reference drugs

The plasma protein- and brain tissue binding of the reference drugs were measured using equilibrium dialysis. The ratio of fu brain and fu plasma (fu: unbound fraction) values were used for the correction of Papp *in vivo* data (fu uncorrected Papp *in vivo* in **Table 11**) that had previously been generated in a mouse brain distribution model (211).

Table 11. Unbound fraction in brain (fu brain) and unbound fraction in plasma (fu plasma) of drugs determined using equilibrium dialysis. *In vivo* permeability based on total brain and plasma concentrations (tissue binding uncorrected ***in vivo Papp***) and *in vivo* permeability data corrected with the ratio of unbound fraction in brain to unbound fraction in plasma (***fu brain/fu plasma – corrected in vivo Papp***).

Compound	Tissue binding					*in vivo* Papp (x 10^{-6} cm/s)	**fu brain** / **fu plasma** ratio - ***corrected*** *in vivo* Papp (x 10^{-6} cm/s)
	unbound fraction in brain (**fu brain**)		unbound fraction in plasma (**fu plasma**)		**fu brain** / **fu plasma** ratio		
	mean	S.D.	mean	S.D.			
Antipyrine	0.967	0.067	0.929	0.077	1.04	10.75	11.19
Caffeine	0.927	0.095	0.980	0.029	0.95	11.11	10.50
Verapamil	0.034	0.009	0.079	0.016	0.43	5.69	2.45
Indomethacin	0.082	0.033	0.017	0.003	4.94	0.13	0.64
Quinidine	0.084	0.028	0.283	0.024	0.30	1.69	0.50
Loperamide	0.008	0.003	0.021	0.002	0.38	1.05	0.40
Atenolol	0.848	0.239	0.980	0.058	0.87	0.23	0.20
Vinblastine	0.013	0.003	0.105	0.031	0.12	1.43	0.18
Cimetidine	0.745	0.330	0.836	0.144	0.89	0.20	0.18
Digoxin	0.243	0.018	0.313	0.019	0.77	0.10	0.08

By *in vitro* equilibrium dialysis antipyrine, caffeine, quinidine, atenolol, digoxin and cimetidine proved to be low plasma protein binding drugs (less than 75% binding), as their fu values were higher than 0.25. Verapamil, indomethacin, loperamide and vinblastine appeared to be moderate/high plasma protein binding drugs (binding equal or higher than 90%), with fu of less than or equal to 0.1.

Taking the fu brain values (unbound fraction in brain tissue) determined also with equilibrium dialysis, the fu brain to fu plasma ratios appeared to be close to 1 for

caffeine, antipyrine, atenolol, cimetidine and digoxin. Ratio 1 indicates that the extent of brain tissue binding and plasma protein binding is quite similar for these compounds, and therefore, Papp *in vivo* values corrected with this ratio appears to be similar to the fu uncorrected Papp *in vivo* data.

The brain tissue binding of verapamil, quinidine and loperamide was slightly higher than their plasma protein binding; therefore, correction with fu brain to fu plasma ratio resulted in a lower *in vivo* Papp values than the uncorrected *in vivo* Papp (2-3-fold shift).

The most dramatic shifts in fu corrected Papp *in vivo* appeared for indomethacin (4.9-fold increase) and vinblastine (8-fold decrease). Indomethacin has high plasma protein binding (fu plasma: 0.017) with relative lower brain tissue binding (fu brain: 0.082), but vinblastine has high brain tissue binding (fu brain: 0.013) with relative lower plasma protein (fu plasma: 0.105); therefore, the fu ratios are significantly deviate from one and markedly change the value of the Papp *in vivo*.

4.2.5.2. Effect of tissue binding and P-gp functionality on in vitro – in vivo permeability correlation

The fu corrected or the fu un-corrected Papp *in vivo* data (calculated on the basis of total drug concentrations) of the reference drugs was plotted against the *in vitro* permeability data determined in rat BBB and in native Caco-2, VB-Caco-2, MDCK and MDCK-MDR1 models. When tissue binding uncorrected Papp *in vivo* data was used, no substantial correlation was observed in any of the models *($r^2 < 0.45$)* for the tested reference compounds (**Table 12**). On the contrary, when the *in vitro* permeabilities were plotted against tissue binding corrected Papp *in vivo* data, a correlation was obtained (r^2 = 0.7989-0.6053); the goodness of fit was similar in the models (**Table 12**, **Fig. 22**), meaning that the correction of *in vivo* permeability with tissue binding substantially improves the correlation. Those compounds with a significant deviation of the fu brain to fu plasma ratio from 1, such as indomethacin (fu brain to plasma 4.9) and vinblastine (fu brain to plasma 0.12), are outliers if uncorrected data is plotted, whereas corrected values substantially improve the power of correlation.

DOI: 10.14753/SE.2013.1815

Table 12. The r^2 values of correlations between *in vitro* permeability (Papp) determined in the different cell based models of drug permeability and the fu brain/fu plasma ratio corrected or the tissue binding uncorrected *in vivo* Papp values. BBB, triple co-culture blood-brain barrier model.

Permeability model	r^2 value	
	in vitro Papp versus. fu brain / fu plasma ratio corrected Papp *in vivo*	*in vitro* Papp versus. tissue binding un-corrected Papp *in vivo*
Rat BBB	0.7989	0.4391
Caco-2	0.6053	0.4430
VB-Caco-2	0.7206	0.3851
MDCK	0.6809	0.4217
MDCK-MDR1	0.7782	0.3352

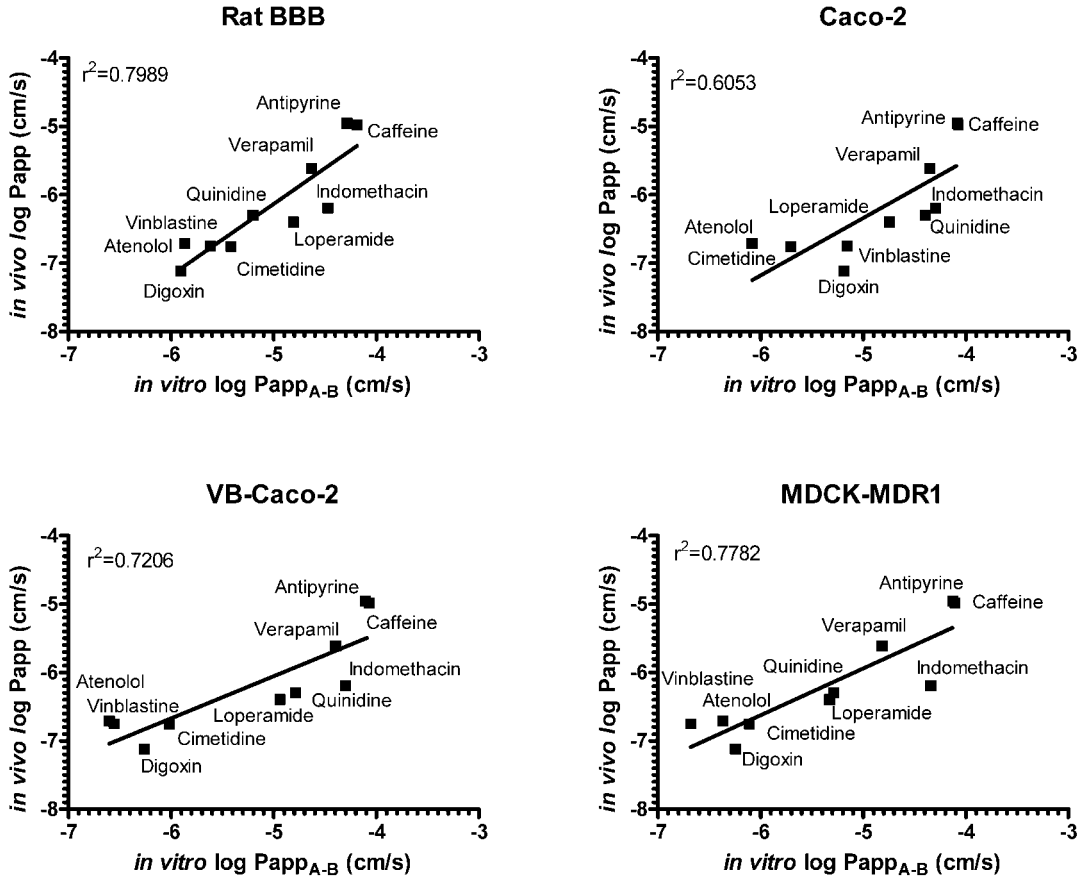

Fig. 22. Plots of *in vitro* permeability (Papp) of reference drugs determined in rat BBB, native Caco-2, VB-Caco-2 and MDCK-MDR1 models with their tissue binding corrected Papp *in vivo* data. The Papp *in vivo* data are based on total brain and total plasma concentrations derived from mouse brain distribution model (211) and corrected with the ratio of fu brain/fu plasma determined in equilibrium dialysis.

DOI: 10.14753/SE.2013.1815

The results also show the positive effect of P-gp functionality in the models on the goodness of *in vitro – in vivo* correlations. The high and low P-gp functionality counterparts VB-Caco-2 versus Caco-2 and MDCK-MDR1 versus MDCK models clearly point to the trend of better predictivity (higher r^2 value) of the high P-gp functionality model in comparison with its low P-gp counterpart (VB-Caco-2 versus native Caco-2 r^2 = 0.7206 versus 0.6053 and MDCK-MDR1 versus MDCK r^2 = 0.7782 versus 0.6809 **Table 12**).

4.2.6. Comparison of high P-gp activity models: VB-Caco-2 versus MDCK-MDR1

In vitro permeability (Papp *in vitro*) was determined for a large set of chemically diverse drugs (n = 59) (**Table 13 and 10**) and NCEs (n = 62) in VB-Caco-2 and the well accepted surrogate BBB model of MDCK-MDR1. A strong correlation was found in terms of the permeability (**Fig. 23**) in the models.

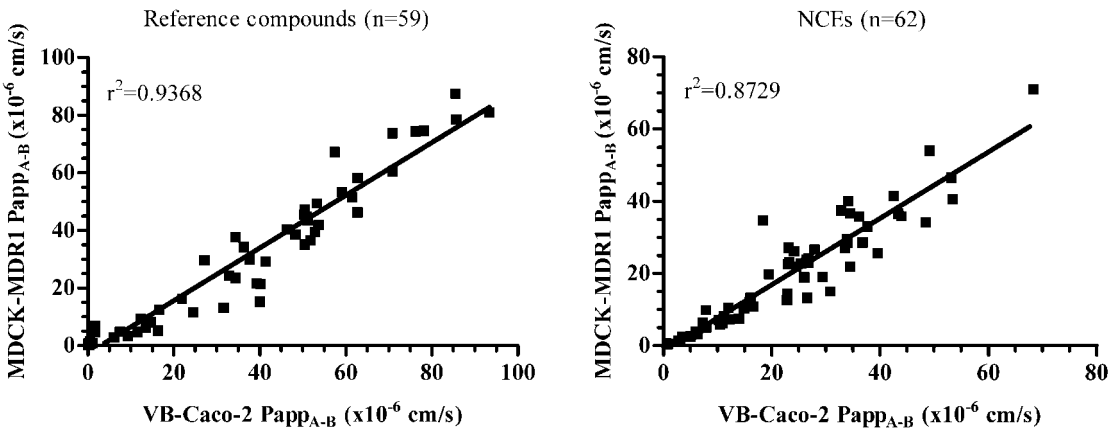

Fig. 23. Correlation between permeability (Papp) data of reference drugs (n=59) and NCEs (n=62) determined in VB-Caco-2 and in MDCK-MDR1 models.

Table 13. Permeability values and efflux ratios of reference drugs measured in VB-Caco-2 and MDCK-MDR1 models.

Compound	VB-Caco-2		MDCK-MDR1			Compound	VB-Caco-2		MDCK-MDR1		
	$Papp_{A-B}$ x10^{-6} cm/s	Efflux ratio	$Papp_{A-B}$ x10^{-6} cm/s	Efflux ratio	Efflux ratio corrected		$Papp_{A-B}$ x10^{-6} cm/s	Efflux ratio	$Papp_{A-B}$ x10^{-6} cm/s	Efflux ratio	Efflux ratio corrected
Aldosterone	32,8	1,4	24,3	2,7	2,5	Alprenolol	51,7	0,9	36,5	0,8	1,1
Estradiol	50,9	0,9	44,8	0,8	1,3	Labetalol	9,3	4,6	3,4	15,3	11,3
Hydrocortisone	21,9	2,3	16,2	6,3	4,6	Risperidone	41,3	1,5	29,2	2,1	1,6
Lidocaine	70,8	0,8	73,7	1,1	1,1	Sulfadiazine	7,4	0,9	4,8	0,7	0,9
Omeprazole	53,2	1,2	49,4	1,7	2,1	Amiloride	1,7	0,5	4,6	0,3	0,9
Phenytoin	62,7	0,9	46,2	1,1	1,0	Guanabenz	51,1	0,9	43,4	1,1	1,0
Progesterone	46,3	1,0	40,3	1,0	1,1	Lisinopril [a]	1,6	1,3	6,9	0,4	0,8
Propranolol	37,6	1,2	29,9	1,0	1,0	Cetirizine	6,1	2,9	2,9	7,7	4,0
Metoprolol	57,4	1,0	67,2	0,8	1,0	Diazepam	70,9	0,9	60,5	0,9	1,0
Colchicine	0,4	29,9	0,8	24,4	3,9	Theophylline	36,2	1,2	34,2	1,1	0,9
Salicylic acid	12,3	1,1	9,3	0,8	1,0	Varenicline	50,4	0,9	47,3	1,0	1,3
Theobromine	34,4	1,0	37,6	1,7	1,1	Donepezil	48,3	1,1	38,5	1,2	1,2
Corticosterone	62,7	0,9	58,2	1,0	1,0	Galantamine	52,8	1,0	39,4	1,4	1,4
Acetaminophen	34,4	0,9	23,5	1,0	1,2	Aniracetam	93,4	0,7	80,9	0,9	1,3
Ketoconazole	27,1	1,2	29,6	1,2	1,1	SB-258585	24,5	2,1	11,6	3,8	2,2
Dexamethasone	13,5	2,9	6,2	8,6	5,6	Dextromethorphan	59,0	0,8	53,3	1,2	1,2
Ranitidine	0,5	3,5	1,5	4,1	2,2	Dextrorphan	40,2	1,1	21,3	2,6	2,0
Chlorothiazide [a]	0,1	21,9	0,7	1,3	1,0	Clomipramine	14,7	0,8	8,1	1,4	1,1
Furosemide [a]	0,3	72,6	0,7	1,6	0,9	Escitalopram	39,2	0,9	21,7	1,5	1,8
Sulfasalazine [a]	0,2	65,8	0,4	1,1	1,0	Duloxetine	16,6	0,9	12,4	1,0	1,0
Doxorubicin [a]	0,1	60,3	0,2	16,6	4,4	Riluzole	85,5	0,9	87,5	0,9	0,9
Talinolol	0,3	35,6	0,4	27,7	5,0	Desipramine	31,5	0,9	13,1	1,4	1,4
Ibuprofen	76,2	0,7	74,3	0,9	0,8	Venlafaxine	50,4	0,8	35,1	1,1	1,5
Warfarin	53,6	0,9	41,8	1,2	1,3	Rhodamine 123 [b]	0,2	19,7	0,2	12,9	3,3
Lamotrigine	61,4	0,9	51,5	0,9	1,0						

Compouds were measured at 10 µM unless otherwise stated. [a] Compounds were measured at 50 µM . [b] Compound was measured at 1 µM.

DOI: 10.14753/SE.2013.1815

DOI: 10.14753/SE.2013.1815

5. Discussion

5.1. Drug penetration model of vinblastine-treated Caco-2 cultures

The P-gp has an impact on the ADME of many substrate drugs, since it is present at the major body barriers such as the epithelial cells of the intestine and kidney, canalicular membranes of hepatocytes and the endothelial cells of the blood-brain barrier. This influence is especially significant by the CNS and by the intestine for the low penetrability or dissolution limited drug substrates (240).

The need for cost-effective critical knowledge on NCEs in early development supports the fast killing of drugs with undesired properties. Penetrability and P-gp liability are among the critical features which determine effective drug levels in the periphery and in the CNS. An *in vitro* model displaying both reliable passive penetrability and P-gp functionality could effectively screen simultaneously for drug penetration and P-gp liability, so it could considerably support the selection of successful development candidates with drug-like properties.

The prediction of human absorption on the ground of Caco-2 based penetration assay is routinely performed during drug development. However, the highly variable, rather low expression of P-gp in Caco-2 cells is normally a limiting factor that does not allow the sensitive and reproducible recognition of P-gp substrates.

In our study, chronic exposure of Caco-2 cells to vinblastine gave the cell population a homogeneous appearance which is in contrast to that of Caco-2 cultures, the latter being known to have a highly heterogeneous morphology (241,242). The VB-Caco-2 cultures display a significantly higher level of P-gp mRNA and protein, and the penetration model based on it maintains high and steady P-gp functionality with negligible variation through a broad passage range of the cells.

Whether it is selection, induction or both, the exact mechanism by which co-incubation with vinblastine leads to the elevation of P-gp level in Caco-2 cultures is not clear. The human pregnane X receptor (hPXR) is described as a major nuclear receptor involved in the regulation of P-gp and several human CYP enzymes like 3A4, 2C8, 2C9 and 2C19. However, studies either report vinblastine as an inducer of the hPXR-ligand

binding domain, but a weak activator of the receptor itself (243), or they describe the relative lack of PXR in Caco-2 cells (244,245) and assume a direct interaction between the drug and the transporter mRNA leading to the induction of P-gp, independent of PXR (145).

An increase in the activity of CYP enzymes – regulated by PXR or in other ways – were not observed in our vinblastine treated Caco-2 cultures. In contrast to unchanged CYP enzymes, the elevation of the P-gp level was clearly apparent.

A selection mechanism applies to the acquisition of drug resistance in many types of cancers. An explanation for this may be that cancer cells express a different array of drug-resistance genes, and overgrowth of the sensitive cells by the drug-resistant variant may occur due to the effect of the anticancer drug (246). In clinical settings the rate of P-gp expression shows correlation with the drug resistance. The selection of drug-resistant cells may be the case in this study as well. Subpopulations with different P-gp activity have been described in Caco-2 cultures (146). Vinblastine, a toxic antimicrotubule drug, enters cells with low P-gp activity, and it may simply select those with strong efflux, resulting in cultures populated with cells with a high level of P-gp mRNA, protein and related functionality. This hypothesis may be supported by the observation that withdrawal of vinblastine did not result in a loss of P-gp protein or P-gp functionality in VB-Caco-2, and the cultures maintained a high level of these features even after a prolonged absence of the drug. In Caco-2 cells Hoskins and co-workers (247) demonstrated that desacetylvinblastine sulfate (DAVLB) evoked selection of resistance in a citotoxicity assay, and unaltered P-gp expression on the cell surface, which was present long after DAVLB withdrawal.

The high sensitivity of VB-Caco-2 for identifying P-gp substrates has been demonstrated in our long term study, in which through 150 passages the eleven reference P-gp substrates tested were all positively recognized by the VB-Caco-2 in bi-directional transport assay. In contrast, standard Caco-2 failed to identify verapamil, quinidine, dexamethasone, loperamide, labetalol, ranitidine and atenolol in the investigated interval (ca 60 passages); even when low (1-10 μM) concentrations were applied.

Untreated Caco-2 cultures did not show efflux for the high permeability verapamil either in our or others' laboratory (147,149). Although our VB-Caco-2

culture is rather sensitive, verapamil was recognised only at a low drug concentration. A similar finding was published by Döppenschmitt et al. (148). The failure of Caco-2 to identify quinidine and ranitidine as P-gp substrates has also been reported (144,145,77); however, other labs were able to detect efflux for quinidine (248,249). The expression level of P-gp in Caco-2 cultures has been reported to be sensitive to simple culture conditions such as the type of supporting membranes (polycarbonate or PET filters) the cells grown on, serum, the length of the cultivation period and the number of seeded cells, which may go some way to explaining the interlaboratory differences (86,91). Shirasaka et al (145) demonstrated 1.4-3.3-fold higher efflux ratios for quinidine, verapamil, vinblastine and digoxin using short term (5 days) Caco-2 cultures grown in 10 nM vinblastine containing special differentiation medium, in comparison to normal Caco-2. The apical to basolateral permeability of vinblastine and quinidine was highly comparable with those measured with MDCK-MDR1. In comparison to Shirasaka's results in our long term (19-21 days) VB-Caco-2 cultures, the efflux response for quinidine, verapamil and vinblastine was even higher; from 2.9 to 29-fold.

The importance of sensitively recognising P-gp substrates is underlined by the fact that the *in vivo* P-gp liability of these exemplary drugs and many others is notable; they demonstrate efflux limited absorption and/or BBB penetration and consequently low brain level (250,251,252,253,254). The results obtained suggest that VB-Caco-2 cells have a major advantage in that they are capable of recognising the P-gp substrates in drug screening more sensitively and consistently than Caco-2. The reliable use of vinblastine treated cultures for penetration testing was demonstrated with maintained P-gp functionality throughout a broad passage range between 40 and 201. Caco-2 is routinely used for permeability testing for a narrower passage range of ca. 10-40 (241,58) and it shows variable P-gp functionality.

The applicability and superiority of VB-Caco-2 culture in penetration screening have also been supported by the test results of 91 new chemical entities from 16 different structure families that emerged from Richter's preclinical research program. Using the VB-Caco-2 based penetrability model, 37% of NCEs were found to be P-gp substrate, in contrast only 9% by Caco-2. It is important to point out that passively penetrating drugs show similar permeability values in both models. Caco-2 is mentioned among the best predictors, if not the best predictor, of passive penetrability even for

brain penetration (143,59). However, VB-Caco-2, with its high and steady P-gp functionality, appears to be a more complex and sensitive model for permeability screening of drug candidates. In addition, the long-term use of VB-Caco-2 for testing P-gp inhibitors in calcein AM assay is also possible based on our results.

5.2. Challenging brain penetration modelling with VB-Caco-2:

Comparison of brain capillary endothelial cell-based and epithelial cell-based surrogate BBB penetration models

The preferred *in vitro* models of brain penetration are based either on brain capillary endothelial cells or on epithelial cells, such as the MDR1-transfected dog kidney MDCK. The human intestinal Caco-2 cells are also frequently challenged for similar application.

These cells of these penetration models originate from distinct anatomical regions of living organisms. A characteristic they share is that they form barriers and express tight intercellular junctional complexes, influx and efflux transport systems. They are genetically programmed to best serve the corresponding organ function. Therefore, it is somewhat surprising that cells of such differing origins could all serve as valuable tools for *in vitro* BBB studies, and cells of non-cerebral origin are capable of providing acceptable predictions of brain penetration. In order to overcome all these contradictions, we studied the critical BBB features like the presence of restrictive paracellular pathway, the BBB-like selective transcellular penetration and functionality of a major brain drug efflux transporter P-gp using reference drugs. We compared the decisive characteristics of human native Caco-2-, the high P-gp expressing VB-Caco-2- and the MDCK-MDR1 epithelial models and the rat brain capillary endothelial cell model grown in triple co-culture with astrocytes and pericytes.

As expected, the electron microscopical morphology of rat brain capillary endothelial cells is greatly different from that of epithelial cell lines, the native Caco-2 and VB-Caco-2 and of MDCK-MDR1. Theoretically, cell morphology and membrane composition determine functionality and consequently drug penetration via the monolayers created by the cells. The TEER and permeability for paracellular low molecular weight tracers are well accepted measures of tightness between cells both *in*

vivo and *in vitro* (200). In our hands, the low molecular weight, low molecular radius paracellular marker sodium fluorescein, also a substrate of MRPs (255), revealed a significantly higher permeability in endothelial cell monolayers than in the epithelial type cells like VB-Caco-2 or MDCK-MDR1 with MRP activity. The data show that despite the differing complexity of the tight junctions (lengths, composition, unity with adherens junctions) and the manner in which the cells tightly attach (apically positioned in epithelial cells versus found along overlapping plasmalemma in brain capillary endothelial cells), epithelial monolayers like VB-Caco-2 and MDCK-MDR1 still provide integrity that is very much on a par with that of brain capillary endothelial monolayers.

TEER, with the exception of MDCKII type monolayers, was well above a 150 Ωcm^2 preferable limit for Caco-2, VB-Caco-2 and rat BBB models (200). Similarly low TEER values for MDCKII cells were published by others as well (143). Low TEER but high integrity for paracellular marker molecules has been reported both in endothelial and epithelial cells (256,223,257). In kidney epithelial cells, where ionic reabsorption is a physiological function, the apparent contradiction between TEER values and low paracellular permeability might be explained by the view that TEER reflects monolayer integrity to movement of ions not only through paracellular pathways but also via ion channels, transporters and ion pores like certain members of claudins. Monolayers with tight paracellular pathways for molecules can have low TEER values if they express high level of ion pores supporting ion movement. Claudin-2, -7, -10, -15 and -16 have pore forming function, and may facilitate cation permeability, thereby decrease TEER (258). According to our yet unpublished results, MDCK and MDCK-MDR1 cells have higher gene expression of claudin-2, -10 and -16 than Caco-2, VB-Caco-2 or rat BBB cells. Low TEER value may not indicate per se disturbed or not well elaborated paracellular pathways or leaky monolayers if paracellular tightness was found high by both morphological and functional methods.

Transcellular penetration is a function of many factors including the distance that has to be travelled by the drug, the lipid composition of membranes and also the involvement of active transporters. The huge differences (10-20-fold) in the average height of brain capillary endothelial cells and of epithelial cell types, and the somewhat differing membrane compositions, may have a notable effect on the transcellular

penetration of drugs. In our study, in the relatively passive model of native Caco-2 a slightly higher permeability rates generally appeared for the different mechanisms of the tested reference drugs in comparison to the rat brain model. For the clearly passive compounds like antipyrine, caffeine and indomethacin this difference varies only slightly, between 1.3 and 1.5-fold. This may mean that the surface area-enhancing microvilli could compensate or slightly overcompensate for the longer route of penetration through the epithelial cells with higher cell thickness.

In our studies, the highest number of P-gp substrates were recognized by the MDCK-MDR1 and VB-Caco-2 models (5 substrates), while the native Caco-2 and the rat BBB model identified only 3 and 1 P-gp substrate drugs, respectively. For drugs intended for CNS penetration identification of efflux (e.g. P-gp) liability is especially important considering the limiting effect of efflux on brain entry and distribution. For peripheral drugs to be substrate of P-gp is advantageous considering that significantly less CNS side effect is expected due to limited brain penetration. Quinidine, vinblastine, loperamide and digoxin are important substrates of P-gp *in vivo* (250,251,253), and were all recognized by the VB-Caco-2 and MDCK-MDR1 models, but not by the rat BBB model applied at an identical test drug concentration. Comparing all the tested drugs and permeability markers, the lowest BBB permeability value measured *in vivo* was obtained with digoxin. Similar result was obtained on the *in vitro* BBB model. Interestingly, on the epithelial models, the multiple efflux pump ligand vinblastine and the paracellular marker atenolol revealed lower penetrability.

The high permeability P-gp substrate verapamil and the low permeability mixed transport mechanism atenolol (paracellular with P-gp efflux) were not identified as P-gp substrates by any of these models at the 10 μM test concentration. As a rule of thumb potential efflux substrates with high passive permeability therefore needs to be tested at a low concentration, when efflux transporters can cope with the influx. Verapamil was only recognized as P-gp substrate by the MDCK-MDR1 (data not show) and the VB-Caco-2 at low concentrations. At a concentration as high as 10 μM, when the high passive inward flux overwhelms limited efflux these two models also failed.

In contrast to verapamil, paracellularly permeable atenolol was detectable as a P-gp substrate reliable at a higher (e.g., 50 μM) concentration, and only by the VB-Caco-2 and MDCK-MDR1 models (data not shown). A similar phenomenon was also found by

others as well (144), where in the case of a paracellular mechanism, low permeability drugs were not detected as P-gp substrates at low cellular concentrations. However, the transporter substrate qualification lacks pharmacological relevance at concentrations that far exceed the therapeutic range.

We measured the permeability of 59 reference drugs and 61 NCEs in the VB-Caco-2 drug penetration model that have not been used before for BBB permeability predictions and in the frequently referenced MDCK-MDR1 surrogate BBB model. The results showed that the VB-Caco-2 model measured passively permeable compounds and P-gp substrates are in excellent correlation with the MDCK-MDR1 model. It is worth mentioning that three highly permeable drugs like aldosterone, omeprazole and dextrorphan were only identified as efflux substrates by the MDCK-MDR1 model. In contrast, sulfasalazine, chlorothiazide, furosemide only qualified as efflux modulated in VB-Caco-2. A plausible explanation for this disturbing finding is that these drugs are known to be substrates of efflux transporters other than P-gp, such as MRPs and BCRP, which are highly expressed in the VB-Caco-2 model, but not in the MDCK-MDR1 model. BCRP and MRPs are also important efflux transporters at BBB involved in drug efflux (5,17,259) besides P-gp. Sulfasalazine is a known BCRP substrate.

With regard to the P-gp mediated efflux functionality of the models, the VB-Caco-2 and MDCK-MDR1 were more sensitive than the rat BBB model. Otherwise, it is clear that among the models tested, the brain capillary endothelial cells are programmed genetically for expressing most transporters that function *in vivo* on the BBB. Using substrate drugs (n = 7) in bidirectional permeability assay, we provide a large set of data on P-gp functionality in brain capillary endothelial monolayers and show their lower capability in comparison with VB-Caco-2 and MDCK-MDR1, for identifying P-gp substrate drugs.

It was suggested that MDCK cell line having low expression of transporters offers a good base for study of passive permeability (260). However, in our study, activity of the canine efflux transporter was shown in agreement with Brayden et al (261), as our parent MDCK model recognized two drugs as efflux substrate (vinblastine and digoxin). Therefore, efflux ratio measured in the MDCK-MDR1 model was corrected with the efflux ratio of the parent cell model in order to eliminate the effect of the canine transporters, in agreement with the FDA.

DOI: 10.14753/SE.2013.1815

Besides the action of the transporters, factors like drug binding in plasma and brain tissue, brain metabolism and the bulk flow toward the cerebrospinal fluid all influence the complex process that determines the rate and extent of brain penetration (262). Several studies highlight that the relative degree of tissue binding between plasma and the brain modulates the penetration of drugs into the brain, and indicate that nonspecific binding is a significant component of the brain-plasma partition coefficient (Kp) (226,263,228,221). It has generally been held that only the extent of brain penetration is influenced by nonspecific binding, but it was recently demonstrated that this factor also determines the rate of brain penetration (233). The results of Summerfield et al. show that the *in situ* brain permeability (P) of drugs determined even in short (30 s) lasting *in situ* brain perfusion is influenced by the binding of drugs to the brain tissue. For those sets of marketed CNS drugs (n=50) the brain tissue was thought to act as a sink helping to drive CNS drug uptake.

In our study, the rate of penetration (Papp) of 10 reference drugs with both a passive and efflux mechanism has been determined in the rat brain endothelial model of BBB and in Caco-2, VB-Caco-2, MDCK and MDCK-MDR1. Plotting the *in vivo* permeability data of all 10 drugs tested against the *in vitro* Papp data resulted in a linear correlation when a tissue binding correction was applied for them. No correlation was seen if we used the total drug concentration-based Papp *in vivo* data in the plots or if we did not exclude the data of indomethacin and vinblastine from this latter plot. The Papp *in vivo* data of indomethacin and vinblastine have been changed most intensely when tissue binding corrections were applied and this correction modified markedly the outcome of correlations.

Hypothetically, a higher brain tissue binding relative to plasma protein binding acts as a driving force that helps to maintain a dynamic diffusion gradient across the BBB. This may even attenuate the effect of efflux transporters, and not just help the brain entry of an otherwise low permeability drug (221), like in the case of vinblastine. For indomethacin, this driving force is absent, having much lower brain tissue binding relative to its plasma protein binding, and so results in lower penetrability (Papp *in vivo*) than expected based on its *in vitro* intrinsic permeability (in agreement with Fridén et al., (264)).

DOI: 10.14753/SE.2013.1815

6. Conclusions and novel findings

A high P-gp expressing VB-Caco-2 culture was developed via vinblastine treatment of Caco-2 cells and characterized in comparison to Caco-2 culture. The VB-Caco-2 cells show compact, homogenous monolayers, similar passive permeability as Caco-2 model in bidirectional transport assay, but the VB-Caco-2 model is more sensitive in identifying P-gp substrates and could reliably be used with steady P-gp features through long passages. It is suitable when using in bidirectional transport assay for the prediction of drug absorption, examination of P-gp mediated interactions and for studying of P-gp inhibitors in calcein AM assay. We showed that omitting vinblastine from established VB-Caco-2 cultures did not affect either the protein level or the functionality of P-gp, which confirms the selectional mechanism of vinblastine.

Furthermore, comparison of epithelial cell-based models, including the VB-Caco-2 model, as possible surrogate BBB models, was performed with the primary brain capillary endothelial BBB model (EPA). Despite the different morphology, epithelial-based models provide integrity that is very much on a par with that of rat BBB model, and the models show similar passive transcellular permeability, which makes them highly comparable to the rat BBB model. While the functionality of the most important BBB efflux transporter P-gp in the rat BBB model was low, the VB-Caco-2 and the MDCK-MDR1 models identified the highest number of P-gp substrate drugs.

Significant correlation was obtained between the *in vitro* and *in vivo* brain permeability using all models if the *in vivo* values were corrected with the ratio of free fraction of brain and plasma. It was first shown that correction of the *in vivo* Papp obtained in mouse brain distribution model with the ratio of unbound fractions improve the *in vitro – in vivo* correlations.

A strong correlation was found in terms of the permeability in the VB-Caco-2 and the well accepted surrogate BBB model of MDCK-MDR1 for a large set of chemically diverse drugs and NCEs.

DOI: 10.14753/SE.2013.1815

In conclusion, the VB-Caco-2 culture provides a reliable tool for the penetration screening of drugs and NCEs. The VB-Caco-2 model with steady P-gp features is suitable for the identification of P-gp substrates with drug-drug interaction potential. The VB-Caco-2 model may provide an alternative of the widely recognized surrogate BBB model MDCK-MDR1 and the more labour-intense and expensive brain capillary endothelial-based BBB model for fast screening of drug candidates for brain permeability.

DOI: 10.14753/SE.2013.1815

7. Summary

The permeability of new chemical entities (NCE) is routinely screened in preclinical drug research. It is important for the prediction of human absorption as well as brain penetration of NCEs. Caco-2 is a well-established model for human absorption, but the identification of P-glycoprotein (P-gp) substrates and therefore, the predictive accuracy of this model is not always satisfactory. Vinblastine has been reported to affect P-gp expression in Caco-2 cells. Therefore, the effect of sustained vinblastine treatment on the expression and functionality of P-gp was studied, using RT-PCR, Western blot techniques and bidirectional transport assay. Completion of culture medium with vinblastine increased the P-gp mRNA and the expression at protein level. The vinblastine-treated Caco-2 (VB-Caco-2) model shows similar passive permeability as Caco-2 model in bidirectional transport assay, but the VB-Caco-2 model is more sensitive in identifying P-gp substrates. The P-gp expression and activity remains consistently high in the VB-Caco-2 cell line over 150 passages. Furthermore, comparison of epithelial cell-based models, including the VB-Caco-2 model and the well accepted surrogate BBB model of MDCK-MDR1, as possible surrogate BBB models, was performed with the primary brain capillary endothelial BBB model (EPA). Epithelial-based models provide integrity that is very much on a par with that of rat BBB model, and the models show similar passive transcellular permeability. While the P-gp functionality of the rat BBB model was low, the VB-Caco-2 and the MDCK-MDR1 models identified the highest number of P-gp substrate drugs. Significant correlation was obtained between the *in vitro* and *in vivo* brain permeability using all models if the *in vivo* values were corrected with the ratio of free fraction of brain and plasma. The VB-Caco-2 culture provides a reliable tool for the penetration screening of drugs and NCEs. The VB-Caco-2 model with steady P-gp features is suitable for the identification of P-gp substrates with drug-drug interaction potential. The VB-Caco-2 model may provide an alternative of the MDCK-MDR1 model and the more labour-intense and expensive brain capillary endothelial-based BBB model for fast screening of drug candidates for brain permeability.

DOI: 10.14753/SE.2013.1815

8. Összefoglalás

Az újonnan szintetizált vegyületek és gyógyszerjelölt molekulák permeábilitásának szűrése a preklinikai vizsgálatok fontos része, ami a molekulák intesztinális felszívódásának és az agyi penetrációjának előrejelzése miatt szükséges. A Caco-2 egy gyakran alkalmazott, hatékony humán abszorpciós modell, de a P-glikoprotein (P-gp) szubsztrátokat bizonytalanul mutatja ki, ami rontja a predikciós értékét. A vinblasztinról kimutatták, hogy Caco-2 sejtekben befolyásolja a P-gp expresszióját. Kísérleteinkben a krónikus vinblasztin kezelés hatását vizsgáltuk a Caco-2 sejtek P-gp szintjére és funkcionalitására RT-PCR-rel, Western blottal és kétirányú transzport esszé segítségével. A médiumhoz adott vinblasztin növelte a P-gp mRNS és fehérje szintjét. A vinblasztinnal kezelt Caco-2 (VB-Caco-2) modell a passzív permeábilitású vegyületeket a natív Caco-2 modellhez hasonlóan méri, de a P-gp szubsztrátokat érzékenyebben ismeri fel. Kimutattuk, hogy a P-gp aktivitása egyenletesen magas marad a vizsgált 150 passzáláson keresztül. A továbbiakban összehasonlítottuk a VB-Caco-2 és a széles körben alkalmazott MDCK-MDR1 epiteliális alapú modelleket, mint lehetséges agyi endotélt helyettesítő BBB modelleket a primer kapilláris endotél alapú hármas kultúra modellel (EPA). A modellek hasonlóan alacsony permeábilitást mutatnak a paracelluláris markerekre, és hasonló transzcelluláris passzív penetrációt. Míg az agyi endotél modell gyenge P-gp funkcionalitást mutatott, a VB-Caco-2 és az MDCK-MDR1 modellek mutatták ki a legtöbb vizsgált P-gp szubsztrát gyógyszert. Az *in vitro* - *in vivo* agyi permeábilitás között mindegyik modellben szignifikáns korreláció áll fenn, ha az *in vivo* értékeket korrigáljuk az agyi és a plazma szabad frakciók hányadosával. A VB-Caco-2 sejtkultúra a gyógyszerek és gyógyszerjelöltek szkrínelésére kiválóan alkalmas modell. A magas és stabil P-gp expresszió miatt az interakciós potenciállal rendelkező P-gp szubsztrátok azonosítására, vizsgálatára is alkalmas. A VB-Caco-2 modell megfelelő szkrín alternatívája lehet a széles körben elfogadott agyi endotélt helyettesítő MDCK-MDR1 modellnek, illetve a drága és nehezebben kivitelezhető agyi kapilláris endotél alapú modellnek.

DOI: 10.14753/SE.2013.1815

9. References

1. Buxton ILO, Benet LZ. Pharmacokinetics: The dynamics of drug absorption, distribution, metabolism, and elimination. In: Brunton LL, Chabner BA, Knollmann BC (Eds.), Goodman and Gilman's The Pharmacological Basis of Therapeutics. The McGraw-Hill Companies, Inc., New York, 2011: 17-39.

2. Giacomini KMSY. Membrane transporters and drug response. In: Brunton LL, Chabner BA, Knollmann BC (Eds.), Goodman and Gilman's The Pharmacological Basis of Therapeutics. The McGraw-Hill Companies, Inc., New York, 2011: 89-121.

3. Aller SG, Yu J, Ward A, Weng Y, Chittaboina S, Zhuo R, Harrell PM, Trinh YT, Zhang Q, Urbatsch IL, Chang G. (2009) Structure of P-glycoprotein reveals a molecular basis for poly-specific drug binding. Science, 323: 1718-1722.

4. Ayrton A, Morgan P. (2001) Role of transport proteins in drug absorption, distribution and excretion. Xenobiotica, 31: 469-497.

5. Begley DJ. (2004) ABC transporters and the blood-brain barrier. Curr Pharm Des, 10: 1295-1312.

6. Lin JH. (2003) Drug-drug interaction mediated by inhibition and induction of P-glycoprotein. Adv Drug Deliv Rev, 55: 53-81.

7. Chan LM, Lowes S, Hirst BH. (2004) The ABCs of drug transport in intestine and liver: efflux proteins limiting drug absorption and bioavailability. Eur J Pharm Sci, 21: 25-51.

8. del Amo EM, Heikkinen AT, Monkkonen J. (2009) In vitro-in vivo correlation in P-glycoprotein mediated transport in intestinal absorption. Eur J Pharm Sci, 36: 200-211.

9. Lin JH. (2004) How significant is the role of P-glycoprotein in drug absorption and brain uptake? Drugs Today (Barc), 40: 5-22.

10. Suzuki H, Sugiyama Y. (2000) Role of metabolic enzymes and efflux transporters in the absorption of drugs from the small intestine. Eur J Pharm Sci, 12: 3-12.

11. Bernsdorf A, Giessmann T, Modess C, Wegner D, Igelbrink S, Hecker U, Haenisch S, Cascorbi I, Terhaag B, Siegmund W. (2006) Simvastatin does not influence the intestinal P-glycoprotein and MPR2, and the disposition of talinolol after chronic medication in healthy subjects genotyped for the ABCB1, ABCC2 and SLCO1B1 polymorphisms. Br J Clin Pharmacol, 61: 440-450.

12. Giessmann T, May K, Modess C, Wegner D, Hecker U, Zschiesche M, Dazert P, Grube M, Schroeder E, Warzok R, Cascorbi I, Kroemer HK, Siegmund W. (2004) Carbamazepine regulates intestinal P-glycoprotein and multidrug resistance protein MRP2 and influences disposition of talinolol in humans. Clin Pharmacol Ther, 76: 192-200.

13. Masuda S, Uemoto S, Goto M, Fujimoto Y, Tanaka K, Inui K. (2004) Tacrolimus therapy according to mucosal MDR1 levels in small-bowel transplant recipients. Clin Pharmacol Ther, 75: 352-361.

14. Murakami T, Takano M. (2008) Intestinal efflux transporters and drug absorption. Expert Opin Drug Metab Toxicol, 4: 923-939.

15. Westphal K, Weinbrenner A, Zschiesche M, Franke G, Knoke M, Oertel R, Fritz P, von RO, Warzok R, Hachenberg T, Kauffmann HM, Schrenk D, Terhaag B, Kroemer HK, Siegmund W. (2000) Induction of P-glycoprotein by rifampin

increases intestinal secretion of talinolol in human beings: a new type of drug/drug interaction. Clin Pharmacol Ther, 68: 345-355.

16. Takano M, Yumoto R, Murakami T. (2006) Expression and function of efflux drug transporters in the intestine. Pharmacol Ther, 109: 137-161.

17. Giacomini KM, Huang SM, Tweedie DJ, Benet LZ, Brouwer KL, Chu X, Dahlin A, Evers R, Fischer V, Hillgren KM, Hoffmaster KA, Ishikawa T, Keppler D, Kim RB, Lee CA, Niemi M, Polli JW, Sugiyama Y, Swaan PW, Ware JA, Wright SH, Yee SW, Zamek-Gliszczynski MJ, Zhang L. (2010) Membrane transporters in drug development. Nat Rev Drug Discov, 9: 215-236.

18. Rivera S.M., Goodman Gilman A. Drug invention and the pharmaceutical industry. In: Brunton LL, Chabner BA, Knollman BC (Eds.), Goodman and Gilman's The Pharmacological Basis of Therapeutics. The McGraw-Hill Companies, Inc., New York, 2011: 3-16.

19. Walker DK. (2004) The use of pharmacokinetic and pharmacodynamic data in the assessment of drug safety in early drug development. Br J Clin Pharmacol, 58: 601-608.

20. Kola I, Landis J. (2004) Can the pharmaceutical industry reduce attrition rates? Nat Rev Drug Discov, 3: 711-715.

21. Dahan AS, Amidon GL. Gastrointestinal dissolution and absorption of class II drugs. In: Waterbeemd H, Testa B (Eds.), Drug bioavailability. Wiley VCH, Weinheim, 2009: 191-215.

22. Iatropoulos MJ. Morphology of the gastrointestinal tract. In: Rozman K, Hannen O (Eds.), Gastrointestinal toxicology. Elsevier, Amsterdam, 1986: 246-266.

23. Kaminsky LS, Zhang QY. (2003) The small intestine as a xenobiotic-metabolizing organ. Drug Metab Dispos, 31: 1520-1525.

24. Lin JH, Chiba M, Baillie TA. (1999) Is the role of the small intestine in first-pass metabolism overemphasized? Pharmacol Rev, 51: 135-158.

25. Rhoades R, Pflanzer R. (1992) The Gastrointestinal System. Human Physiology. 777-822.

26. Avdeef A, Tam KY. (2010) How well can the Caco-2/Madin-Darby canine kidney models predict effective human jejunal permeability? J Med Chem, 53: 3566-3584.

27. Barrett KE, Barman S.M., Boitano S, Brooks HL. (2010) Ganong's review of medical physiology.

28. Agoram B, Woltosz WS, Bolger MB. (2001) Predicting the impact of physiological and biochemical processes on oral drug bioavailability. Adv Drug Deliv Rev, 50 Suppl 1:S41-67.: S41-S67.

29. Fallingborg J, Christensen LA, Ingeman-Nielsen M, Jacobsen BA, Abildgaard K, Rasmussen HH. (1989) pH-profile and regional transit times of the normal gut measured by a radiotelemetry device. Aliment Pharmacol Ther, 3: 605-613.

30. Hilgendorf C, Ahlin G, Seithel A, Artursson P, Ungell AL, Karlsson J. (2007) Expression of thirty-six drug transporter genes in human intestine, liver, kidney, and organotypic cell lines. Drug Metab Dispos, 35: 1333-1340.

31. Mouly S, Paine MF. (2003) P-glycoprotein increases from proximal to distal regions of human small intestine. Pharm Res, 20: 1595-1599.

32. Paine MF, Khalighi M, Fisher JM, Shen DD, Kunze KL, Marsh CL, Perkins JD, Thummel KE. (1997) Characterization of interintestinal and intraintestinal variations in human CYP3A-dependent metabolism. J Pharmacol Exp Ther, 283: 1552-1562.

33. Paine MF, Hart HL, Ludington SS, Haining RL, Rettie AE, Zeldin DC. (2006) The human intestinal cytochrome P450 "pie". Drug Metab Dispos, 34: 880-886.

34. Davis SS. (2005) Formulation strategies for absorption windows. Drug Discov Today, 10: 249-257.

35. Lipinski CA. (2000) Drug-like properties and the causes of poor solubility and poor permeability. J Pharmacol Toxicol Methods, 44: 235-249.

36. Veber DF, Johnson SR, Cheng HY, Smith BR, Ward KW, Kopple KD. (2002) Molecular properties that influence the oral bioavailability of drug candidates. J Med Chem, 45: 2615-2623.

37. Zhao YH, Le J, Abraham MH, Hersey A, Eddershaw PJ, Luscombe CN, Butina D, Beck G, Sherborne B, Cooper I, Platts JA. (2001) Evaluation of human intestinal absorption data and subsequent derivation of a quantitative structure-activity relationship (QSAR) with the Abraham descriptors. J Pharm Sci, 90: 749-784.

38. Lennernas H. (1997) Human jejunal effective permeability and its correlation with preclinical drug absorption models. J Pharm Pharmacol, 49: 627-638.

39. Dokoumetzidis A, Kalantzi L, Fotaki N. (2007) Predictive models for oral drug absorption: from in silico methods to integrated dynamical models. Expert Opin Drug Metab Toxicol, 3: 491-505.

40. Hou T, Li Y, Zhang W, Wang J. (2009) Recent developments of in silico predictions of intestinal absorption and oral bioavailability. Comb Chem High Throughput Screen, 12: 497-506.

41. Metcalfe PD, Thomas S. (2010) Challenges in the prediction and modeling of oral absorption and bioavailability. Curr Opin Drug Discov Devel, 13: 104-110.

42. Wang J, Skolnik S. (2010) Mitigating permeability-mediated risks in drug discovery. Expert Opin Drug Metab Toxicol, 6: 171-187.

43. Hamalainen MD, Frostell-Karlsson A. (2004) Predicting the intestinal absorption potential of hits and leads. Drug Discov Today: Technologies, 1: 397-405.

44. Clark DE. (1999) Rapid calculation of polar molecular surface area and its application to the prediction of transport phenomena. 1. Prediction of intestinal absorption. J Pharm Sci, 88: 807-814.

45. Palm K, Stenberg P, Luthman K, Artursson P. (1997) Polar molecular surface properties predict the intestinal absorption of drugs in humans. Pharm Res, 14: 568-571.

46. Demel MA, Schwaha R, Kramer O, Ettmayer P, Haaksma EE, Ecker GF. (2008) In silico prediction of substrate properties for ABC-multidrug transporters. Expert Opin Drug Metab Toxicol, 4: 1167-1180.

47. Winiwarter S, Hilgendorf C. (2008) Modeling of drug-transporter interactions using structural information. Curr Opin Drug Discov Devel, 11: 95-103.

48. Corti G, Maestrelli F, Cirri M, Furlanetto S, Mura P. (2006) Development and evaluation of an in vitro method for prediction of human drug absorption I. Assessment of artificial membrane composition. Eur J Pharm Sci, 27: 346-353.

49. Corti G, Maestrelli F, Cirri M, Zerrouk N, Mura P. (2006) Development and evaluation of an in vitro method for prediction of human drug absorption II. Demonstration of the method suitability. Eur J Pharm Sci, 27: 354-362.

50. Danelian E, Karlen A, Karlsson R, Winiwarter S, Hansson A, Lofas S, Lennernas H, Hamalainen MD. (2000) SPR biosensor studies of the direct

interaction between 27 drugs and a liposome surface: correlation with fraction absorbed in humans. J Med Chem, 43: 2083-2086.

51. Pidgeon C, Ong S, Liu H, Qiu X, Pidgeon M, Dantzig AH, Munroe J, Hornback WJ, Kasher JS, Glunz L, . (1995) IAM chromatography: an in vitro screen for predicting drug membrane permeability. J Med Chem, 38: 590-594.

52. Avdeef A, Bendels S, Di L, Faller B, Kansy M, Sugano K, Yamauchi Y. (2007) PAMPA--critical factors for better predictions of absorption. J Pharm Sci, 96: 2893-2909.

53. Kansy M, Senner F, Gubernator K. (1998) Physicochemical high throughput screening: parallel artificial membrane permeation assay in the description of passive absorption processes. J Med Chem, 41: 1007-1010.

54. Kansy M, Avdeef A, Fischer H. (2004) Advances in screening for membrane permeability: high-resolution PAMPA for medicinal chemists. Drug Discovery Today: Technologies, 1: 349-355.

55. Balimane PV, Chong S, Morrison RA. (2000) Current methodologies used for evaluation of intestinal permeability and absorption. J Pharmacol Toxicol Methods, 44: 301-312.

56. Mahida YR, Makh S, Hyde S, Gray T, Borriello SP. (1996) Effect of Clostridium difficile toxin A on human intestinal epithelial cells: induction of interleukin 8 production and apoptosis after cell detachment. Gut, 38: 337-347.

57. Moyer MP. (1983) Culture of human gastrointestinal epithelial cells. Proc Soc Exp Biol Med, 174: 12-15.

58. Hubatsch I, Ragnarsson EG, Artursson P. (2007) Determination of drug permeability and prediction of drug absorption in Caco-2 monolayers. Nat Protoc, 2: 2111-2119.

59. Ungell AL. (2004) Caco-2 replace or refine? Drug Discov Today: Technol, 1: 423-430.

60. Delie F, Rubas W. (1997) A human colonic cell line sharing similarities with enterocytes as a model to examine oral absorption: advantages and limitations of the Caco-2 model. Crit Rev Ther Drug Carrier Syst, 14: 221-286.

61. Anderle P, Rakhmanova V, Woodford K, Zerangue N, Sadee W. (2003) Messenger RNA expression of transporter and ion channel genes in undifferentiated and differentiated Caco-2 cells compared to human intestines. Pharm Res, 20: 3-15.

62. Seithel A, Karlsson J, Hilgendorf C, Bjorquist A, Ungell AL. (2006) Variability in mRNA expression of ABC- and SLC-transporters in human intestinal cells: comparison between human segments and Caco-2 cells. Eur J Pharm Sci, 28: 291-299.

63. Sun D, Lennernas H, Welage LS, Barnett JL, Landowski CP, Foster D, Fleisher D, Lee KD, Amidon GL. (2002) Comparison of human duodenum and Caco-2 gene expression profiles for 12,000 gene sequences tags and correlation with permeability of 26 drugs. Pharm Res, 19: 1400-1416.

64. Spahn-Langguth H, Langguth P. (2001) Grapefruit juice enhances intestinal absorption of the P-glycoprotein substrate talinolol. Eur J Pharm Sci, 12: 361-367.

65. Lin X, Skolnik S, Chen X, Wang J. (2011) Attenuation of intestinal absorption by major efflux transporters: quantitative tools and strategies using a Caco-2 model. Drug Metab Dispos, 39: 265-274.

66. Balimane PV, Marino A, Chong S. (2008) P-gp inhibition potential in cell-based models: which "calculation" method is the most accurate? AAPS J, 10: 577-586.

67. Ming X, Thakker DR. (2010) Role of basolateral efflux transporter MRP4 in the intestinal absorption of the antiviral drug adefovir dipivoxil. Biochem Pharmacol, 79: 455-462.

68. Wang Q, Strab R, Kardos P, Ferguson C, Li J, Owen A, Hidalgo IJ. (2008) Application and limitation of inhibitors in drug-transporter interactions studies. Int J Pharm, 356: 12-18.

69. Annaert P, Ye ZW, Stieger B, Augustijns P. (2010) Interaction of HIV protease inhibitors with OATP1B1, 1B3, and 2B1. Xenobiotica, 40: 163-176.

70. Maeda T, Takahashi K, Ohtsu N, Oguma T, Ohnishi T, Atsumi R, Tamai I. (2007) Identification of influx transporter for the quinolone antibacterial agent levofloxacin. Mol Pharm, 4: 85-94.

71. Yamakawa Y, Hamada A, Shuto T, Yuki M, Uchida T, Kai H, Kawaguchi T, Saito H. (2011) Pharmacokinetic impact of SLCO1A2 polymorphisms on imatinib disposition in patients with chronic myeloid leukemia. Clin Pharmacol Ther, 90: 157-163.

72. Gram LK, Rist GM, Lennernas H, Steffansen B. (2009) Impact of carriers in oral absorption: Permeation across Caco-2 cells for the organic anions estrone-3-sulfate and glipizide. Eur J Pharm Sci, 37: 378-386.

73. Kis O, Zastre JA, Ramaswamy M, Bendayan R. (2010) pH dependence of organic anion-transporting polypeptide 2B1 in Caco-2 cells: potential role in antiretroviral drug oral bioavailability and drug-drug interactions. J Pharmacol Exp Ther, 334: 1009-1022.

74. Sai Y, Kaneko Y, Ito S, Mitsuoka K, Kato Y, Tamai I, Artursson P, Tsuji A. (2006) Predominant contribution of organic anion transporting polypeptide OATP-B (OATP2B1) to apical uptake of estrone-3-sulfate by human intestinal Caco-2 cells. Drug Metab Dispos, 34: 1423-1431.

75. Artursson P, Palm K, Luthman K. (2001) Caco-2 monolayers in experimental and theoretical predictions of drug transport. Adv Drug Deliv Rev, 46: 27-43.

76. Lennernas H. (1998) Human intestinal permeability. J Pharm Sci, 87: 403-410.

77. Skolnik S, Lin X, Wang J, Chen XH, He T, Zhang B. (2010) Towards prediction of in vivo intestinal absorption using a 96-well Caco-2 assay. J Pharm Sci, 99: 3246-3265.

78. Huang SM, Strong JM, Zhang L, Reynolds KS, Nallani S, Temple R, Abraham S, Habet SA, Baweja RK, Burckart GJ, Chung S, Colangelo P, Frucht D, Green MD, Hepp P, Karnaukhova E, Ko HS, Lee JI, Marroum PJ, Norden JM, Qiu W, Rahman A, Sobel S, Stifano T, Thummel K, Wei XX, Yasuda S, Zheng JH, Zhao H, Lesko LJ. (2008) New era in drug interaction evaluation: US Food and Drug Administration update on CYP enzymes, transporters, and the guidance process. J Clin Pharmacol, 48: 662-670.

79. Anderle P, Niederer E, Rubas W, Hilgendorf C, Spahn-Langguth H, Wunderli-Allenspach H, Merkle HP, Langguth P. (1998) P-Glycoprotein (P-gp) mediated efflux in Caco-2 cell monolayers: the influence of culturing conditions and drug exposure on P-gp expression levels. J Pharm Sci, 87: 757-762.

80. Korjamo T, Monkkonen J, Uusitalo J, Turpeinen M, Pelkonen O, Honkakoski P. (2006) Metabolic and efflux properties of Caco-2 cells stably transfected with nuclear receptors. Pharm Res, 23: 1991-2001.

81. Lampen A, Bader A, Bestmann T, Winkler M, Witte L, Borlak JT. (1998) Catalytic activities, protein- and mRNA-expression of cytochrome P450 isoenzymes in intestinal cell lines. Xenobiotica, 28: 429-441.

82. Prueksaritanont T, Gorham LM, Hochman JH, Tran LO, Vyas KP. (1996) Comparative studies of drug-metabolizing enzymes in dog, monkey, and human small intestines, and in Caco-2 cells. Drug Metab Dispos, 24: 634-642.

83. Sun H, Chow EC, Liu S, Du Y, Pang KS. (2008) The Caco-2 cell monolayer: usefulness and limitations. Expert Opin Drug Metab Toxicol, 4: 395-411.

84. Chong S, Dando SA, Soucek KM, Morrison RA. (1996) In vitro permeability through caco-2 cells is not quantitatively predictive of in vivo absorption for peptide-like drugs absorbed via the dipeptide transporter system. Pharm Res, 13: 120-123.

85. Balimane PV, Han YH, Chong S. (2006) Current industrial practices of assessing permeability and P-glycoprotein interaction. AAPS J, 8: E1-13.

86. Behrens I, Kissel T. (2003) Do cell culture conditions influence the carrier-mediated transport of peptides in Caco-2 cell monolayers? Eur J Pharm Sci, 19: 433-442.

87. Wikman A, Karlsson J, Carlstedt I, Artursson P. (1993) A drug absorption model based on the mucus layer producing human intestinal goblet cell line HT29-H. Pharm Res, 10: 843-852.

88. Wils P, Warnery A, Phung-Ba V, Scherman D. (1994) Differentiated intestinal epithelial cell lines as in vitro models for predicting the intestinal absorption of drugs. Cell Biol Toxicol, 10: 393-397.

89. Barthe L, Woodley J, Houin G. (1999) Gastrointestinal absorption of drugs: methods and studies. Fundam Clin Pharmacol, 13: 154-168.

90. Haslam IS, Jones K, Coleman T, Simmons NL. (2008) Induction of P-glycoprotein expression and function in human intestinal epithelial cells (T84). Biochem Pharmacol, 76: 850-861.

91. Volpe DA. (2008) Variability in Caco-2 and MDCK cell-based intestinal permeability assays. J Pharm Sci, 97: 712-725.

92. Irvine JD, Takahashi L, Lockhart K, Cheong J, Tolan JW, Selick HE, Grove JR. (1999) MDCK (Madin-Darby canine kidney) cells: A tool for membrane permeability screening. J Pharm Sci, 88: 28-33.

93. Wang Q, Rager JD, Weinstein K, Kardos PS, Dobson GL, Li J, Hidalgo IJ. (2005) Evaluation of the MDR-MDCK cell line as a permeability screen for the blood-brain barrier. Int J Pharm, 288: 349-359.

94. Tavelin S, Milovic V, Ocklind G, Olsson S, Artursson P. (1999) A conditionally immortalized epithelial cell line for studies of intestinal drug transport. J Pharmacol Exp Ther, 290: 1212-1221.

95. Le FE, Chesne C, Artusson P, Brayden D, Fabre G, Gires P, Guillou F, Rousset M, Rubas W, Scarino ML. (2001) In vitro models of the intestinal barrier. The report and recommendations of ECVAM Workshop 46. European Centre for the Validation of Alternative methods. Altern Lab Anim, 29: 649-668.

96. Quastel JH. (1961) Technics for studies of intestinal absorption in vitro. Methods Med Res, 9: 273-286.

97. Fisher RB, Parsons DS. (1949) A preparation of surviving rat small intestine for the study of absorption. J Physiol, 110: 36-46, pl.

98. Andlauer W, Kolb J, Stehle P, Furst P. (2000) Absorption and metabolism of genistein in isolated rat small intestine. J Nutr, 130: 843-846.

99. Plauth M, Raible A, Bauder-Gross D, Vieillard-Baron D, Furst P, Hartmann F. (1991) Effects of dexamethasone on glutamine metabolism in the isolated vascularly perfused rat small intestine. Res Exp Med (Berl), 191: 349-357.

100. Wei Y, Neves LA, Franklin T, Klyuchnikova N, Placzek B, Hughes HM, Curtis CG. (2009) Vascular perfused segments of human intestine as a tool for drug absorption. Drug Metab Dispos, 37: 731-736.

101. Hidalgo IJ. (2001) Assessing the absorption of new pharmaceuticals. Curr Top Med Chem, 1: 385-401.

102. Carreno-Gomez B, Duncan R. (2000) Everted rat intestinal sacs: a new model for the quantitation of P-glycoprotein mediated-efflux of anticancer agents. Anticancer Res, 20: 3157-3161.

103. Leppert PS, Fix JA. (1994) Use of everted intestinal rings for in vitro examination of oral absorption potential. J Pharm Sci, 83: 976-981.

104. Barthe L, Woodley JF, Kenworthy S, Houin G. (1998) An improved everted gut sac as a simple and accurate technique to measure paracellular transport across the small intestine. Eur J Drug Metab Pharmacokinet, 23: 313-323.

105. Lacombe O, Woodley J, Solleux C, Delbos JM, Boursier-Neyret C, Houin G. (2004) Localisation of drug permeability along the rat small intestine, using markers of the paracellular, transcellular and some transporter routes. Eur J Pharm Sci, 23: 385-391.

106. Ballent M, Lifschitz A, Virkel G, Sallovitz J, Lanusse C. (2006) Modulation of the P-glycoprotein-mediated intestinal secretion of ivermectin: in vitro and in vivo assessments. Drug Metab Dispos, 34: 457-463.

107. Bouer R, Barthe L, Philibert C, Tournaire C, Woodley J, Houin G. (1999) The roles of P-glycoprotein and intracellular metabolism in the intestinal absorption of methadone: in vitro studies using the rat everted intestinal sac. Fundam Clin Pharmacol, 13: 494-500.

108. Lafforgue G, Arellano C, Vachoux C, Woodley J, Philibert C, Dupouy V, Bousquet-Melou A, Gandia P, Houin G. (2008) Oral absorption of ampicillin: role of paracellular route vs. PepT1 transporter. Fundam Clin Pharmacol, 22: 189-201.

109. Arellano C, Philibert C, Vachoux C, Woodley J, Houin G. (2007) The metabolism of midazolam and comparison with other CYP enzyme substrates during intestinal absorption: in vitro studies with rat everted gut sacs. J Pharm Pharm Sci, 10: 26-36.

110. Maeda Y, Omoda K, Konishi T, Takahashi M, Kihira K, Hibino S, Tsukiai S. (1993) Effects of aluminium-containing antacid on bioavailability of ofloxacin following oral administration of pivaloyloxymethyl ester of ofloxacin as prodrug. Biol Pharm Bull, 16: 594-599.

111. Quevedo MA, Brinon MC. (2009) In vitro and in vivo pharmacokinetic characterization of two novel prodrugs of zidovudine. Antiviral Res, 83: 103-111.

112. Yang CY, Chao PD, Hou YC, Tsai SY, Wen KC, Hsiu SL. (2006) Marked decrease of cyclosporin bioavailability caused by coadministration of ginkgo and onion in rats. Food Chem Toxicol, 44: 1572-1578.

113. Cornaire G, Woodley JF, Saivin S, Legendre JY, Decourt S, Cloarec A, Houin G. (2000) Effect of polyoxyl 35 castor oil and Polysorbate 80 on the intestinal absorption of digoxin in vitro. Arzneimittelforschung, 50: 576-579.

114. Ussing HH, Zerahn K. (1951) Active transport of sodium as the source of electric current in the short-circuited isolated frog skin. Acta Physiol Scand, 23: 110-127.

115. Clarke LL. (2009) A guide to Ussing chamber studies of mouse intestine. Am J Physiol Gastrointest Liver Physiol, 296: G1151-G1166.

116. Hillgren KM, Kato A, Borchardt RT. (1995) In vitro systems for studying intestinal drug absorption. Med Res Rev, 15: 83-109.

117. Mardones P, Andrinolo D, Csendes A, Lagos N. (2004) Permeability of human jejunal segments to gonyautoxins measured by the Ussing chamber technique. Toxicon, 44: 521-528.

118. Matysiak-Budnik T, Coffin B, Lavergne-Slove A, Sabate JM, Megraud F, Heyman M. (2004) Helicobacter pylori increases the epithelial permeability to a food antigen in human gastric biopsies. Am J Gastroenterol, 99: 225-232.

119. Wallon C, Braaf Y, Wolving M, Olaison G, Soderholm JD. (2005) Endoscopic biopsies in Ussing chambers evaluated for studies of macromolecular permeability in the human colon. Scand J Gastroenterol, 40: 586-595.

120. Nishimura T, Amano N, Kubo Y, Ono M, Kato Y, Fujita H, Kimura Y, Tsuji A. (2007) Asymmetric intestinal first-pass metabolism causes minimal oral bioavailability of midazolam in cynomolgus monkey. Drug Metab Dispos, 35: 1275-1284.

121. van de Kerkhof EG, Ungell AL, Sjoberg AK, de Jager MH, Hilgendorf C, de G, I, Groothuis GM. (2006) Innovative methods to study human intestinal drug metabolism in vitro: precision-cut slices compared with ussing chamber preparations. Drug Metab Dispos, 34: 1893-1902.

122. Kikuchi A, Nozawa T, Wakasawa T, Maeda T, Tamai I. (2006) Transporter-mediated intestinal absorption of fexofenadine in rats. Drug Metab Pharmacokinet, 21: 308-314.

123. Sugiyama T, Yamamoto A, Kawabe Y, Uchiyama T, Quan YS, Muranishi S. (1997) Effects of various absorption enhancers on the intestinal absorption of water soluble drugs by in vitro Ussing chamber method: correlation with an in situ absorption experiment. Biol Pharm Bull, 20: 812-814.

124. Bohets H, Annaert P, Mannens G, Van BL, Anciaux K, Verboven P, Meuldermans W, Lavrijsen K. (2001) Strategies for absorption screening in drug discovery and development. Curr Top Med Chem, 1: 367-383.

125. Jezyk N, Rubas W, Grass GM. (1992) Permeability characteristics of various intestinal regions of rabbit, dog, and monkey. Pharm Res, 9: 1580-1586.

126. Stavchansky S, Berndt C. Experimental and theoretical methods to study drug permeability. In: Amidon G, Lesko L, Midha K, Shah V, Hilfinger J (Eds.), International bioequivalence standards: A new era. TSRL Inc., Ann Arbor, 2006: 49-115.

127. Kaddoumi A, Fleisher D, Heimbach T, Li LY, Cole S. (2006) Factors influencing regional differences in intestinal absorption of UK-343,664 in rat: possible role in dose-dependent pharmacokinetics. J Pharm Sci, 95: 435-445.

128. Sababi M, Borga O, Hultkvist-Bengtsson U. (2001) The role of P-glycoprotein in limiting intestinal regional absorption of digoxin in rats. Eur J Pharm Sci, 14: 21-27.

129. Song NN, Li QS, Liu CX. (2006) Intestinal permeability of metformin using single-pass intestinal perfusion in rats. World J Gastroenterol, 12: 4064-4070.

130. Blanchard J, Tang LM, Earle ME. (1990) Reevaluation of the absorption of carbenoxolone using an in situ rat intestinal technique. J Pharm Sci, 79: 411-414.

131. Uhing MR, Kimura RE. (1995) The effect of surgical bowel manipulation and anesthesia on intestinal glucose absorption in rats. J Clin Invest, 95: 2790-2798.

132. Yuasa H, Matsuda K, Watanabe J. (1995) Influence of anesthetic regimens on the intestinal absorption of 5-fluorouracil in rats. Biol Pharm Bull, 18: 747-752.

133. de Zwart LL, Rompelberg CJM, Sips AJAM, Welink J, van Engelen JGM, (1999) Anatomical and physiological differences between various species used in studies on the pharmacokinetics and toxicology of xenobiotics. A review of literature. Report National Istitute of Public Health and the Environment, RIVM, Bilthoven, Netherlands.

134. DeSesso JM, Jacobson CF. (2001) Anatomical and physiological parameters affecting gastrointestinal absorption in humans and rats. Food Chem Toxicol, 39: 209-228.

135. He YL, Murby S, Warhurst G, Gifford L, Walker D, Ayrton J, Eastmond R, Rowland M. (1998) Species differences in size discrimination in the paracellular pathway reflected by oral bioavailability of poly(ethylene glycol) and D-peptides. J Pharm Sci, 87: 626-633.

136. Gres MC, Julian B, Bourrie M, Meunier V, Roques C, Berger M, Boulenc X, Berger Y, Fabre G. (1998) Correlation between oral drug absorption in humans, and apparent drug permeability in TC-7 cells, a human epithelial intestinal cell line: comparison with the parental Caco-2 cell line. Pharm Res, 15: 726-733.

137. Hayeshi R, Hilgendorf C, Artursson P, Augustijns P, Brodin B, Dehertogh P, Fisher K, Fossati L, Hovenkamp E, Korjamo T, Masungi C, Maubon N, Mols R, Mullertz A, Monkkonen J, O'Driscoll C, Oppers-Tiemissen HM, Ragnarsson EG, Rooseboom M, Ungell AL. (2008) Comparison of drug transporter gene expression and functionality in Caco-2 cells from 10 different laboratories. Eur J Pharm Sci, 35: 383-396.

138. Lentz KA, Hayashi J, Lucisano LJ, Polli JE. (2000) Development of a more rapid, reduced serum culture system for Caco-2 monolayers and application to the biopharmaceutics classification system. Int J Pharm, 200: 41-51.

139. Liang E, Chessic K, Yazdanian M. (2000) Evaluation of an accelerated Caco-2 cell permeability model. J Pharm Sci, 89: 336-345.

140. Uchida M, Fukazawa T, Yamazaki Y, Hashimoto H, Miyamoto Y. (2009) A modified fast (4 day) 96-well plate Caco-2 permeability assay. J Pharmacol Toxicol Methods, 59: 39-43.

141. Yamashita S, Konishi K, Yamazaki Y, Taki Y, Sakane T, Sezaki H, Furuyama Y. (2002) New and better protocols for a short-term Caco-2 cell culture system. J Pharm Sci, 91: 669-679.

142. Mariadason JM, Rickard KL, Barkla DH, Augenlicht LH, Gibson PR. (2000) Divergent phenotypic patterns and commitment to apoptosis of Caco-2 cells during spontaneous and butyrate-induced differentiation. J Cell Physiol, 183: 347-354.

143. Garberg P, Ball M, Borg N, Cecchelli R, Fenart L, Hurst RD, Lindmark T, Mabondzo A, Nilsson JE, Raub TJ, Stanimirovic D, Terasaki T, Oberg JO, Osterberg T. (2005) In vitro models for the blood-brain barrier. Toxicol In Vitro, 19: 299-334.

144. Lentz KA, Polli JW, Wring SA, Humphreys JE, Polli JE. (2000) Influence of passive permeability on apparent P-glycoprotein kinetics. Pharm Res, 17: 1456-1460.

145. Shirasaka Y, Kawasaki M, Sakane T, Omatsu H, Moriya Y, Nakamura T, Sakaeda T, Okumura K, Langguth P, Yamashita S. (2006) Induction of human P-glycoprotein in Caco-2 cells: development of a highly sensitive assay system for P-glycoprotein-mediated drug transport. Drug Metab Pharmacokinet, 21: 414-423.

146. Horie K, Tang F, Borchardt RT. (2003) Isolation and characterization of Caco-2 subclones expressing high levels of multidrug resistance protein efflux transporter. Pharm Res, 20: 161-168.

147. Korjamo T, Honkakoski P, Toppinen MR, Niva S, Reinisalo M, Palmgren JJ, Monkkonen J. (2005) Absorption properties and P-glycoprotein activity of modified Caco-2 cell lines. Eur J Pharm Sci, 26: 266-279.

148. Doppenschmitt S, Spahn-Langguth H, Regardh CG, Langguth P. (1999) Role of P-glycoprotein-mediated secretion in absorptive drug permeability: An approach using passive membrane permeability and affinity to P-glycoprotein. J Pharm Sci, 88: 1067-1072.

149. Shirasaka Y, Sakane T, Yamashita S. (2008) Effect of P-glycoprotein expression levels on the concentration-dependent permeability of drugs to the cell membrane. J Pharm Sci, 97: 553-565.

150. Siissalo S, Laitinen L, Koljonen M, Vellonen KS, Kortejarvi H, Urtti A, Hirvonen J, Kaukonen AM. (2007) Effect of cell differentiation and passage number on the expression of efflux proteins in wild type and vinblastine-induced Caco-2 cell lines. Eur J Pharm Biopharm, 67: 548-554.

151. Eneroth A, Astrom E, Hoogstraate J, Schrenk D, Conrad S, Kauffmann HM, Gjellan K. (2001) Evaluation of a vincristine resistant Caco-2 cell line for use in a calcein AM extrusion screening assay for P-glycoprotein interaction. Eur J Pharm Sci, 12: 205-214.

152. Laska DA, Houchins JO, Pratt SE, Horn J, Xia X, Hanssen BR, Williams DC, Dantzig AH, Lindstrom T. (2002) Characterization and application of a vinblastine-selected CACO-2 cell line for evaluation of p-glycoprotein. In Vitro Cell Dev Biol Anim, 38: 401-410.

153. Doppenschmitt S, Spahn-Langguth H, Regardh CG, Langguth P. (1998) Radioligand-binding assay employing P-glycoprotein-overexpressing cells: testing drug affinities to the secretory intestinal multidrug transporter. Pharm Res, 15: 1001-1006.

154. Doppenschmitt S, Langguth P, Regardh CG, Andersson TB, Hilgendorf C, Spahn-Langguth H. (1999) Characterization of binding properties to human P-glycoprotein: development of a [3H]verapamil radioligand-binding assay. J Pharmacol Exp Ther, 288: 348-357.

155. Abbott NJ. (2004) Evidence for bulk flow of brain interstitial fluid: significance for physiology and pathology. Neurochem Int, 45: 545-552.

156. Abbott NJ, Ronnback L, Hansson E. (2006) Astrocyte-endothelial interactions at the blood-brain barrier. Nat Rev Neurosci, 7: 41-53.

157. Abbott NJ, Patabendige AA, Dolman DE, Yusof SR, Begley DJ. (2010) Structure and function of the blood-brain barrier. Neurobiol Dis, 37: 13-25.

158. Schlageter KE, Molnar P, Lapin GD, Groothuis DR. (1999) Microvessel organization and structure in experimental brain tumors: microvessel populations with distinctive structural and functional properties. Microvasc Res, 58: 312-328.

159. Wilhelm I, Fazakas C, Krizbai IA. (2011) In vitro models of the blood-brain barrier. Acta Neurobiol Exp (Wars), 71: 113-128.

160. Hellstrom M, Gerhardt H, Kalen M, Li X, Eriksson U, Wolburg H, Betsholtz C. (2001) Lack of pericytes leads to endothelial hyperplasia and abnormal vascular morphogenesis. J Cell Biol, 153: 543-553.

161. Lai CH, Kuo KH. (2005) The critical component to establish in vitro BBB model: Pericyte. Brain Res Brain Res Rev, 50: 258-265.

162. Zlokovic BV. (2008) The blood-brain barrier in health and chronic neurodegenerative disorders. Neuron, 57: 178-201.

163. Kacem K, Lacombe P, Seylaz J, Bonvento G. (1998) Structural organization of the perivascular astrocyte endfeet and their relationship with the endothelial glucose transporter: a confocal microscopy study. Glia, 23: 1-10.

164. Hawkins BT, Davis TP. (2005) The blood-brain barrier/neurovascular unit in health and disease. Pharmacol Rev, 57: 173-185.

165. Tontsch U, Bauer HC. (1989) Isolation, characterization, and long-term cultivation of porcine and murine cerebral capillary endothelial cells. Microvasc Res, 37: 148-161.

166. Wolburg H, Lippoldt A. (2002) Tight junctions of the blood-brain barrier: development, composition and regulation. Vascul Pharmacol, 38: 323-337.

167. Deli MA. Drug Transport and the Blood-Brain Barrier. In: Tihanyi K, Vastag M (Eds.), Solubility, delivery and ADME problems of drugs and drug candidates. Bentham Science, 2011: 144-165.

168. Begley DJ, Brightman MW. (2003) Structural and functional aspects of the blood-brain barrier. Prog Drug Res, 61:39-78.: 39-78.

169. el-Bacha RS, Minn A. (1999) Drug metabolizing enzymes in cerebrovascular endothelial cells afford a metabolic protection to the brain. Cell Mol Biol (Noisy -le-grand), 45: 15-23.

170. Bauer B, Hartz AM, Lucking JR, Yang X, Pollack GM, Miller DS. (2008) Coordinated nuclear receptor regulation of the efflux transporter, Mrp2, and the phase-II metabolizing enzyme, GSTpi, at the blood-brain barrier. J Cereb Blood Flow Metab, 28: 1222-1234.

171. Minn A, Ghersi-Egea JF, Perrin R, Leininger B, Siest G. (1991) Drug metabolizing enzymes in the brain and cerebral microvessels. Brain Res Brain Res Rev, 16: 65-82.

172. Cserr HF, Bundgaard M. (1984) Blood-brain interfaces in vertebrates: a comparative approach. Am J Physiol, 246: R277-R288.

173. Bernacki J, Dobrowolska A, Nierwinska K, Malecki A. (2008) Physiology and pharmacological role of the blood-brain barrier. Pharmacol Rep, 60: 600-622.

174. Gingrich MB, Junge CE, Lyuboslavsky P, Traynelis SF. (2000) Potentiation of NMDA receptor function by the serine protease thrombin. J Neurosci, 20: 4582-4595.

175. Nadal A, Fuentes E, Pastor J, McNaughton PA. (1995) Plasma albumin is a potent trigger of calcium signals and DNA synthesis in astrocytes. Proc Natl Acad Sci U S A, 92: 1426-1430.

176. Banks WA. (2009) Characteristics of compounds that cross the blood-brain barrier. BMC Neurol, 9 Suppl 1: S3.

177. Pardridge WM. (2002) Drug and gene targeting to the brain with molecular Trojan horses. Nat Rev Drug Discov, 1: 131-139.

178. Enerson BE, Drewes LR. (2006) The rat blood-brain barrier transcriptome. J Cereb Blood Flow Metab, 26: 959-973.

179. del Amo EM, Urtti A, Yliperttula M. (2008) Pharmacokinetic role of L-type amino acid transporters LAT1 and LAT2. Eur J Pharm Sci, 35: 161-174.

180. Dallas S, Miller DS, Bendayan R. (2006) Multidrug resistance-associated proteins: expression and function in the central nervous system. Pharmacol Rev, 58: 140-161.

181. Fricker G, Miller DS. (2004) Modulation of drug transporters at the blood-brain barrier. Pharmacology, 70: 169-176.

182. Ohtsuki S, Terasaki T. (2007) Contribution of carrier-mediated transport systems to the blood-brain barrier as a supporting and protecting interface for the brain; importance for CNS drug discovery and development. Pharm Res, 24: 1745-1758.

183. Terasaki T, Ohtsuki S. (2005) Brain-to-blood transporters for endogenous substrates and xenobiotics at the blood-brain barrier: an overview of biology and methodology. NeuroRx, 2: 63-72.

184. Loscher W, Potschka H. (2005) Drug resistance in brain diseases and the role of drug efflux transporters. Nat Rev Neurosci, 6: 591-602.

185. Banks WA. (1999) Physiology and pathology of the blood-brain barrier: implications for microbial pathogenesis, drug delivery and neurodegenerative disorders. J Neurovirol, 5: 538-555.

186. Joo F. (1996) Endothelial cells of the brain and other organ systems: some similarities and differences. Prog Neurobiol, 48: 255-273.

187. Gonzalez-Mariscal L, Betanzos A, Nava P, Jaramillo BE. (2003) Tight junction proteins. Prog Biophys Mol Biol, 81: 1-44.

188. Furuse M, Hirase T, Itoh M, Nagafuchi A, Yonemura S, Tsukita S, Tsukita S. (1993) Occludin: a novel integral membrane protein localizing at tight junctions. J Cell Biol, 123: 1777-1788.

189. Martin-Padura I, Lostaglio S, Schneemann M, Williams L, Romano M, Fruscella P, Panzeri C, Stoppacciaro A, Ruco L, Villa A, Simmons D, Dejana E. (1998) Junctional adhesion molecule, a novel member of the immunoglobulin superfamily that distributes at intercellular junctions and modulates monocyte transmigration. J Cell Biol, 142: 117-127.

190. Furuse M, Fujita K, Hiiragi T, Fujimoto K, Tsukita S. (1998) Claudin-1 and -2: novel integral membrane proteins localizing at tight junctions with no sequence similarity to occludin. J Cell Biol, 141: 1539-1550.

191. Breier G, Breviario F, Caveda L, Berthier R, Schnurch H, Gotsch U, Vestweber D, Risau W, Dejana E. (1996) Molecular cloning and expression of murine vascular endothelial-cadherin in early stage development of cardiovascular system. Blood, 87: 630-641.

192. Vorbrodt AW, Dobrogowska DH. (2004) Molecular anatomy of interendothelial junctions in human blood-brain barrier microvessels. Folia Histochem Cytobiol, 42: 67-75.

193. Itoh M, Morita K, Tsukita S. (1999) Characterization of ZO-2 as a MAGUK family member associated with tight as well as adherens junctions with a binding affinity to occludin and alpha catenin. J Biol Chem, 274: 5981-5986.

194. Vastag M, Keseru GM. (2009) Current in vitro and in silico models of blood-brain barrier penetration: a practical view. Curr Opin Drug Discov Devel, 12: 115-124.

195. Veszelka SKÁ, Deli MA. Tools for Modelling Blood-Brain Barrier Penetrability. In: Tihanyi K, Vastag M (Eds.), Solubility, delivery and ADME problems of drugs and drug candidates. Bentham Science, 2011: 166-188.

196. Abbott NJ, Dolman DE, Patabendige AK. (2008) Assays to predict drug permeation across the blood-brain barrier, and distribution to brain. Curr Drug Metab, 9: 901-910.

197. Gumbleton M, Audus KL. (2001) Progress and limitations in the use of in vitro cell cultures to serve as a permeability screen for the blood-brain barrier. J Pharm Sci, 90: 1681-1698.

198. Vastag M, Hellinger É, Bakk ML, Tihanyi K. (2011) Cell based models of blood-brain barrier penetration. Ther Deliv, 2: 549-553.

199. Crone C, Olesen SP. (1982) Electrical resistance of brain microvascular endothelium. Brain Res, 241: 49-55.

200. Deli MA, Abraham CS, Kataoka Y, Niwa M. (2005) Permeability studies on in vitro blood-brain barrier models: physiology, pathology, and pharmacology. Cell Mol Neurobiol, 25: 59-127.

201. Ohno K, Pettigrew KD, Rapoport SI. (1978) Lower limits of cerebrovascular permeability to nonelectrolytes in the conscious rat. Am J Physiol, 235: H299-H307.

202. Avdeef A. High-Throughput Measurement of Permeability Profiles. In: van de Waterbeemd H, Lennernas P, Artursson P (Eds.), Drug bioavailability. Estimation of solubility, permeability, absorption and bioavailability. Wiley-VCH, Weinheim, 2003: 46-71.

203. Reichel A. (2006) The role of blood-brain barrier studies in the pharmaceutical industry. Curr Drug Metab, 7: 183-203.

204. Dehouck MP, Meresse S, Delorme P, Fruchart JC, Cecchelli R. (1990) An easier, reproducible, and mass-production method to study the blood-brain barrier in vitro. J Neurochem, 54: 1798-1801.

205. Bachmeier CJ, Trickler WJ, Miller DW. (2006) Comparison of drug efflux transport kinetics in various blood-brain barrier models. Drug Metab Dispos, 34: 998-1003.

206. Nakagawa S, Deli MA, Nakao S, Honda M, Hayashi K, Nakaoke R, Kataoka Y, Niwa M. (2007) Pericytes from brain microvessels strengthen the barrier

integrity in primary cultures of rat brain endothelial cells. Cell Mol Neurobiol, 27: 687-694.

207. Berezowski V, Landry C, Dehouck MP, Cecchelli R, Fenart L. (2004) Contribution of glial cells and pericytes to the mRNA profiles of P-glycoprotein and multidrug resistance-associated proteins in an in vitro model of the blood-brain barrier. Brain Res, 1018: 1-9.

208. El HB, Chappey O, Piciotti M, Debray M, Boval B, Roux F. (1997) Modulation of P-glycoprotein activity by glial factors and retinoic acid in an immortalized rat brain microvessel endothelial cell line. Neurosci Lett, 236: 107-111.

209. Zhang Y, Li CS, Ye Y, Johnson K, Poe J, Johnson S, Bobrowski W, Garrido R, Madhu C. (2006) Porcine brain microvessel endothelial cells as an in vitro model to predict in vivo blood-brain barrier permeability. Drug Metab Dispos, 34: 1935-1943.

210. Culot M, Lundquist S, Vanuxeem D, Nion S, Landry C, Delplace Y, Dehouck MP, Berezowski V, Fenart L, Cecchelli R. (2008) An in vitro blood-brain barrier model for high throughput (HTS) toxicological screening. Toxicol In Vitro, 22: 799-811.

211. Nakagawa S, Deli MA, Kawaguchi H, Shimizudani T, Shimono T, Kittel A, Tanaka K, Niwa M. (2009) A new blood-brain barrier model using primary rat brain endothelial cells, pericytes and astrocytes. Neurochem Int, 54: 253-263.

212. Perriere N, Demeuse P, Garcia E, Regina A, Debray M, Andreux JP, Couvreur P, Scherrmann JM, Temsamani J, Couraud PO, Deli MA, Roux F. (2005) Puromycin-based purification of rat brain capillary endothelial cell cultures. Effect on the expression of blood-brain barrier-specific properties. J Neurochem, 93: 279-289.

213. Cecchelli R, Dehouck B, Descamps L, Fenart L, Buee-Scherrer V, V, Duhem C, Lundquist S, Rentfel M, Torpier G, Dehouck MP. (1999) In vitro model for evaluating drug transport across the blood-brain barrier. Adv Drug Deliv Rev, 36: 165-178.

214. Cecchelli R, Berezowski V, Lundquist S, Culot M, Renftel M, Dehouck MP, Fenart L. (2007) Modelling of the blood-brain barrier in drug discovery and development. Nat Rev Drug Discov, 6: 650-661.

215. Kasa P, Pakaski M, Joo F, Lajtha A. (1991) Endothelial cells from human fetal brain microvessels may be cholinoceptive, but do not synthesize acetylcholine. J Neurochem, 56: 2143-2146.

216. Perriere N, Yousif S, Cazaubon S, Chaverot N, Bourasset F, Cisternino S, Decleves X, Hori S, Terasaki T, Deli M, Scherrmann JM, Temsamani J, Roux F, Couraud PO. (2007) A functional in vitro model of rat blood-brain barrier for molecular analysis of efflux transporters. Brain Res, 1150:1-13. Epub;%2007 Mar 12.: 1-13.

217. Roux F, Durieu-Trautmann O, Chaverot N, Claire M, Mailly P, Bourre JM, Strosberg AD, Couraud PO. (1994) Regulation of gamma-glutamyl transpeptidase and alkaline phosphatase activities in immortalized rat brain microvessel endothelial cells. J Cell Physiol, 159: 101-113.

218. Weksler BB, Subileau EA, Perriere N, Charneau P, Holloway K, Leveque M, Tricoire-Leignel H, Nicotra A, Bourdoulous S, Turowski P, Male DK, Roux F, Greenwood J, Romero IA, Couraud PO. (2005) Blood-brain barrier-specific properties of a human adult brain endothelial cell line. FASEB J, 19: 1872-1874.

219. Cucullo L, Couraud PO, Weksler B, Romero IA, Hossain M, Rapp E, Janigro D. (2008) Immortalized human brain endothelial cells and flow-based vascular modeling: a marriage of convenience for rational neurovascular studies. J Cereb Blood Flow Metab, 28: 312-328.

220. Carrara S, Reali V, Misiano P, Dondio G, Bigogno C. (2007) Evaluation of in vitro brain penetration: optimized PAMPA and MDCKII-MDR1 assay comparison. Int J Pharm, 345: 125-133.

221. Summerfield SG, Stevens AJ, Cutler L, del Carmen OM, Hammond B, Tang SP, Hersey A, Spalding DJ, Jeffrey P. (2006) Improving the in vitro prediction of in vivo central nervous system penetration: integrating permeability, P-glycoprotein efflux, and free fractions in blood and brain. J Pharmacol Exp Ther, 316: 1282-1290.

222. Hakkarainen JJ, Jalkanen AJ, Kaariainen TM, Keski-Rahkonen P, Venalainen T, Hokkanen J, Monkkonen J, Suhonen M, Forsberg MM. (2010) Comparison of in vitro cell models in predicting in vivo brain entry of drugs. Int J Pharm, 402: 27-36.

223. Lohmann C, Huwel S, Galla HJ. (2002) Predicting blood-brain barrier permeability of drugs: evaluation of different in vitro assays. J Drug Target, 10: 263-276.

224. Feng B, LaPerle JL, Chang G, Varma MV. (2010) Renal clearance in drug discovery and development: molecular descriptors, drug transporters and disease state. Expert Opin Drug Metab Toxicol, 6: 939-952.

225. Kusuhara H, Sugiyama Y. (2009) In vitro-in vivo extrapolation of transporter-mediated clearance in the liver and kidney. Drug Metab Pharmacokinet, 24: 37-52.

226. Hammarlund-Udenaes M, Friden M, Syvanen S, Gupta A. (2008) On the rate and extent of drug delivery to the brain. Pharm Res, 25: 1737-1750.

227. Hammarlund-Udenaes M. (2010) Active-site concentrations of chemicals - are they a better predictor of effect than plasma/organ/tissue concentrations? Basic Clin Pharmacol Toxicol, 106: 215-220.

228. Reichel A. (2009) Addressing central nervous system (CNS) penetration in drug discovery: basics and implications of the evolving new concept. Chem Biodivers, 6: 2030-2049.

229. Shen DD, Artru AA, Adkison KK. (2004) Principles and applicability of CSF sampling for the assessment of CNS drug delivery and pharmacodynamics. Adv Drug Deliv Rev, 56: 1825-1857.

230. Hammarlund-Udenaes M. (2000) The use of microdialysis in CNS drug delivery studies. Pharmacokinetic perspectives and results with analgesics and antiepileptics. Adv Drug Deliv Rev, 45: 283-294.

231. Maurer TS, Debartolo DB, Tess DA, Scott DO. (2005) Relationship between exposure and nonspecific binding of thirty-three central nervous system drugs in mice. Drug Metab Dispos, 33: 175-181.

232. van de WH, Smith DA, Jones BC. (2001) Lipophilicity in PK design: methyl, ethyl, futile. J Comput Aided Mol Des, 15: 273-286.

233. Summerfield SG, Read K, Begley DJ, Obradovic T, Hidalgo IJ, Coggon S, Lewis AV, Porter RA, Jeffrey P. (2007) Central nervous system drug disposition: the relationship between in situ brain permeability and brain free fraction. J Pharmacol Exp Ther, 322: 205-213.

234. Evers R, Kool M, Smith AJ, van DL, de HM, Borst P. (2000) Inhibitory effect of the reversal agents V-104, GF120918 and Pluronic L61 on MDR1 Pgp-, MRP1- and MRP2-mediated transport. Br J Cancer, 83: 366-374.

235. Lowry OH, Rosebrough NJ, Farr AL, Randall RJ. (1951) Protein measurement with the Folin phenol reagent. J Biol Chem, 193: 265-275.

236. Schwab D, Fischer H, Tabatabaei A, Poli S, Huwyler J. (2003) Comparison of in vitro P-glycoprotein screening assays: recommendations for their use in drug discovery. J Med Chem, 46: 1716-1725.

237. Bauer B, Miller DS, Fricker G. (2003) Compound profiling for P-glycoprotein at the blood-brain barrier using a microplate screening system. Pharm Res, 20: 1170-1176.

238. Ungell AL, Karlsson J. Cell cultures in drug discovery: An industrial perspective. In: van de Waterbeemd H, Lennernas H, Artursson P (Eds.), Drug bioavailability. Estimation of solubility, permeability, absorption and bioavailability. Wiley-VCH, Weinheim, 2003: 90-131.

239. Polli JW, Wring SA, Humphreys JE, Huang L, Morgan JB, Webster LO, Serabjit-Singh CS. (2001) Rational use of in vitro P-glycoprotein assays in drug discovery. J Pharmacol Exp Ther, 299: 620-628.

240. Szakacs G, Varadi A, Ozvegy-Laczka C, Sarkadi B. (2008) The role of ABC transporters in drug absorption, distribution, metabolism, excretion and toxicity (ADME-Tox). Drug Discov Today, 13: 379-393.

241. Briske-Anderson MJ, Finley JW, Newman SM. (1997) The influence of culture time and passage number on the morphological and physiological development of Caco-2 cells. Proc Soc Exp Biol Med, 214: 248-257.

242. Walter E, Kissel T. (1995) Heterogeneity in the human intestinal cell line Caco-2 leads to differences in the transepithelial transport. Eur J Pharm Sci, 3: 215-230.

243. Smith NF, Mani S, Huang H, Bates SE, Figg WD, Sparreboom A. (2006) Induction of cytochrome P450 3A4 (CYP3A4) by vinblastine. Clin Pharmacol Ther, 79: 35.

244. Mitin T, Von Moltke LL, Court MH, Greenblatt DJ. (2004) Levothyroxine up-regulates P-glycoprotein independent of the pregnane X receptor. Drug Metab Dispos, 32: 779-782.

245. Thummel KE, Brimer C, Yasuda K, Thottassery J, Senn T, Lin Y, Ishizuka H, Kharasch E, Schuetz J, Schuetz E. (2001) Transcriptional control of intestinal cytochrome P-4503A by 1alpha,25-dihydroxy vitamin D3. Mol Pharmacol, 60: 1399-1406.

246. Gottesman MM. (2002) Mechanisms of cancer drug resistance. Annu Rev Med, 53: 615-627.

247. Hoskins J, DeHerdt SV, Moore RE, Bumol TF. (1993) The development and characterization of Vinca alkaloid-resistant Caco-2 human colorectal cell lines expressing mdr-1. Int J Cancer, 53: 680-688.

248. Neuhoff S, Ungell AL, Zamora I, Artursson P. (2003) pH-dependent bidirectional transport of weakly basic drugs across Caco-2 monolayers: implications for drug-drug interactions. Pharm Res, 20: 1141-1148.

249. Troutman MD, Thakker DR. (2003) Efflux ratio cannot assess P-glycoprotein-mediated attenuation of absorptive transport: asymmetric effect of P-glycoprotein on absorptive and secretory transport across Caco-2 cell monolayers. Pharm Res, 20: 1200-1209.

250. Kusuhara H, Suzuki H, Terasaki T, Kakee A, Lemaire M, Sugiyama Y. (1997) P-Glycoprotein mediates the efflux of quinidine across the blood-brain barrier. J Pharmacol Exp Ther, 283: 574-580.

251. Mizuno N, Niwa T, Yotsumoto Y, Sugiyama Y. (2003) Impact of drug transporter studies on drug discovery and development. Pharmacol Rev, 55: 425-461.

252. Sadeque AJ, Wandel C, He H, Shah S, Wood AJ. (2000) Increased drug delivery to the brain by P-glycoprotein inhibition. Clin Pharmacol Ther, 68: 231-237.

253. Schinkel AH, Wagenaar E, van DL, Mol CA, Borst P. (1995) Absence of the mdr1a P-Glycoprotein in mice affects tissue distribution and pharmacokinetics of dexamethasone, digoxin, and cyclosporin A. J Clin Invest, 96: 1698-1705.

254. Schinkel AH, Wagenaar E, Mol CA, van DL. (1996) P-glycoprotein in the blood-brain barrier of mice influences the brain penetration and pharmacological activity of many drugs. J Clin Invest, 97: 2517-2524.

255. Hawkins BT, Ocheltree SM, Norwood KM, Egleton RD. (2007) Decreased blood-brain barrier permeability to fluorescein in streptozotocin-treated rats. Neurosci Lett, 411: 1-5.

256. Gaillard PJ, de Boer AG. (2000) Relationship between permeability status of the blood-brain barrier and in vitro permeability coefficient of a drug. Eur J Pharm Sci, 12: 95-102.

257. Madara JL. (1998) Regulation of the movement of solutes across tight junctions. Annu Rev Physiol, 60:143-59.: 143-159.

258. Krause G, Winkler L, Mueller SL, Haseloff RF, Piontek J, Blasig IE. (2008) Structure and function of claudins. Biochim Biophys Acta, 1778: 631-645.

259. Koshiba S, An R, Saito H, Wakabayashi K, Tamura A, Ishikawa T. (2008) Human ABC transporters ABCG2 (BCRP) and ABCG4. Xenobiotica, 38: 863-888.

260. Braun A, Hammerle S, Suda K, Rothen-Rutishauser B, Gunthert M, Kramer SD, Wunderli-Allenspach H. (2000) Cell cultures as tools in biopharmacy. Eur J Pharm Sci, 11 Suppl 2: S51-S60.

261. Brayden DJ, Griffin J. (2008) Avermectin transepithelial transport in MDR1- and MRP-transfected canine kidney monolayers. Vet Res Commun, 32: 93-106.

262. Liu X, Smith BJ, Chen C, Callegari E, Becker SL, Chen X, Cianfrogna J, Doran AC, Doran SD, Gibbs JP, Hosea N, Liu J, Nelson FR, Szewc MA, Van DJ. (2005) Use of a physiologically based pharmacokinetic model to study the time to reach brain equilibrium: an experimental analysis of the role of blood-brain barrier permeability, plasma protein binding, and brain tissue binding. J Pharmacol Exp Ther, 313: 1254-1262.

263. Jeffrey P, Summerfield SG. (2007) Challenges for blood-brain barrier (BBB) screening. Xenobiotica, 37: 1135-1151.

264. Friden M, Ljungqvist H, Middleton B, Bredberg U, Hammarlund-Udenaes M. (2010) Improved measurement of drug exposure in the brain using drug-specific correction for residual blood. J Cereb Blood Flow Metab, 30: 150-161.

DOI: 10.14753/SE.2013.1815

10. Publications

Publications related to the dissertation:

Hellinger É, Veszelka S, Tóth AE, Walter F, Kittel Á, Bakk ML, Tihanyi K, Háda V, Nakagawa S, Dinh Ha Duy T, Niwa M, Deli MA, Vastag M. (2012) Comparison of brain capillary endothelial cell-based and epithelial (MDCK-MDR1, Caco-2 and VB-Caco-2) cell-based surrogate blood-brain barrier penetration models. Eur J Pharm Biopharm, 82: 340-351. IF_{2010}: 4.304

Vastag M, **Hellinger É**, Bakk ML, Tihanyi K. (2011) Cell-based models of blood-brain barrier penetration. Ther Deliv, 2: 549-553.

Hellinger É, Bakk ML, Pócza P, Tihanyi K, Vastag M. (2010) Drug penetration model of vinblastine-treated Caco-2 cultures. Eur J Pharm Sci, 41: 96-106. IF: 3.291

Book chapter: **Hellinger É**, Vastag M. Intestinal absorption and models of penetration. In: Tihanyi K, Vastag M, (eds.), Solubility, delivery and ADME problems of drugs and drug-candidates. Bentham Science Publishers. 2011: 86-101.

Other publications:

Tihanyi K, Bakk ML, **Hellinger É**, Vastag M. (2010) CYP inhibition-mediated drug-drug interactions. Curr Enzyme Inhib, 6: 130-145.

Boer K, **Hellinger É**, Hellinger A, Pocza P, Pos Z, Demeter P, Baranyai Z, Dede K, Darvas Z. Falus A. (2008) Decreased expression of histamine H1 and H4 receptors suggests disturbance of local regulation in human colorectal tumours by histamine. Eur J Cell Biol, 87: 227-236. IF: 3.955

DOI: 10.14753/SE.2013.1815

Jókúti A, **Hellinger É**, Hellinger A, Darvas Z, Falus A, Thurmond RL, Hirschberg A. (2007) Histamine H4 receptor expression is elevated in human nasal polyp tissue. Cell Biol Int, 31: 1367-1370. IF: 1.547

DOI: 10.14753/SE.2013.1815

Acknowledgements

The greatest part of the experimental work of this dissertation has been done at Laboratory of In-Vitro Metabolism Research, at Gedeon Richter Plc, under the supervision of **Dr. Károly Tihanyi**. I am very thankful to him for giving me advice, support and encouragement and for giving me the possibility to do my PhD work at Gedeon Richter Plc. I would like to thank **Dr. Monika Vastag**, the head of the In-Vitro Metabolism Laboratory, for the enormous help, support and attention. I am also very grateful to her for introducing me into the different methods and supporting me in all aspects of the research described in the current thesis. I would also like to thank the contribution of all my colleagues in the laboratory; **Andrea Tóth-Major, Andrea Jánki, Erika Czank, Mónika Laura Bakk, Marianna Borsos, Szilvia Baranyi, Teréz Merkl, Ildikó Bakonyi and Dr. Emese Kápolna**, and also my ex-colleague, **Dr. János Leibinger**. I am also grateful to **the workers of Laboratory of Molecular Cell Biology, Developmental Drug Metabolism and Pharmacokinetics, Discovery Pharmacokinetic** and to **Dr. Viktor Háda** from Spectroscopic Research for their help in the studies.

Some experiments from the PhD work was done in the Laboratory of Molecular Neurobiology, Institute of Biophysics, Biological Research Center of the Hungarian Academy of Sciences, Szeged with the help and support of **Dr. Mária Deli**, to whom I am very grateful, and I also thank the help of **Dr. Szilvia Veszelka, Andrea Tóth** and **Fruzsina Walter** from the laboratory. I would like to thank **Dr. Shinsuke Nakagawa, Dr. Dinh Ha Duy Thuy,** and **Prof. Masami Niwa** from Nagasaki University Graduate School of Biomedical Sciences, Japan for providing their experimental data. I am also thankful to **Dr. Ágnes Kittel** (Institute of Experimental Medicine, Hungarian Academy of Sciences) for the electron micrographs and to **Dr. Péter Pócza** (Department of Genetics, Cell and Immunobiology, Semmelweis University) for the RT-PCR measurement.

I would like to thank all my family and my husband for their endless patience and support.

DOI: 10.14753/SE.2013.1815

Appendix (Paper I-IV)